



SYNTHESIS OF AG-DOPED TiO_2 NANOPARTICLES VIA SOL-GEL
METHOD FOR ANTIBACTERIAL AIR FILTER

BY

MISS SIRIPOND PHROMMA

A THESIS SUBMITTED IN PARTIAL FULFILLMENT OF THE REQUIREMENTS
FOR THE DEGREE OF MASTER DEGREE OF ENGINEERING
(ENERGY AND ENVIRONMENTAL TECHNOLOGY MANAGEMENT)
DEPARTMENT OF CHEMICAL ENGINEERING FACULTY OF ENGINEERING
THAMMASAT UNIVERSITY
ACADEMIC YEAR 2017
COPYRIGHT OF THAMMASAT UNIVERSITY

SYNTHESIS OF AG-DOPED TiO_2 NANOPARTICLES VIA SOL-GEL
METHOD FOR ANTIBACTERIAL AIR FILTER

BY

MISS SIRIPOND PHROMMA



A THESIS SUBMITTED IN PARTIAL FULFILLMENT OF THE REQUIREMENTS
FOR THE DEGREE OF MASTER DEGREE OF ENGINEERING
(ENERGY AND ENVIRONMENTAL TECHNOLOGY MANAGEMENT)
DEPARTMENT OF CHEMICAL ENGINEERING FACULTY OF ENGINEERING
THAMMASAT UNIVERSITY
ACADEMIC YEAR 2017
COPYRIGHT OF THAMMASAT UNIVERSITY

THAMMASAT UNIVERSITY
FACULTY OF ENGINEERING

THESIS

BY

MISS SIRIPOND PHROMMA

ENTITLED

SYNTHESIS OF AG-DOPED TiO_2 NANOPARTICLES VIA SOL-GEL METHOD FOR
ANTIBACTERIAL AIR FILTER

was approved as partial fulfillment of the requirements for the degree of Master of
Engineering (Energy and Environmental Technology Management)

On August 9, 2018

Chairman

Worane

(Associate. Professor. Woranee Mungalasiri, Ph.D.)

Member and Advisor

Tippabust

(Assistant. Professor. Tippabust Eksangri, D.Eng.)

Member and Co-advisor

Chaweewan Sapcharoenkun

(Chaweewan Sapcharoenkun, Ph.D.)

Member

Suwimon Boonrungsiman

(Suwimon Boonrungsiman, Ph.D.)

Dean

Thira J.

(Associate. Professor. Thira Jearsiripongkul, Ph.D.)

Thesis Title	SYNTHESIS OF AG-DOPED TiO ₂ NANOPARTICLES VIA SOL-GEL METHOD FOR ANTIBACTERIAL AIR FILTER
Author	Miss Siripond Phromma
Degree	Master of Engineering
Major Field/Faculty/University	Energy and Environmental Technology Management Faculty of Engineering Thammasat University
Thesis Advisor	Asst. Prof. Tippabust Eksangsri, D.Eng.
Thesis Co-Advisor	Chaweewan Sapcharoenkun, Ph.D.
Academic Years	2017

ABSTRACT

Titanium dioxide (TiO₂) is well-known for its high antibacterial activity. The application of TiO₂ for antibacterial air filter has been recognized but the limitation of photocatalytic reaction on dependency of UV light has still been a challenge. TiO₂ modified with silver (Ag-TiO₂) has attracted much attention and applied in a wide range of applications especially as an antibacterial agent in recent years. However, its low photocatalytic activity, antibacterial activity, and surface area limit the potential use and capabilities in antibacterial air filter. In this study, Ag-TiO₂ were synthesized via dry and wet ball milling sol-gel method (DWBMS) and dip coated on commercial air filter to produce antibacterial air filter, which can be used under UV light and dark condition. First, synthesis of TiO₂ nanoparticles (NPs) via DWBMS was conducted. The influences of various alcohol types used and varied calcination temperature were investigated. The results suggested the optimal synthesis conditions to be applied for the synthesis of Ag-TiO₂ NPs in the next step. Methanol as a solvent was found to be the most suitable reagent for TiO₂ synthesis with smallest particle size and narrow size

distribution of 8.1 ± 2.1 nm and highest photocatalytic efficiency of $8.5 \times 10^{-4} \text{ min}^{-1}$ compared to ethanol and isopropanol. Calcination temperature in the range of 300-800°C was observed. It was found that the calcination temperature plays an essential role for phase transition, crystallite size, particle size, and crystallinity of TiO₂. The high amount of anatase phase mixed with brookite and rutile phases had a strong effect on the photocatalytic activity between 300 and 600°C while the crystallite and particle size of TiO₂ had a dominant influence on the photocatalytic activity from 600 to 700°C. The highest photocatalytic activity with the kinetic constant rate of $1.70 \times 10^{-3} \text{ min}^{-1}$ was achieved with TiO₂ calcined at 600 °C. Next, Ag-TiO₂ NPs were synthesized via DWBMS with methanol as solvent, and calcination temperature of 600°C. Photocatalytic and antibacterial activities of Ag-TiO₂ were determined by the effect concentration of Ag from 3% to 10% by mole of Ag. It was found that the optimal amount at 5% Ag-TiO₂ showed the highest photocatalytic activity with the kinetic constant rate of $2.02 \times 10^{-3} \text{ min}^{-1}$. At last, the effect of dipping speed, binder concentration, and coating solution concentration were investigated to propose the optimal coating conditions. Then, the solution of synthesized 5% Ag-TiO₂ was dip-coated on F9 air filter. The selected conditions were; 0.50 mm/s dipping speed, 1%v/v PPG-4000 as binder, and 10%w/v of 5% Ag-TiO₂. It was clearly seen that the coated air filter offered the bacterial reduction efficiency up to 99.99%, under both UV-light and dark conditions.

Keyword: Antibacterial air filter, Ag doped titanium dioxide, Dry and wet ball milling sol-gel method, Photocatalytic activity, Self-cleaning, Antibacterial activity

หัวข้อวิทยานิพนธ์	การสังเคราะห์อนุภาคนาโนไทเทเนียมไดออกไซด์ที่มีการเจือโลหะเงินด้วยวิธีการโซลเจลเพื่อประยุกต์ใช้สำหรับแผ่นกรองอากาศยับยั้งแบคทีเรีย
ชื่อผู้เขียน	นางสาวศิริพร พรหมมา
ชื่อปริญญา	วิศวกรรมศาสตรมหาบัณฑิต
สาขา/คณะ/มหาวิทยาลัย	เทคโนโลยีการจัดการพลังงานและสิ่งแวดล้อม วิศวกรรมศาสตร์ มหาวิทยาลัยธรรมศาสตร์
อาจารย์ที่ปรึกษาวิทยานิพนธ์	ผู้ช่วยศาสตราจารย์ ดร. ทิพบุษย์ เอกแสงศรี
อาจารย์ที่ปรึกษาวิทยานิพนธ์ร่วม	ดร. ฉวีวรรณ ทรัพย์เจริญกุล
ปีการศึกษา	2560

บทคัดย่อ

ไทเทเนียมไดออกไซด์ (TiO_2) เป็นสารที่มีประสิทธิภาพในการยับยั้งแบคทีเรียสูง ปัจจุบันมีการนำ TiO_2 มาประยุกต์ใช้กับแผ่นกรองอากาศเพื่อเพิ่มประสิทธิภาพในการยับยั้งแบคทีเรีย แต่ข้อจำกัดของแผ่นกรองอากาศที่เคลือบด้วย TiO_2 นั้นจำเป็นต้องใช้แสงยูวีเพื่อกระตุ้นให้ TiO_2 เกิดปฏิกิริยาเร่งด้วยแสงและมีฤทธิ์ในการยับยั้งแบคทีเรีย ดังนั้นจึงมีการดัดแปลง TiO_2 ด้วยการเติมโลหะเงิน (Ag) (Ag-TiO_2) ซึ่งเป็นสารที่น่าสนใจและถูกนำมาประยุกต์ใช้อย่างกว้างขวาง โดยเฉพาะอย่างยิ่งนำมาเป็นสารยับยั้งแบคทีเรีย แต่อย่างไรก็ตามแผ่นกรองอากาศที่เคลือบด้วยสารยับยั้งแบคทีเรียยังพบปัญหาเรื่องการเกิดปฏิกิริยาเร่งด้วยแสงและประสิทธิภาพการยับยั้งแบคทีเรียเกิดได้ไม่ดีมากนัก และสารเคลือบมีพื้นที่ผิวสัมผัสในการเกิดปฏิกิริยาได้น้อย ดังนั้นในงานวิจัยนี้ต้องการสังเคราะห์อนุภาค Ag-TiO_2 ด้วยวิธีการโซลเจลร่วมกับการบดแบบแห้งและแบบเปียก (DWBMS) และนำสาร Ag-TiO_2 ที่สังเคราะห์ได้ไปเคลือบบนแผ่นกรองอากาศทางการค้า เพื่อให้มีประสิทธิภาพในการยับยั้งเชื้อแบคทีเรียทั้งภายใต้แสงยูวีและในที่มืด ในขั้นตอนแรกทำการสังเคราะห์อนุภาค TiO_2 โดยทำการศึกษาผลของชนิดแอลกอฮอล์และอุณหภูมิที่ใช้ในการเผาอนุภาคที่แตกต่างกัน ซึ่งผลการทดลองที่ได้จากการสังเคราะห์อนุภาค TiO_2 ทำให้ทราบสภาวะที่เหมาะสมสำหรับสังเคราะห์อนุภาค Ag-TiO_2 ในขั้นต่อไป ผลการทดลองพบว่า อนุภาค TiO_2 ที่สังเคราะห์ได้โดยใช้เมทานอลเป็นตัวทำละลายทำให้ได้อนุภาคที่มีขนาดเล็กที่สุดและมีการกระจายตัวของอนุภาคที่แคบ โดยมีค่าเท่ากับ 8.1 ± 2.1 นาโนเมตรและเกิดปฏิกิริยาเร่งด้วยแสงได้มากที่สุดเท่ากับ 8.5×10^{-4} ต่อนาที เมื่อ

เปรียบเทียบกับ TiO_2 ที่สังเคราะห์โดยใช้เอทานอลและไอโซโพรพานอล จากการศึกษาผลของอุณหภูมิที่ใช้ในการเผาอนุภาค TiO_2 ในช่วง 300°C ถึง 800°C พบว่าส่งผลต่อการเปลี่ยนแปลงเฟสขนาดของผลึก (crystallite size) ขนาดอนุภาค และความเป็นผลึกของอนุภาค TiO_2 การเกิดปฏิกิริยาเร่งด้วยแสงของอนุภาค TiO_2 เกิดแตกต่างกัน โดยในช่วงอุณหภูมิ 300°C ถึง 600°C เป็นผลมาจากปริมาณของเฟสอะนาเทสที่มีมากผสมกับเฟสรูไทล์และ บรูกไคต์ ในขณะที่อนุภาค TiO_2 ที่ถูกเผาในช่วงอุณหภูมิ 600°C - 700°C การเกิดปฏิกิริยาเร่งด้วยแสงเป็นผลมาจากขนาด crystallite size การเกิดปฏิกิริยาเร่งด้วยแสงได้ดีที่สุดพบที่อุณหภูมิ 600°C มีค่าคงที่อัตราเท่ากับ 1.70×10^{-3} ต่อนาที ในขั้นถัดมาทำการสังเคราะห์อนุภาค Ag-TiO_2 ด้วยวิธี DWBMS จึงเลือกใช้เมทานอลเป็นตัวทำละลายและอุณหภูมิที่ใช้ในการเผาคือ 600°C และศึกษาผลความเข้มข้นของ Ag ตั้งแต่ 3% ถึง 10% โดยโมลต่อการเกิดปฏิกิริยาเร่งด้วยแสงและประสิทธิภาพยับยั้งแบคทีเรีย พบว่าความเข้มข้นของ Ag ที่เหมาะสมคือ 5% Ag-TiO_2 เกิดปฏิกิริยาเร่งด้วยแสงได้ดีที่สุดมีค่าคงที่อัตราเท่ากับ 2.02×10^{-3} ต่อนาที ในขั้นสุดท้ายในงานวิจัยนี้สนใจศึกษาสภาวะที่เหมาะสมต่อการเคลือบสารบนแผ่นกรองอากาศ โดยศึกษาผลอัตราเร็วในการจุ่มเคลือบ ความเข้มข้นของสารยึดติด (PPG-4000) และความเข้มข้นของสารเคลือบ จากนั้นอนุภาค Ag-TiO_2 จะถูกเคลือบบนแผ่นกรองอากาศทางการค้าชนิด F9 ซึ่งพบว่าสภาวะที่เหมาะสมต่อการเคลือบคือ อัตราเร็วในการจุ่มเคลือบแผ่นกรองอากาศเท่ากับ 0.50 mm/s , ความเข้มข้นของสารยึดติด (PPG-4000) เท่ากับ 1%v/v และความเข้มข้นของ 5% Ag-TiO_2 เท่ากับ 10%w/v พบว่าแผ่นกรองอากาศมีประสิทธิภาพในการยับยั้งแบคทีเรียได้ถึง 99.99% ภายใต้สภาวะที่ไม่มีแสงและมีแสงยูวี

คำสำคัญ: แผ่นกรองอากาศยับยั้งแบคทีเรีย, การเจืออนุภาคเงินในอนุภาคนาโนไทเทเนียมไดออกไซด์, วิธีการโซลเจลร่วมกับการบดแบบแห้งและแบบเปียก, ปฏิกิริยาเร่งด้วยแสง, การทำความสะอาดด้วยตัวเอง, การยับยั้งแบคทีเรีย

ACKNOWLEDGEMENTS

I would like to thank my advisor, Asst. Prof. Tippabust Eksangsri for good recommendation and support me everything to do research in the thesis.

I would like to thank co-advisor Dr. Chaweewan Sapcharoenkun for good suggestion about the knowledge of nanomaterial, support me for analysis the data and consult with the equipment to use in thesis. Moreover, I would like to thank member of National Nanotechnology Center (NANOTEC) and National Metal and Material Technology Center (MTEC) for supporting me to understand work and provided the equipment for experiment in the thesis.

Finally, I would like to thank my parent to support and always standing side by side me to do the thesis and thank myself for patience and did not discouraged with obstacles.

Miss Siripond Phomma

TABLE OF CONTENTS

	Page
ABSTRACT	(1)
ACKNOWLEDGEMENTS	(5)
LIST OF TABLES	(10)
LIST OF FIGURES	(13)
LIST OF ABBREVIATIONS	(18)
CHAPTER 1 INTRODUCTION	1
1.1 Background	1
1.2 Objectives	4
1.3 Scope of this work	4
CHAPTER 2 REVIEW OF LITERATURE	6
2.1 Air filter	6
2.2 Nanoparticle for antibacterial activity	9
2.2.1 TiO ₂ nanoparticles	9
2.2.2 Modified TiO ₂ for visible light	12
2.3 Method for synthesis of Ag-TiO ₂ NPs	14
2.3.1 Sol-gel method	15
2.4 Method for coating of Ag-TiO ₂ NPs on air filter	18
2.4.1 Dip and spin coating	18

CHAPTER 3 RESEARCH METHODOLOGY	21
3.1 Synthesis of TiO ₂ nanoparticles	21
3.1.1 Materials	21
3.1.2 Effect of alcohol types on TiO ₂ powder synthesis with DWBMS method	21
3.1.3 Effect of calcination temperatures on TiO ₂ powder synthesis with DWBMS method	22
3.2 Synthesis of Ag-TiO ₂ nanoparticle	23
3.2.1 Materials	23
3.2.2 Effect concentration of Ag NPs on synthesis of Ag-TiO ₂ powder with DWBMS method	23
3.2.3 Characterization of TiO ₂ and Ag-TiO ₂ powder	24
3.2.4 Preparation of photocatalytic activity of TiO ₂ , P25, and Ag-TiO ₂ powder	25
3.2.5 Preparation of antibacterial activity of TiO ₂ , P25, and Ag-TiO ₂ powder	25
3.3 Coating Ag-TiO ₂ NPs on air filter for self-cleaning, and antibacterial activity	26
3.3.1 Materials	26
3.3.2 Preparation dip coating with various dipping speed of P25 NPs on air filter	27
3.3.3 Preparation dip coating with various IPA, PPG-4000, and P25 on air filter	27
3.3.4 Preparation dip coating with various concentration of PPG-4000 NPs on air filter	27
3.3.5 Preparation dip coating with various concentration of P25 NPs on air filter	28
3.3.6 Preparation dip coating with P25, TiO ₂ , and 5% Ag-TiO ₂ NPs on air filter	28

3.3.7 Preparation dip coating for self-cleaning test on air filters	28
3.3.8 Antibacterial activity test of air filters	29
CHAPTER 4 RESULTS AND DISCUSSION	30
4.1 Synthesis of TiO ₂ NPs	30
4.1.1 Effect of alcohol types on TiO ₂ synthesis	30
4.1.2 Effect of calcination temperatures on TiO ₂ synthesis	34
4.2 Synthesis of Ag-TiO ₂ powder	44
4.2.1 Effect of different concentration of Ag on photocatalytic activity of Ag-TiO ₂	44
4.2.2 Effect of different concentration of Ag on antibacterial activity	55
4.3 Dip coating of TiO ₂ , P25, and Ag-TiO ₂ NPs on air filter	60
4.3.1 Effect of dipping speed on air filters for self-cleaning, and antibacterial activity application	60
4.3.2 Effect of PPG-4000, IPA, and P25 NPs self-cleaning, and antibacterial on air filter	63
4.3.3 Effect of concentration of PPG-4000 on self-cleaning, and antibacterial air filter	65
4.3.4 Effect of concentration of P25 NPs on self-cleaning, and antibacterial air filters	69
4.3.5 Effect of different materials including of 10%w/v P25 NPs, TiO ₂ , and 5% Ag-TiO ₂ on self-cleaning, and antibacterial air filters	72
CHAPTER 5 CONCLUSIONS AND RECOMMENDATIONS	76
5.1 Conclusions	76
5.2 Recommendations and outlook	76

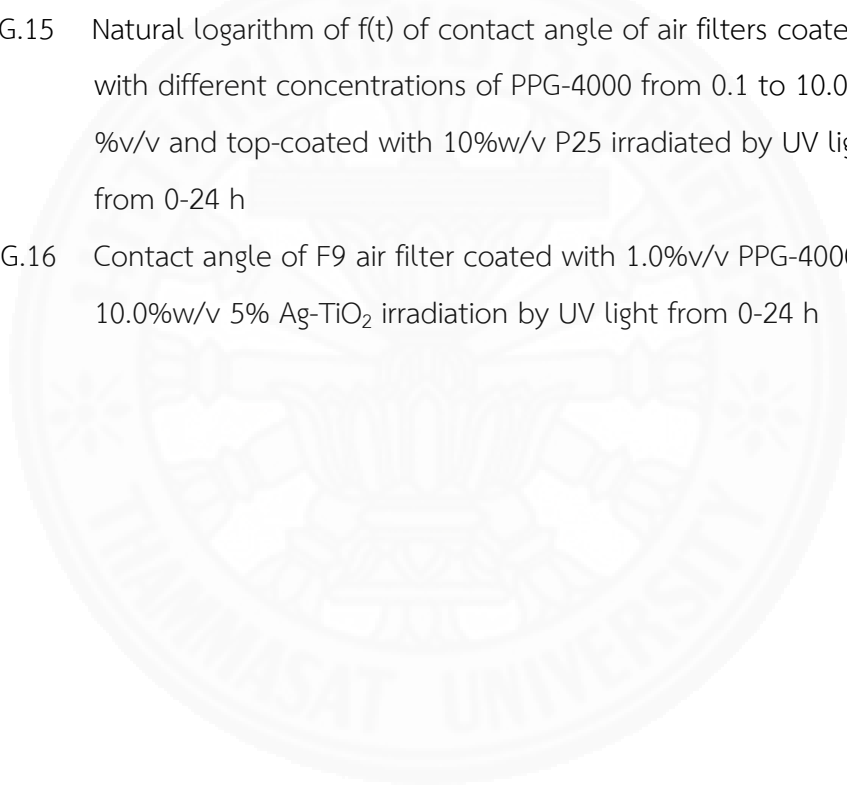
REFERENCES	78
APPENDICES	
APPENDIX A: Particle size and size distribution of TiO ₂ was synthesized via DWBMS method with different calcination temperature	85
APPENDIX B: Particle size and size distribution of Ag-TiO ₂ was synthesized via DWBMS method with different concentration of Ag	87
APPENDIX C: Energy dispersive spectroscopy (EDS) from FE-SEM of Ag-TiO ₂ NPs	89
APPENDIX D: Pore size distribution of TiO ₂ and Ag-TiO ₂ with different concentrations of Ag from 3 to 10% by mole	92
APPENDIX E: Energy band gap of TiO ₂ and Ag-TiO ₂ powder with different concentrations of Ag	93
APPENDIX F: Self-cleaning rate on air filter with different speeds and concentrations of PPG-4000, P25 NPs, TiO ₂ , and 5% Ag-TiO ₂	94
BIOGRAPHY	112

LIST OF TABLES

Tables	Page
2.1 Classification of air filter of ASHRAF 52.1, 52.2-1992	7
2.2 Classification of air filter of EN 779: 2012	8
2.3 Classification of air filter of EN 1822: 2009	8
4.1 Particle size of TiO ₂ with different solvents from DLS	33
4.2 Crystallite size of synthesized TiO ₂ with calcination temperatures	41
4.3 Kinetic constant of TiO ₂ and Ag-TiO ₂ with different concentrations of Ag	47
4.4 Percentage of crystallinity and amorphous of synthesized TiO ₂ and 3-10% by mole of Ag-TiO ₂	50
4.5 Surface area, pore volume, and pore diameter of TiO ₂ and 3-10% by mole of Ag-TiO ₂	52
4.6 Minimum inhibitory concentration (MIC) and minimum bactericidal concentration (MBC) of TiO ₂ , P25, and Ag-TiO ₂ at different concentration of Ag under dark and UV light conditions	58
4.7 Energy band gap of TiO ₂ and 3-10% by mole of Ag-TiO ₂	59
4.8 Self-cleaning rate of air filters coated with various dipping speeds from 0.167 to 1.000 mm/s	62
4.9 Self-cleaning rate of air filters coated with various concentration of PPG-4000 from 0.1 to 1.0%v/v combined with P25 NPs	68
4.10 Self-cleaning rate of air filters coated with various concentration of P25 from 0.1 to 1.0%w/v	71
4.11 Self-cleaning rate of air filters coated with 10%w/v P25 NPs, TiO ₂ , and 5% Ag-TiO ₂	75
F.1 Concentration of <i>E. coli</i> on F9 air filters coated with different dipping speeds	94

F.2	Concentration of <i>E. coli</i> on F9 air filters coated with different concentration of PPG-4000	95
F.3	Concentration of <i>E. coli</i> on F9 air filters coated with different concentration of PPG-4000 and 10%w/v P25	95
F.4	Concentration of <i>E. coli</i> on F9 air filters coated with different concentration of P25	96
F.5	Concentration of <i>E. coli</i> on F9 air filters coated with P25, TiO ₂ and 5% Ag-TiO ₂	96
G.1	Contact angle of F9 air filters coated with 10%w/v P25 NPs with 0.167 mm/s irradiated by UV light from 0 to 24 h	97
G.2	Contact angle of F9 air filter coated with 10%w/v P25 NPs with 0.250 mm/s irradiated by UV light from 0 to 24 h	98
G.3	Contact angle of air filter coated with 10%w/v P25 NPs with 0.500 mm/s irradiated by UUV light from 0 to 24 h	99
G.4	Contact angle of air filter coated with 10%w/v P25 NPs with 1.000 mm/s irradiated by UV light from 0 to 24 h	100
G.5	Natural logarithm of f(t) of contact angle of air filters coated with P25 NPs with different dipping speeds irradiated by UV light from 0 to 24 h	101
G.6	Contact angle of F9 air filter coated with 0.1%v/v PPG-4000 and 10%w/v P25 NPs irradiated by UV light from 0 to 24 h	102
G.7	Contact angle of F9 air filter coated with 1.0%v/v PPG-4000 and 10%w/v P25 NPs irradiated by UV light from 0 to 24 h	103
G.8	Contact angle of F9 air filter coated with 5.0%v/v PPG-4000 and 10%w/v P25 NPs irradiated by UV light from 0 to 24 h	104
G.9	Contact angle of F9 air filter coated with 10.0% v/v PPG-4000 and 10%w/v P25 NPs irradiated from 0-24 h	105
G.10	Natural logarithm of f(t) contact angle of air filters coated with different concentrations of PPG-4000 from 0.1 to 10.0%v/v and top-coated with 10%w/v P25 irradiated by UV light from 0-24 h	106

G.11	Contact angle of F9 air filter coated with 1.0%v/v PPG-4000 and 0.1%w/v P25 NPs irradiated by UV light from 0-24h	107
G.12	Contact angle of F9 air filter coated with 1.0%v/v PPG-4000 and 1.0%w/v P25 NPs from 0-24 h	108
G.13	Contact angle of F9 air filter coated with 1.0% v/v PPG-4000 and 5.0%w/v P25 NPs irradiated by UV light from 0-24 h	109
G.14	Contact angle of F9 air filter coated with 1.0% v/v PPG-4000 and 10.0% w/v P25 NPs irradiated by UV light from 0-24 h	109
G.15	Natural logarithm of f(t) of contact angle of air filters coated with different concentrations of PPG-4000 from 0.1 to 10.0 %v/v and top-coated with 10%w/v P25 irradiated by UV light from 0-24 h	110
G.16	Contact angle of F9 air filter coated with 1.0%v/v PPG-4000 and 10.0%w/v 5% Ag-TiO ₂ irradiation by UV light from 0-24 h	111



LIST OF FIGURES

Figures	Page	
2.1	Crystal structure of TiO ₂	10
2.2	Photocatalytic activity of TiO ₂ nanoparticles under UV light	11
2.3	Mechanism antibacterial activity of Ag nanoparticles	13
2.4	Schematic diagrams show photocatalytic activity of Ag modified TiO ₂ and Ag-TiO ₂	14
2.5	The transformation form sol to gel formation in sol-gel method	15
2.6	Flow chart preparation of doped TiO ₂ nanoparticle via sol-gel method	16
2.7	Particle size and size distribution of original boron, after wet ball milling and after dry ball milling for 4 h	17
2.8	Stages of dip coating process	19
2.9	Stages of spin coating process	19
3.1	Synthesis of TiO ₂ NPs with various alcohol types via DWBM method	22
3.2	Synthesis of TiO ₂ NPs with various calcination temperatures via DWBM method	23
4.1	TEM images and size distribution of synthesized TiO ₂ with different solvents	32
4.2	Particle size and size distribution of TiO ₂ with different solvent form DLS	32
4.3	Photocatalytic activity with the degradation of MB solution of synthesized TiO ₂ particles obtained from different solvents	34
4.4	XRD pattern of TiO ₂ particles before and after calcination at different temperatures	35
4.5	Relationship between calcination temperatures and phase content	36

4.6	TEM image of TiO ₂ particle calcined at different calcination temperatures	38
4.7	Selected area electron diffraction (SAED) image of TiO ₂ particle calcined at different calcination temperature	39
4.8	Photocatalytic degradation of MB of synthesized TiO ₂ with different calcination temperatures and P25 NPs under UV irradiation	43
4.9	Relationship between kinetic constant and calcination temperatures from 300°C to 800°C	43
4.10	XRD patterns of synthesized TiO ₂ , Ag and 3-10% by mole Ag-TiO ₂ after calcination at 600°C for 4h	46
4.11	Photocatalytic activity of TiO ₂ and 3-10% by mole of Ag-TiO ₂ under UV light for 2 h	46
4.12	Crystallite size of anatase, rutile and brookite phases of 3-10% by mole of Ag-TiO ₂	47
4.13	Relationship between % phase content and % Ag concentration of TiO ₂ and Ag-TiO ₂	48
4.14	TEM images with d-spacing of TiO ₂ and 3-10% by mole Ag-TiO ₂	48
4.15	Selected area electron diffraction images of TiO ₂ and 3-10% by mole Ag-TiO ₂	49
4.16	Isotherm of TiO ₂ and 3-10% by mole Ag-TiO ₂ from N ₂ adsorption-desorption	52
4.17	Back scattered electron (BSE) images of TiO ₂ and 3-10% by mole Ag-TiO ₂	53
4.18	Energy Dispersive Spectroscopy (EDS) mapping of 3% Ag-TiO ₂	54
4.19	Mechanism of photocatalytic activity of Ag-TiO ₂ powder under UV light	54
4.20	Mechanism antibacterial activity of Ag-TiO ₂ powder under dark and UV light conditions	58

4.21	Diffuse reflectance spectra (DRS) of TiO ₂ and 3-10% by mole Ag-TiO ₂ nanoparticles	59
4.22	Reduction rate of <i>E. coli</i> with air filters coated with different dipping speeds under dark and UV light condition	63
4.23	FE-SEM images of uncoated F9 air filter and coated air filters with 9%v/v of PPG-4000 and 10%w/v of P25 NPs with different dipping speeds	63
4.24	Reduction of <i>E. coli</i> on different F9 air filters with different coating agents including PPG, IPA, P25, and PPG+P25+IPA employing AATCC 100-1999 and ISO 27447 under dark and UV light conditions for 6h	64
4.25	Reduction rate of <i>E. coli</i> on air filter coated with different concentrations of PPG-4000 employing modified AATCC 100 and ISO 27447 under dark and UV light conditions	66
4.26	Reduction rate of <i>E. coli</i> on air filter coated with different concentrations of PPG-4000 and then coated with 10%w/v P25 NPs tested by of AATCC 100 under dark and UV light conditions	68
4.27	FE-SEM images of uncoated F9 air filter and air filters was coated with different concentrations of PPG-4000	69
4.28	FE-SEM images of uncoated F9 air filter and air filters coated with various concentrations of P25	71
4.29	Reduction rate of <i>E. coli</i> on air filters coated with different concentrations of P25 NPs from 0.1% to 10.0%w/v and 1.0% v/v PPG-4000 employing the modified AATCC 100 under dark and UV light conditions	72
4.30	FE-SEM images of uncoated F9 air filter and air filter coated with 10% P25, TiO ₂ and 5% Ag-TiO ₂	74

4.31	Reduction rate of <i>E. coli</i> on air filter with 10%w/v P25, TiO ₂ and 5% Ag-TiO ₂ employing the modified AATCC 100 under dark and UV light conditions	74
4.32	FE-SEM image of air filter coated with 10%w/v of 5% Ag-TiO ₂ and EDS mapping	75
A.1	TEM images of TiO ₂ powder with various calcination temperatures	85
A.2	Size distribution of TiO ₂ powder with various calcination temperatures	86
B.1	TEM images of Ag-TiO ₂ powder TiO ₂ and 3-10% by mole Ag-TiO ₂	87
B.2	Size distribution of Ag-TiO ₂ powder with 3-10% by mole Ag-TiO ₂	88
C.1	Energy Dispersive Spectroscopy (EDS) mapping of 5% by mole Ag-TiO ₂ particles	89
C.2	Energy Dispersive Spectroscopy (EDS) mapping of 6% by mole Ag-TiO ₂ particles	90
C.3	Energy Dispersive Spectroscopy (EDS) mapping of 10% by mole Ag-TiO ₂ particles	91
D.1	Pore size distribution of TiO ₂ and 3-10% by mole Ag-TiO ₂	92
E.1	Energy band gap of TiO ₂ and 3-10% by mole Ag-TiO ₂	93
G.1	Relationship between UV irradiation time and ln f(t) of F9 air filters coated with different dipping speeds of 10%w/v P25 solution	102
G.2	Relationship between UV irradiation time and ln f(t) of F9 air filter coated with different concentrations of PPG-4000 from 0.1% to 10.0%v/v	106
G.3	Relationship between UV irradiation time and ln f(t) of F9 air filter coated with different concentration of P25 NPs from 0.1% to 10.0%w/v	110

G.4	Relationship between UV irradiation time and $\ln f(t)$ of F9 air filter coated with 10%w/v of 5% Ag-TiO ₂	111
-----	---	-----



LIST OF ABBREVIATIONS

Symbols/Abbreviations	Terms
DWBMS	Dry and Wet Ball Milling Sol-Gel Method
Ag-TiO ₂	Silver doped Titanium dioxide
NPs	Nanoparticles
<i>B. subtilis</i>	<i>Bacillus subtilis</i>
<i>E. coli</i>	<i>Escherichia coli</i>
<i>S. aureus</i>	<i>Staphylococcus aureus</i>
PCO	Photocatalytic oxidation
TEM	Transmission electron microscopy
HEPA	High Efficiency Particulate Air Filter
PPG	Polypropylene glycol
XRD	X-ray diffraction
SEM	Scanning Electron Microscopy
FE-SEM	Field Emission Scanning Electron Microscopy
DRS	Diffuse Reflectance Spectroscopy
BET	Brunauer-Emmett-Teller
MIC	Minimum Inhibitory Concentration
MBC	Minimum Bactericidal Concentration
VOC	Volatile Organic Compound
ASHRAE	American Society of Heating, Refrigeration and Air Condition Engineers
EN	The European Standard
ISO	International Organization for Standardization
<i>P.aeruginosa</i>	<i>Pseudomonas aeruginosa</i>
<i>S. epidermidis</i>	<i>Staphylococcus epidermidis</i>



O_2^-	Superoxide anion
OH^\bullet	Hydroxyl radical
ROS	Reactive Oxygen Species
TTIP	Titanium tetraisopropoxide
MeOH	Methanol
EtOH	Ethanol
IPA	Isopropanol
HNO_3	Nitric acid
DI	Deionized water
$AgNO_3$	Silver nitrate
MB	Methylene blue
DMSO	Dimethyl sulfoxide
P25	Commercial P25 TiO_2
JCPDF	Joint Committee on Powder Diffraction Standard
SAED	Selected Area Electron Diffraction
SPR	Surface Plasmon Resonance
BSE	Black Scattering Electron Microscopy

CHAPTER 1

INTRODUCTION

1.1 Background

The problem of bioaerosol including viruses, bacteria, fungi and pollen is everywhere in the environment. These bioaerosols are significantly attracted much attention because they cause human health effect. Particularly, bacteria can rapidly spread through the air flow which affects to an increase of the human diseases. According to WHO report in 2017, 10.4 million of people around the world were infected by tuberculosis disease. In Thailand, there was a significant increase the number of people who suffer from respiratory infection with *Mycobacterium tuberculosis* bacteria. 119,000 people per year (people in Thailand) were diagnosed with tuberculosis⁽¹⁾. A number of researches are interested in study and development of antibacterial air filter. At the present, High Efficiency Particulate Air Filter (HEPA) shows the high efficiency of 99.97% of filtering small particles ($>0.3 \mu\text{m}$) and can remove some bioaerosol airborne pollutants. However, it cannot effectively kill them. Thus, it becomes necessary to develop air purification system, device or method for the treatment of air contaminate with bioaerosol, specifically bacteria. Antibacterial air filter is an alternative device that can help in the filtering and inhibit the growth of bacteria. For improvement of air filter for antibacterial activity, silver nanoparticles (Ag NPs) was coated on air filter for high antibacterial activity. Because Ag NPs is well known high antibacterial agent since it can penetrate into the cell membrane of cell bacteria and causing of bacteria death⁽²⁾. Yoon *et al.* (2008) studied the antibacterial ability of the Ag NPs coated on activated carbon fiber (ACF) filter⁽³⁾. An ACF filter showed higher antibacterial efficacy against *B. subtilis* than that against *E. coli* by using disk diffusion method. Joe *et al.* (2013) studied antibacterial ability of Ag NPs coated on HEPA air filter⁽⁴⁾. It was observed that Ag NPs showed antibacterial activity of *S. epidermis* more than *E. coli* bacteria on HEPA air filter. However, Ag NPs show high antibacterial activity but, it can easily be oxidized with oxygen and unstable on air filter. Currently, there

has been a new trend for control pollutant contamination by photocatalytic oxidation (PCO) using TiO_2 photocatalyst into water treatment and air purification for the disinfection of microbial contamination. Because it is inexpensive, non-toxic, chemical and physical stability, and strong antibacterial agent when it occurs the photocatalytic activity under UV light⁽⁵⁾. Chuaybamroong *et al.* (2010) studied photocatalytic oxidation (PCO) of TiO_2 on HEPA air filter for disinfection of airborne microorganism⁽⁶⁾. They found that HEPA air filter with TiO_2 loading of $1870 \pm 169 \text{ mg/m}^2$ with humidity condition of $45 \pm 5\%$ showed the 60-80% eliminating of air borne microorganism under UV-A light. Limmongkon *et al.* (2013) studied the preparation of TiO_2 coated on air filter and used with an electrostatic air filter for removal xylene gas⁽⁷⁾. It was observed that using 5% Degussa P25 (commercial TiO_2) coated on HEPA air filter with four layers of ESF filters showed the highest efficiency of 100% removal xylene gas and provided safely for human health under UV-A light. Using TiO_2 nanoparticles for antibacterial activity, UV light is needed in order to generate hydroxyl free radical (OH^{\bullet}) from photocatalytic activity reaction to inhibit the growth of bacteria⁽⁸⁾. This make it difficult to use in conventional air filtration system. Researcher are interested in modifying TiO_2 for antibacterial activity under dark and UV light by doping with silver (Ag) metal⁽⁹⁾. Ag metal act as electron sink, promote the electron-hole pair separation and prevent electron-hole pair recombination when TiO_2 showed photocatalytic activity reaction under UV light. Then, the optimal Ag concentration for doping is importance parameter for the highest photocatalytic and antibacterial activity under dark and UV light. Tobaldi *et al.* (2014) studied antibacterial activity of Ag- TiO_2 powder, they found that the optimal amount of Ag was 2% by mole of modified TiO_2 powders showed higher antibacterial activity for *E. coli* and *S. aureus* than TiO_2 under visible light⁽¹⁰⁾. Pham and Lee (2104) studied the synthesis of Ag- TiO_2 by sol-gel method to enhance the efficiency of antibacterial activity of *Staphylococcus aureus* coating on fiberglass in order to improve the quality of indoor air filter. It was found that the addition of 7.5% wt. of Ag- TiO_2 coating on fiberglass provided the best photocatalytic and antibacterial activity⁽¹¹⁾.

There are many methods for synthesis of Ag-TiO₂ nanoparticles such as hydrothermal⁽¹²⁾ and sol-gel method⁽¹³⁾. Hydrothermal method synthesized under high pressure and temperature⁽¹²⁾. Then, sol-gel method is promising for synthesis of Ag-TiO₂ nanoparticles because it present high purity, easy to control size and shape which synthesized under atmosphere at room temperature⁽¹³⁾. Moreover, grinding step in sol-gel method showed aggregation of particles and used long time to produce narrow size distribution. Jung *et al.* (2015) studied physicochemical property of boron particles between dry and wet ball milling method. They found that using wet ball milling method provided narrow size distribution and low aggregation of particles than dry ball milling⁽¹⁴⁾. When uniform Ag-TiO₂ powder was synthesized by sol-gel method then, in this study will take Ag-TiO₂ powder to coat on air filter for high antibacterial activity. There are many methods for coating material for instance spin coating and dip coating⁽¹⁵⁾. Kment *et al.* (2012) studied dip and spin coating thin film of TiO₂ from Raman spectroscopy⁽¹⁵⁾. They found that the dip-coated showed smooth and uniformity thin film more than spin coated. Parameter control for dip coating for distribution of nanoparticle for high uniformity on substrate are binder concentration⁽⁷⁾, coating solution concentration and dipping speed⁽¹⁶⁾. Binder is one of the important material required for Ag-TiO₂ coating on air filter for high adhesion on air filter. In this study interested to study polymer polypropylene glycol (PPG) molecular weight 4000 as a binder for dip coating on air filter. Sangkajuntranon *et al.* (2014) studied the effect of different concentration of polyethylene glycol (PEG) 1000 with 5% wt. TiO₂ on air filter. They found that 1% PEG 1000 with 5% wt. TiO₂ showed the highest antibacterial activity of *S. epidermis* under black and white light. Sarah *et al.* (2018) studied the effect of different coating concentration of TiO₂ solution on glass substrate. They found that the optimal concentration for uniform thin film TiO₂ is 0.01 M solution on glass substrate. Moreover, Touam *et al.* (2014) studied effect of dip-coating speed on substrate of TiO₂ thin film. They found that increasing of dip-coating speed from 1 to 3 cm/min, the thickness of thin film increased with large grain size of TiO₂⁽¹⁷⁾. Therefore, in this study have goals study synthesis of Ag-TiO₂ powder for high photocatalytic

activity and coated Ag-TiO₂ on air filter for uniform distribution on air filter and high antibacterial activity.

1.2 Objectives

1.2.1 To synthesize TiO₂ nanoparticles via DWBMS method.

1.2.2 To study the optimal condition for synthesis of Ag-TiO₂ nanoparticles via DWBMS method for high antibacterial activity.

1.2.3 To characterize the physico-chemical properties, photocatalytic and antibacterial activities of TiO₂ and Ag-TiO₂ nanoparticles.

1.2.4 To study the effect of dipping speed binder concentration, and coating solution concentration on Ag-TiO₂ nanoparticles coating on air filters and characterize the physico-chemical properties and antibacterial activity on coated air filters.

1.3 Scopes of this study

1.3.1 Synthesis of Ag-TiO₂ nanoparticles via sol-gel method

1.3.1.1 Synthesis of TiO₂ nanoparticle via DWBMS for high photocatalytic activity

The effect of alcohol types on particles size were studied from synthesis of TiO₂ nanoparticles with various alcohol types namely methanol, ethanol, and isopropanol respectively. Moreover, effect of calcination temperature was studied from synthesis of TiO₂ nanoparticles with various calcination temperatures from 300 to 800°C. All of TiO₂ nanoparticles was characterized by Transmission Electron Microscopy (TEM), X-ray diffraction (XRD), UV-Vis spectroscopy and photocatalytic activity.

1.3.1.2 Synthesis of Ag-TiO₂ nanoparticles via DWBMS method for high photocatalytic and antibacterial activity

The effect of concentration of Ag nanoparticles for high photocatalytic and antibacterial activity was studied from doping with Ag from 3- 10% by mole Ag- TiO₂. Ag- TiO₂ nanoparticles were characterized by TEM, SEM, Diffuse Reflectance Spectroscopy (DRS), Brunauer-Emmett-Teller (BET), N₂ absorption and desorption, XRD, UV- Vis spectroscopy, photocatalytic activity, Minimum Inhibitory Concentration (MIC), and Minimum Bactericidal Concentration (MBC).

1.3.2 Coating of Ag-TiO₂ nanoparticles on air filter

1.3.2.1 Dip coating of Ag-TiO₂ nanoparticles

Air filter was dipped with various speeds of 0.167, 0.250 0.500, and 1.000 mm/s, coated with various concentrations of PPG- 400 from 0.1- 10.0% by volume PPG-4000 and various concentration solution of P25 and 5% Ag-TiO₂ in order to study effect of these for high uniformity of Ag-TiO₂ nanoparticles distribution on air filter and high antibacterial activity. Air filter was coated with various speed, concentration of PPG- 4000, and concentration of solution were characterized self-cleaning, SEM, and antibacterial activity.

CHAPTER 2

REVIEW OF LITERATURE

2.1 Air filter

Air filter is an importance in filtering system because air filter can filter dust, air borne pathogen and volatile organic compound (VOC). At the present, standard for classification and testing of air filter provide 3 classes compost of The American Society of Heating, Refrigeration and Air Condition Engineers (ASHRAE) stand 52.1,52.2-1992, The European Standard (EN 779: 2012) and International Organization for Standardization (ISO) 16890:2017. The classification and testing of air filter of ASHRAE 52.1,52.2-1992 and EN 779:2012, and 1822:2009 as shown in Table 2.1-2.3 respectively.

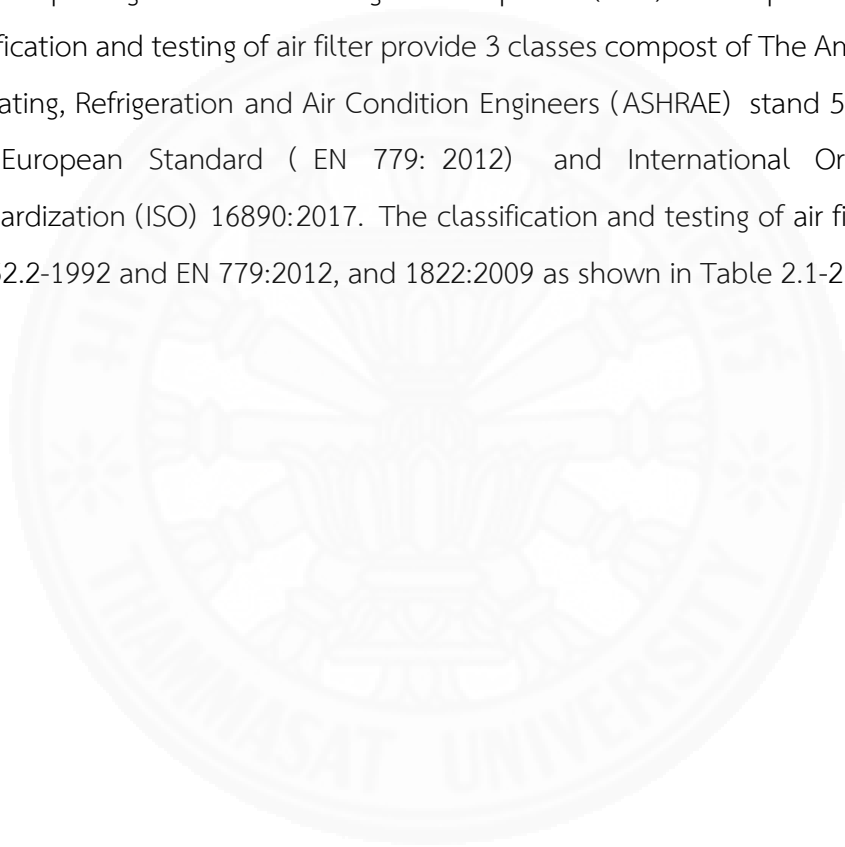


Table 2.1 Classification of air filter of ASHRAE 52.1, 52.2-1992

MERV	ASHRAE 52.2			ASHRAE 52.1	
	Average particle size efficiency (μm) %			Average efficiency (%)	Average dust spot efficiency (%)
	E_1 (0.3-1.0)	E_2 (1.0-3.0)	E_3 (3.0-10.0)		
1	-	-	<20	<65	< 20
2	-	-	<20	<65	< 20
3	-	-	<20	<70	< 20
4	-	-	<20	<75	< 20
5	-	-	≥ 20	80	20
6	-	-	≥ 35	85	20-25
7	-	-	≥ 50	90	25-30
8	-	-	≥ 70	92	30-35
9	-	-	≥ 85	95	40-45
10	-	≥ 50	≥ 85	96	50-55
11	-	≥ 65	≥ 85	97	60-65
12	-	≥ 80	≥ 90	98	70-75
13	-	≥ 90	≥ 90	98	80-85
14	≥ 75	≥ 90	≥ 90	99	90-95
15	≥ 85	≥ 90	≥ 90	99	95
16	≥ 95	≥ 95	≥ 95	100	99

Table 2.2 Classification of air filter of EN 779: 2012

Classification of air filter					
Group	Class	Final pressure drop (test) Pa	Average arrestance (Am) of synthetic dust%	Average efficiency (Em) for 0.4 µm particles %	Minimum efficiency for 0.4 µm particles %
Coarse	G1	250	$50 \leq Am < 65$	-	-
	G2	250	$65 \leq Am < 80$	-	-
	G3	250	$80 \leq Am < 90$	-	-
	G4	250	$90 \leq Am$	-	-
Medium	M5	450	-	$40 \leq Am < 60$	-
	M6	450	-	$60 \leq Am < 80$	-
Fine	F7	450	-	$80 \leq Am < 90$	35
	F8	450	-	$90 \leq Am < 95$	55
	F9	450	-	$95 \leq Am$	70

Table 2.3 Classification of air filter of EN 1822: 2009

class	Local value		Integral value	
	Filtration efficiency in MPPS (%)	Penetration efficiency in MPPS (%)	Filtration efficiency in MPPS (%)	Penetration efficiency in MPPS (%)
E10	85	15	-	-
E11	95	5	-	-
E12	99.5	0.5	-	-
H13	99.95	0.05	99.75	0.25
H14	99.995	0.005	99.975	0.025
U15	99.9995	0.0005	99.9975	0.0025
U16	99.99995	0.00005	99.99975	0.00025
U17	99.999995	0.000005	99.9999	0.0001

(Ref: <https://www.camfil.co.uk/Global/Documents/Brochure/Standards/ASHRAE52.pdf>)

At the present, HEPA shows high efficiency of 99.97% of filtering small particles of 0.3 μm and can remove airborne pathogen. But air filter cannot inhibit growth or kill of bacteria. Therefore, researcher interested in studying coating of nanoparticles on air filter for antibacterial activity air filter.

2.2 Nanoparticles for antibacterial activity

There are many nanoparticles (NPs) for antibacterial activity for instance Ag NPs with particle size rang 1-10 nm with concentration of 25-100 mg/ml can kill *Pseudomonas aeruginosa* (*P. aeruginosa*) and *Escherichia coli* (*E. coli*)⁽¹⁸⁾. Cu NPs particle size of 9 nm showed high antibacterial activity of *E. coli*, *Bacillus subtilis* (*B. subtilis*) and *Staphylococcus aureus* (*S. aureus*)⁽¹⁹⁾. ZnO NPs using of concentration 2×10^{-2} M showed antibacterial activity of *B. subtilis*⁽²⁰⁾. TiO_2 NPs particle size of 20 nm with concentration of 10 mg/ml showed photocatalytic activity antibacteria of *E. coli*, *P. Aeruginosa*, and *S. aureus* under UV light irradiation⁽²¹⁾. From previous research coated nanoparticles on air filter for antibacterial activity. Yoon *et al* (2008). studied the antibacterial ability of the Ag NPs coated on activated carbon fiber (ACF) filter⁽³⁾. They found that an ACF filter showed antibacterial activity with the diameter of the inhibition zones of *B. subtilis* and *E. coli* bacteria was increased from 10.85 ± 0.20 to 11.8 ± 0.28 mm and 11.95 ± 0.21 to 14.55 ± 0.64 mm, respectively. Joe *et al.* (2013) coated Ag NPs coated on HEPA air filter and studied antibacterial activity of *E. coli* and *Staphylococcus epidermidis* (*S. epidermidis*). They found that increasing of Ag NPs, the antibacterial activity of *E. coli* and *S. epidermidis* was increased. However, Ag NPs show high antibacterial activity but, it can easily be oxidized with oxygen and unstable on air filter.

2.2.1 TiO_2 nanoparticles

Photocatalytic oxidation (PCO) using Titanium dioxide (TiO_2) photocatalyst has been new tread for control pollutant of water treatment and air purification. Because TiO_2 has many properties such as resistant chemical, non-toxicity,

chemical and physical stability, antibacterial activity, and strong photocatalytic activity^(22,23). TiO_2 has three crystalline polymorphs structure composed of anatase (tetragonal), rutile (tetragonal), and brookite (orthorhombic) phases, respectively as shown in Figure 2.1. Besides, anatase phase presents indirect band gap structure with energy band gap of 3.02 eV. On the other hand, rutile, and brookite phases present direct band gap structure with energy band gap of 3.02 and 3.30 eV, respectively⁽²⁴⁾.

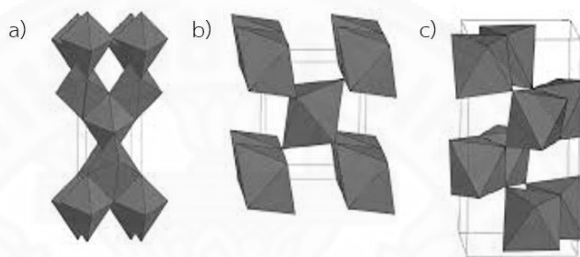


Figure 2.1 Crystal structure of TiO_2 a) anatase, b) rutile and c) brookite phases⁽²⁵⁾.

TiO_2 occurs photocatalytic activity was excited by UV light with wavelength between 100-400 nm with energy equal to or greater than the energy band gap. The electron in valence band was excited to conduction band. Then electron can transfer to surface area of TiO_2 or generate recombination of electron and hole pair. The redox of reaction consist of two reactions are oxidation and reduction. The oxygen in the air can react with electron (e^-) in conduction band and occur the reduction reaction to generate superoxide anion (O_2^-). While the hole in valence band can react with moisture or water to generate hydroxyl radical (OH^*) in oxidation reaction⁽²⁶⁾ as shown in Figure 2.2 and can be written as an these equation from (1) - (5) follows:

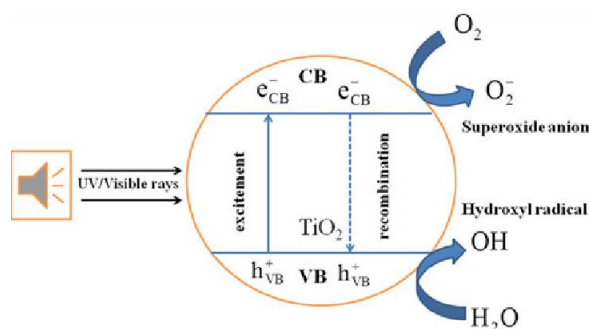


Figure 2.2 Photocatalytic activity of TiO₂ nanoparticles under UV light⁽²⁷⁾.



TiO₂ has strong photocatalytic activity depend on surface area, crystallinity and crystal form⁽²⁸⁾. Bulk TiO₂ showed low surface area and low photocatalytic activity. Therefore, TiO₂ nanoparticles is required for high photocatalytic activity because it shows high surface area. Moreover, different crystal structure of TiO₂ provided different photocatalytic activity under UV light. When considering pure phase of TiO₂ between anatase and rutile phase, anatase phase shows higher photocatalytic activity than rutile phase because anatase phase presents indirect band gap structure and then, anatase phase shows more life time of electron hole pair between conduction band and valance band. Moreover, anatase show average effective mass of photogenerated electron and hole smaller than that of rutile and brookite phase. This indicates that electron in anatase phase can rapidly migrate to the surface of TiO₂ and occur photocatalytic activity faster than rutile and brookite phase. Then, anatase shows low recombination of electron hole pair than rutile phase⁽²⁹⁾. Some research report there are mixture of anatase and rutile phase provide higher photocatalytic activity than single phase because electron of conduction band of anatase phase can

transfer to conduction band of rutile phase. These reduce recombination of electron hole pairs and then, the mixed phase show higher photocatalytic activity than pure phase⁽³⁰⁾.

2.2.2 Modified TiO₂ for visible light

However, TiO₂ is a semiconductor that it requires UV light (100-400 nm) to show photocatalytic activity for antibacterial activity. Therefore, many researches are required to improve the limitation of TiO₂ to be effective in visible light (400-700 nm). There are several ways to modified TiO₂ nanoparticles show photocatalytic activity under visible light. For instance, TiO₂ was synthesized with defect structure by using hydrogen (H₂) treatment with heating from 300°C to 450°C. Then, surface of the crystal structure of TiO₂ occurred lack oxygen atoms. Then, electron from hydrogen atom can reduce Ti⁴⁺ to Ti³⁺ which affects decreasing of energy band gap of TiO₂ and then, visible light can excite TiO₂ for photocatalytic activity⁽³¹⁾. Moreover, TiO₂ was also improved efficiency photocatalytic activity under visible light by doping with non-metal such as N, B, and S or metal such as Ag, Cr and Pt into TiO₂ nanoparticles for photocatalytic activity extent to visible light⁽³²⁾. But, doping with non-metal showed fast recombination of electron-hole pair because it showed reducing of energy band gap in TiO₂. Then, metal doped in TiO₂ is suitable for high photocatalytic activity of TiO₂ under visible light because metal act as electron sink which showed low recombination of electron hole pairs. Ag metal nanoparticle is promising for high antibacterial activity because it showed strong antibacterial activity with low concentration. From previous research of Hajipour *et al.* (2012) reported Ag NPs act as antibacterial agent and can oxidized from Ag⁰ to Ag⁺ ions for antibacterial⁽³³⁾. Because Ag⁺ can good adhesion with the cell wall and penetrate through membrane of cell bacteria. Then, Ag⁺ can destroy mitochondria, DNA and nuclei which they are importance component of bacteria and Ag⁺ can generate reactive oxygen species (ROS) to kill bacteria which causing bacteria death as shown in Figure 2.3

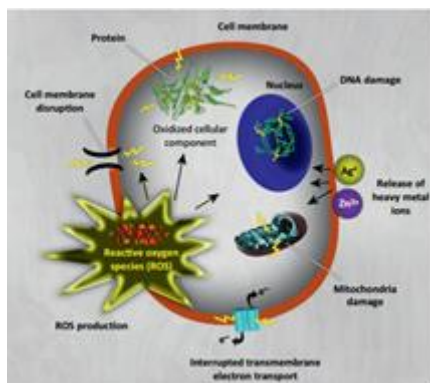


Figure 2.3 Mechanism antibacterial activity of Ag nanoparticles⁽³³⁾.

Therefore, some research studied the optimal amount silver doped titanium dioxide (Ag-TiO_2) in order to improve for high photocatalytic and antibacterial activity under visible light. Liu et al. (2012) improved photocatalytic activity of TiO_2 by doped and deposited of Ag NPs⁽³⁴⁾. They showed diagrams and mechanism of Ag modified TiO_2 as shown in Figure 2.4. It was observed that photocatalytic activity of Ag doped TiO_2 presented lower of energy band gap when compared with TiO_2 . Deposited of Ag in TiO_2 showed Ag act as electron trap at surface of TiO_2 . Therefore, photocatalytic activity of Ag modified TiO_2 showed higher than TiO_2 under visible light. Dunnill et al. (2011) studied Ag doped TiO_2 film for antibacterial activity of *E. coli* under hospital lighting condition⁽³⁵⁾. They were found that Ag doped TiO_2 showed high antibacterial activity than pure TiO_2 under visible light. Tobaldi *et al.* (2014) studied Ag modified nano-titania for high photocatalytic activity and antibacterial agent⁽³⁶⁾. They found that the optimal condition of 2% by mole Ag- TiO_2 showed the highest photocatalytic activity and showed efficiency antibacterial activity of *E. coli* (gram-negative) more than *MRSA* (gram-positive) under UV and visible light.

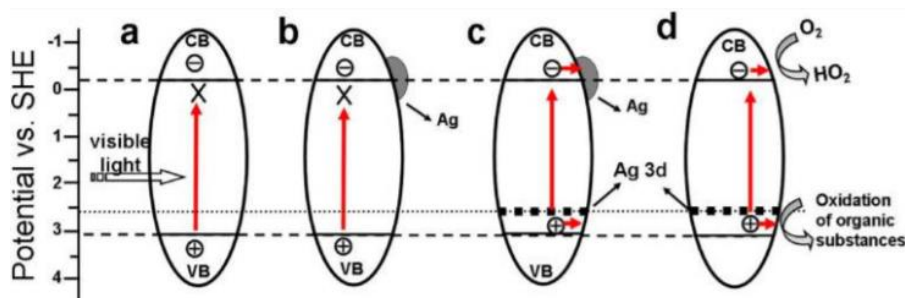


Figure 2.4 Schematic diagrams show photocatalytic activity of Ag modified TiO₂ a) TiO₂ b) Ag deposited c) Ag doped and deposited and d) Ag doped TiO₂ under visible light⁽³⁴⁾.

Mechanism for antibacterial activity of Ag-TiO₂ nanoparticles can explain by photocatalytic activity of TiO₂ under light irradiation and ion releases of Ag⁺ ion. TiO₂ showed photocatalytic activity to generate electron and hole pairs. Hole in valence band can react with water in air or moisture to generate hydroxyl radical (OH[•]). On the other hand, electron in conduction band at surface of TiO₂ can transfer to Ag metal and generate Ag⁻ anion. Ag⁻ anion can react with oxygen to generate superoxide anion (O₂⁻). Free radical of hydroxyl radical and superoxide anion can penetrate of cell membrane and cause the cell bacteria death. The reaction equation can be written as follows⁽³⁷⁾.



2.3 Method for synthesis of Ag-TiO₂ NPs

There are many methods for synthesis of Ag-TiO₂ nanoparticles such as hydrothermal⁽³⁸⁾, photodeposition⁽³⁹⁾ and sol-gel methods⁽⁴⁰⁾. Zhang *et al.* (2017) synthesized of Ag-TiO₂ nanoparticles via hydrothermal method using Teflon-lined

stainless autoclave and used heated 180°C for 24 h⁽³⁸⁾. Hydrothermal method used complex equipment and synthesized Ag-TiO₂ powder under high temperature and pressure in autoclave. Behnajady *et al.* (2008) studied synthesis of Ag-TiO₂ powder via photodeposition for enhancement photocatalytic activity⁽³⁹⁾. However, this method provided easy to synthesized, they found that Ag-TiO₂ powder showed non uniform and irregular shape of Ag-TiO₂ particle. Therefore, sol-gel method is promising for synthesis of Ag-TiO₂ nanoparticles because it present high purity, easily to control size and shape of particles and synthesis under atmosphere at room temperature⁽⁴⁰⁾.

2.3.1 Sol-gel method

Sol-gel method changes the state of the liquid formation in form “Sol” to gel formation. Sol is a colloidal solution suspension of small solid particles and gel is a solid jelly-like material as shown in Figure 2.5.

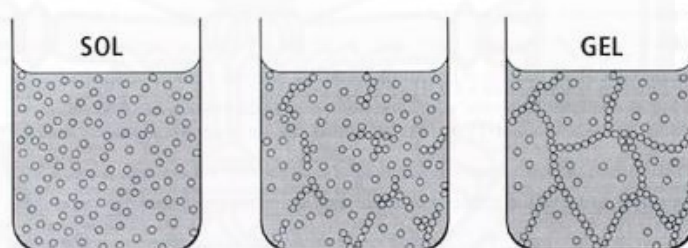
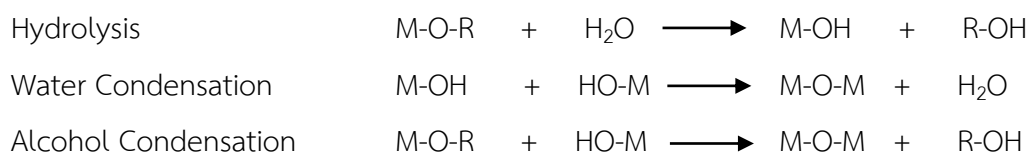


Figure 2.5 The transformation form sol to gel formation in sol-gel method.

(Ref: http://www.uk-finishing.org.uk/N-COAT70/sol_gel.htm)

There are three reactions in sol-gel methods, metal alkoxide react with water in hydrolysis reaction to generate metal hydroxide. Metal hydroxide and metal alkoxide present water and alcohol as a byproduct in condensation reaction and generate metal oxide polymer. The reaction equation can be written as follows⁽⁴¹⁾:



When, M represent a metal such as Si, Zr, Al, Ti, Ce and OR represent alkoxy group such as OC_3H_7 , OCH_3 . Preparation for doping TiO_2 in sol-gel method is shown in Figure 2.6. There are 4 step in sol-gel method compose of mixing, drying, pulverization and calcination.

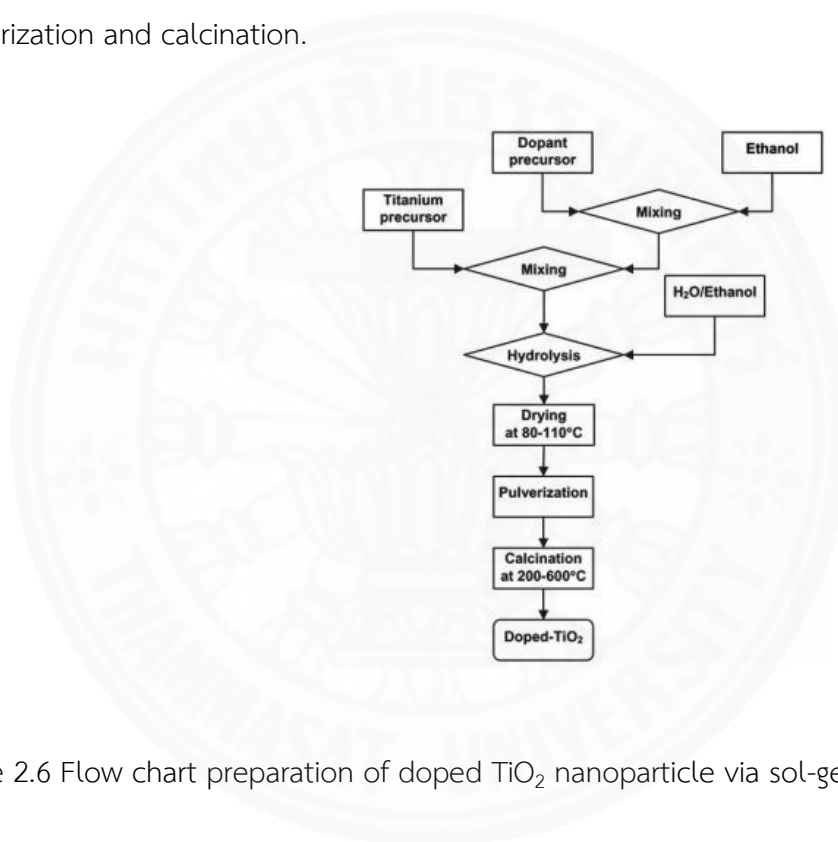


Figure 2.6 Flow chart preparation of doped TiO_2 nanoparticle via sol-gel method⁽³²⁾.

The mixing step is an importance part of sol-gel method for control morphology and particle size of TiO_2 NPs. Behnajady *et al.* (2011) investigated the effect of sol-gel synthesis of TiO_2 nanoparticles on structure and photocatalytic activity⁽⁴²⁾. They found that precursor, solvent and solvent molar percent were parameter to control crystallite size and particle size of TiO_2 NPs for high photocatalytic activity. Especially, the effect of solvent type is an importance for control morphology of particle size and photocatalytic activity. They were observed that using methanol as a solvent with molar ratio of 1:1 (TTIP: methanol) showed the smallest crystallite

size and higher photocatalytic activity than ethanol and isopropanol. *Park et al.* (1997) studied effect of solvent on TiO₂ particles⁽⁴³⁾. They found that synthesis of TiO₂ using n-propanol as a solvent provided small uniform on particle size and less agglomeration of TiO₂ particles. Therefore, in this study is interesting study the effect of alcohol type on synthesis of TiO₂ NPs for high photocatalytic activity. Moreover, pulverization or grinding step is the role important for decreasing particle size of nanoparticles to show high surface area. Then, nanoparticles show high photocatalytic activity. *Mogal et al.* (2014) synthesized of Ag-TiO₂ nanoparticles via sol-gel method and characterized on structure powder⁽⁴⁰⁾. They found that Ag-TiO₂ powder presented aggregation of particle when using dry grinding process. *Serrano et al.* (2009) studied prepared of Ag-TiO₂ powder by modified sol-gel method⁽⁴⁴⁾. It was observed that Ag-TiO₂ powder showed aggregation of small spherical particles. Dry ball milling in sol-gel method preferred aggregation of particle size and then, it showed low surface area for photocatalytic activity. *Jung et al.* (2015) studied physicochemical properties of boron particles between dry and wet ball milling method⁽¹⁴⁾. They found that however, dry ball milling showed small particle size but, wet ball milling presented lower aggregation and narrow size distribution of particles than dry ball milling as shown in Figure 2.7. Therefore, there are mixture of dry and wet ball milling is suitable for synthesis of Ag-TiO₂ nanoparticle for large surface area and narrow size distribution.

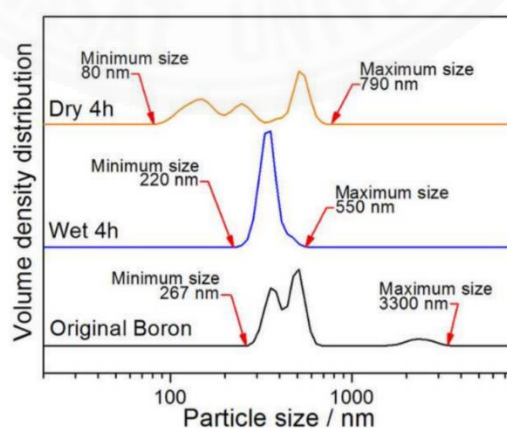


Figure 2.7 Particle size and size distribution of original boron, after wet ball milling and after dry ball milling for 4 h⁽¹⁴⁾.

Phase of Ag-TiO₂ NPs show importance role for high photocatalytic activity. The mixture of anatase and rutile phases show higher photocatalytic activity than single phase. Calcination temperature in sol-gel method is parameter control phase transition in synthesis of Ag-TiO₂ NPs. Mosquera *et al.* (2016) studied the effect of calcination temperature on Ag-TiO₂ thin film⁽⁴⁵⁾. They found that calcination temperature at 400°C of Ag-TiO₂ thin film presented only anatase phase and calcination temperature was increased from 400°C to 800°C showed the mixture of anatase and rutile phases. At calcination temperature above 1,000°C showed only rutile phase. Serrano *et al.* (2009) studied synthesis of Ag-TiO₂ NPs and phase transition⁽⁴⁴⁾. They found that calcination temperature below 450°C, it was observed that only pure anatase and increasing calcination temperature to 600°C showed the mixture anatase and rutile phases. At calcination temperature 750°C presented only rutile phase of Ag-TiO₂ NPs.

2.4 Method for coating of Ag-TiO₂ NPs on air filter

There are many methods coating solution on substrates for thin film for instance dip and spin coating⁽⁴⁶⁾.

2.4.1 Dip and spin coating

Dip coating is continuous process composed of five stages: immersion, start-up, deposition and drainage and evaporation, respectively as shown in Figure 2.8. Spin coating is batch process divided into four stages: deposition, spin-up, spin-off and evaporation as shown in Figure 2.9. Spin coating used less solution for coating on substrate for generate thin film. But dip coating show uniformity distribution of solution on substrate more than spin coating. Therefore, dip coating is suitable for dipping solution on substrate. Kment *et al.* (2012) studied thin film of TiO₂ solution from Raman spectroscopy⁽⁴⁶⁾. They found that the dip-coated showed smooth and uniformity thin film more than spin coated.

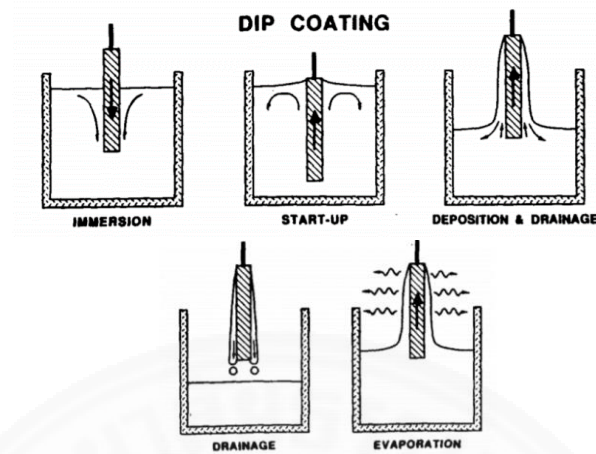


Figure 2.8 Stages of dip coating process⁽⁴⁷⁾

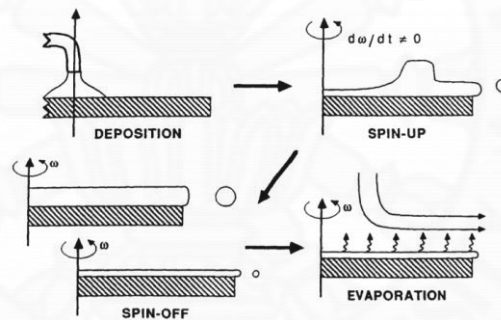


Figure 2.9 Stages of spin coating process⁽⁴⁷⁾

The film thickness in dip coating process is shown equation as follow:

$$h_0 = 0.944 \left(\frac{\eta u_0^3}{\sigma^6 \rho g^2} \right)^{\frac{2}{3}}$$

Where h_0 is the limiting film thickness (cm), u_0 is dipping speed (cm/s), η is solution viscosity (mPa·s), ρ is solution density (g/cm^3), σ is solution surface tension mN/m^{-1} and g is the constant of gravity (cm/s^2)⁽⁴⁸⁾. Parameter control dip coating for distribution of nanoparticles for high uniformity on substrate are dipping

speed and coating concentration⁽¹⁶⁾. Moreover, binder is an importance role for good adhesion between nanoparticles and substrate. In this study are interesting polypropylene glycol molecular weight 4000 (PPG-4000) as bider for dip cotaing on air filter. Because PPG- 4000 showed good stability and adhesion on substrate⁽⁴⁹⁾. Limmongkon *et al.* (2013) studied the effect of binder between polyethylene glycol (PEG) 4000 and Duramax D3005 which coated with TiO₂ solution on air filter⁽⁷⁾. They found that using PEG 4000 showed more adhesive substance than Duramax D3005. Moreover, Touam *et al.* (2014) studied effect speed of dip-coating on structure of TiO₂ thin film. They found that increasing of dip-coating speed from 1 to 3 cm/min, the thickness thin film of TiO₂ was increased with larger grain size of TiO₂⁽¹⁷⁾. Sarah *et al.* (2018) studied the effect of coating concentration of TiO₂ solution from 0.01-0.2 M on substrate⁽⁵⁰⁾. They found that coating concentration TiO₂ solution of 0.01 M showed more uniformity and homogeneous of particles on glass substrate than high concentration of solution. In this study are interesting effect dipping speed, binder concentration and coating concentration souldion for uniformity distribution of material on air filter and show high antibacterial activity.

CHAPTER 3

RESEARCH METHODOLOGY

3.1 Synthesis of TiO₂ nanoparticles

3.1.1 Materials

Titaniumtetra isopropoxide 97%wt-TTIP was used as a precursor and was purchased from Sigma Aldrich. P25 TiO₂ commercial as a TiO₂ reference (75% anatase and 25% rutile) was purchased from ACROS. All solvent such as 99.99%wt-methanol (MeOH), 99.99%wt-ethanol (EtOH) and 99.95%wt-isopropanol (IPA) were purchased from Carlo Erba. 65%wt-nitric acid (HNO₃) was purchased from Carlo Erba as a catalyst. Deionized water (DI) was used all in experiment.

3.1.2 Effect of alcohol types on TiO₂ powder synthesis with DWBMS method

TiO₂ was synthesized which was modified from the previous report of Bahadur *et al*⁽⁵¹⁾. The substitution reaction of TTIP with varied types of alcohol types i.e. MeOH, EtOH and IPA were carried out with a molar ratio of TTIP:alcohol (1:15). Then the hydrolysis reaction of titanium alkoxide was carried out by adding DI water 4 times of molar ratio of TTIP. The solution pH was adjusted to 1.5 by adding 2 ml of HNO₃. The white colloid of TiO₂ sol was observed. The TiO₂ gel mixture was washed with DI water and centrifuged by 10,000 rpm for 15 min. The white jelly-like gel were dried in oven (Mettler UN55) at 110°C for 24 h to remove organic solvents. The yellow-light xerogel was dry ground by 10 mm-ball milling at 300 rpm for 20 min and consequently wet ground by 2 mm-ball milling at 500 rpm for 3 h in IPA solution. The TiO₂ solution was then dried in oven at 110°C for 24 h. Ground powder was calcined in furnace (Nabertherm P330) at 400°C for 4 h with a heating rate of 5°C/min. The nomenclatures of TiO₂ synthesized by MeOH, EtOH and IPA were TiO₂-M, TiO₂-E and TiO₂-P, respectively as shown in Figure 3.1.

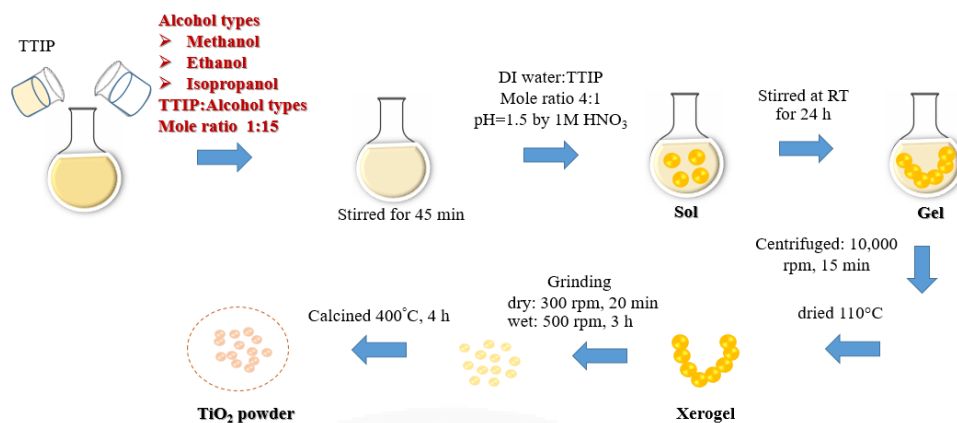


Figure 3.1 Synthesis of TiO₂ NPs with various alcohol types via DWBMS method.

3.1.3 Effect of calcination temperatures on TiO₂ powder synthesis with DWBMS method

The experiments were performed under similar conditions with different alcohol types in 3.1.2 except the calcination temperature condition. The synthesis TiO₂ particles were calcined at different temperatures for 300, 400, 500, 600, 650, 700 and 800°C for 4 h. The nomenclature of TiO₂ synthesized by 300, 400, 500, 600, 650, 700 and 800°C was TiO₂-300, TiO₂-400, TiO₂-500, TiO₂-600, TiO₂-650, TiO₂-700 and TiO₂-800, respectively.

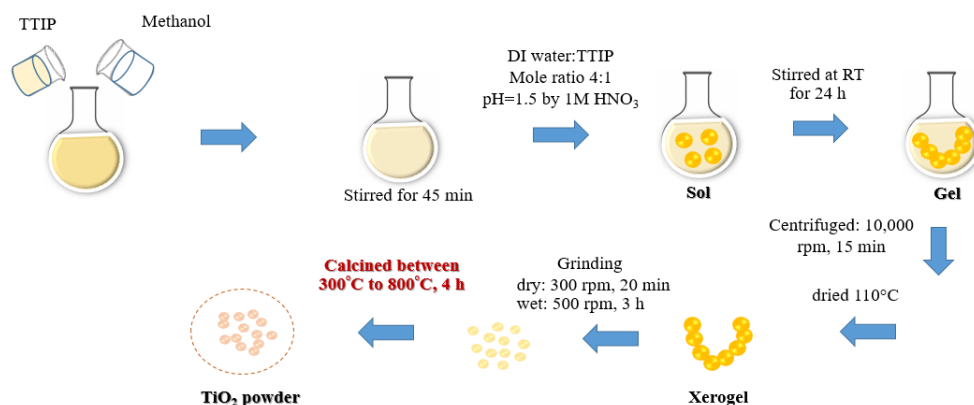


Figure 3.2 Synthesis of TiO_2 NPs with various calcination temperatures via DWBMS method.

3.2 Synthesis of Ag- TiO_2 nanoparticle

3.2.1 Materials

Titaniumtetra isopropoxide 97%wt-TTIP was used as a precursor and was purchased from Sigma Aldrich. P25 TiO_2 commercial as a TiO_2 reference was purchased from ACROS. 99.99%wt-methanol (MeOH) as a solvent was purchased from Carlo Erba. 65% wt-citric acid (HNO_3) was purchased from Carlo Erba as a catalyst. Precursor of Ag is 99.99%-wt-silver nitrate (AgNO_3) was purchased from Sigma Aldrich. 99.99%wt-citric acid used as a reducing agent was purchased from Riedel-de Haen. Deionized water (DI) was used all in experiment.

3.2.2 Effect concentrations of Ag NPs on synthesis of Ag- TiO_2 powder with DWBMS method

Ag- TiO_2 was synthesized under similar condition with preparation TiO_2 NPs with effect of alcohol types. Methanol was used as a solvent. The substitution reaction of TTIP with MeOH was carried out with a molar ratio of TTIP:MeOH (1:15). The solution pH was adjusted to 1.5 by adding 2 ml of HNO_3 . The solution was stirred at room temperature for 45 min. 250 ml of aqueous AgNO_3 (1M) and 500 ml of citric acid (1M) solution was prepared in volumetric flask with DI water as stock solution.

AgNO₃ and citric acid were weighed at 42.47 g and 96.06 g, respectively to prepare 1M concentration. Doping Ag into TiO₂ at 3, 5, 6 and 10% mol of TTIP by pipette of 20.25, 33.78, 40.53 and 67.55 ml from stock solution AgNO₃ and then, added citric acid of 40.53, 67.55, 81.06 and 135.11 ml, respectively for doping 3-10% by mole Ag-TiO₂ to reduce Ag⁺ excess. After string for 24 h, the white gel of Ag-TiO₂ was changes to pale yellow gel of Ag-TiO₂ was observed. The Ag-TiO₂ gel mixture was washed with DI water and centrifuged by 10,000 rpm for 15 min. The pale yellow jelly-like gel were dried at 110°C to remove water and organic solvent. The yellow-light xerogel was dry ground by 10 mm-ball milling at 300 rpm for 20 min and consequently wet ground by 2 mm-ball milling at 500 rpm for 3 h in IPA. The Ag-TiO₂ solution was dried in oven at 110°C for 24 h. Fine powders were calcined at 600°C for 4 h with a heating rate of 5°C/min. The nomenclatures of Ag-TiO₂ synthesized by 3, 5, 6 and 10% by mole of Ag to TiO₂ were 3% Ag-TiO₂, 5% Ag-TiO₂, 6% Ag-TiO₂, and 10% Ag-TiO₂, respectively.

3.2.3 Characterization of TiO₂ and Ag-TiO₂ powder

The morphology and particle size distribution of TiO₂ and Ag-TiO₂ powders were studied using Field emission scanning electron microscope (FE-SEM) operated at low voltage of 2 kV and transmission electron microscope (TEM, JEOL JEM-2100) operated at 200kV. Dynamic light scattering (DSL). X-ray diffraction (XRD) patterns were obtained with a Bruker D8 ADVANCE equipped with Cu source (Cu K_α = 0.154 nm, 40 kV, 40 mA). The scattered radiation was detected in the angular range of 10-80° (2 Θ) with a scan rate of 0.02°. To determine the TiO₂ and Ag-TiO₂ crystallite size, Scherrer's equation⁽⁵²⁾ is employed:

$$D = \frac{0.9\lambda}{\beta \cos\theta}$$

where D is the crystallite size (nm), λ is the X-ray wavelength (Cu K_α = 1.54060 Å), β is the full-width at half-maximum intensity, and θ is the diffraction peak angle. The absorption of TiO₂ and Ag-TiO₂ was investigated by Diffuse reflectance spectroscopy (DRS) with the wavelength rang of 200-800 nm (Agilent carry 5000). Surface area, pore volume, and pore diameter were determined by Brunauer-Emmett-

Teller (BET) (NOVA 2000e) and N₂ adsorption-desorption with pretreatment at 200°C for 3h.

3.2.4 Preparation of photocatalytic activity of TiO₂, P25 and Ag-TiO₂ powder

The degradation of methylene blue (MB) under UV radiation was used as a model system to evaluate the photocatalytic performance of TiO₂, P25 and Ag-TiO₂ powder. The photocatalytic reaction was carried out in the in-house photocatalytic chamber. The initial concentration of methylene blue (C₀) was prepared at 5 ppm. 10 mg of TiO₂, P25 and Ag-TiO₂ powder was mixed with 40 ml of methylene blue solution and then stirred in the photocatalytic chamber. The mixture was kept in the dark for 1 h to ensure the saturation of MB on the surface of the catalysts. The UV light intensity was irradiated at around 0.25 mWcm⁻² at wavelength of 351 nm. At the defined time interval every 1 h until 6 h, the concentration of MB in suspension was analyzed using a UV-Vis spectrophotometer (Agilent carry 5000) in the wavelength of 635 nm. The reaction kinetics follows the pseudo-first-order kinetic model⁽⁵³⁾. The equation is as follows:

$$\ln \left(\frac{C}{C_0} \right) = -k_{app}t$$

where t is the irradiation time, k_{app} is the apparent rate constant (min⁻¹), C is the concentration of the MB and C₀ is an initial MB concentration.

3.2.5 Preparation of antibacterial activity of TiO₂, P25 and Ag-TiO₂ powder

The minimum inhibitory concentration (MIC) value is the lowest concentration of material in aqueous solution that can inhibit the visual growth of bacteria after 24 h. The minimum bactericidal concentration (MBC) value is the lowest concentration of an antibacterial agent required to kill bacteria. MBC can be determined after MIC test.

The MIC of TiO₂, P25 and Ag-TiO₂ with different concentrations was estimated by using *Staphylococcus aureus* (*S. aureus*) 8739 as a gram positive and

Escherichia coli (*E. coli*) 6538P as a gram negative bacteria. Preparation stock solution of *E. Coli* and *S. aureus* number of colony is 10^5 CFU/ml. Preparation of stock solution of TiO_2 , P25 and Ag- TiO_2 , 10 mg of TiO_2 , P25 and 3-10% by mole Ag- TiO_2 dissolved in 1 ml of 20% Dimethyl sulfoxide (DMSO) solution. Pipette 90 μl of TiO_2 , P25 and 3-10% by mole Ag- TiO_2 was dropped into 96 well and mixed with Mueller Hinton Broth (MHB) to made a serial dilution concentration. The plates were incubated under dark and UV light in photocatalytic chamber under $35\pm 2^\circ\text{C}$, 95% relative humidity for 24 h. MBC was determined after know value of MIC. MBC was investigated by spread MIC value and concentration more than MIC on agar plate and incubated plates at $37\pm 2^\circ\text{C}$ for 24 h. When the plate was incubated 24 h, the plate was count the number of colony.

3.3 Coating Ag- TiO_2 NPs on air filter for self-cleaning and antibacterial activity

3.3.1 Materials

A fine air filter with the class F9 from Camfil (Stockholm, Sweden) was cut as a circular shape with a diameter of 4.8 ± 0.01 cm. Commercial P25 TiO_2 (Degussa P25) powders were purchased from ACROS. Polypropylene glycol (PPG) with an average molecular weight of 4,000 (>95% purity) used as a binder was purchased from ACROS. 99.95% wt-isopropanol (IPA) used as a solvent was purchased from Carlo Erba. 100% wt-Oleic acid was purchased from PanReac AppliChem. The *Escherichia coli* (*E. Coil*) ATCC 8739 was used as a bacterial model strain for the gram negative bacteria. Tryptic Soy Agar (TSA) culture and Tryptic Soy Broth (TSB) medium were bought from Difco (USA). 0.85% Sodium chloride (NaCl) as a sterile saline solution and deionized (DI) water were used as a solvent.

3.3.2 Preparation dip coating with of dipping speed of P25 NPs on air filter

9%v/v PPG-4000 was prepared by adding 9 ml of PPG-4000 into 100 ml of IPA solution. 10% P25 was prepared by weighing 8 g of P25 NPs dissolve in 80 ml of IPA. Weighing air filter F9 before dipping followed by dip-coated air filter by 9% v/v PPG-4000 with 0.500 mm/s. The air filter was dried at room temperature for 20 min before the air filter was coated with various dipping speed 0.167, 0.250, and 0.500 mm/s and 1.000 mm/s respectively. The air filter was dried at room temperature for 30 min consequently dried in oven (Memmert) at 110°C for 1 h.

3.3.3 Preparation dip coating with of IPA, PPG-4000 and P25 on air filter

10%v/v PPG-4000 was prepared by adding 10 ml of PPG-4000 into 90 ml of IPA solution. 10%w/v P25 was prepared by weighing 8 g of P25 NPs dissolve in 80 ml of IPA. Weighing air filter F9 before dipping followed by dip-coated air filter with 10%v/v PPG-4000, 10%w/v P25, IPA solution and 10%v/v PPG-4000 and 10%w/v P25 on air filter with dipping speed of 0.500 mm/s. The air filter F9 was weighted after dipping with each solution. The air filter was dried at room temperature for 30 min and dried in oven (Memmert) at 110°C for 1 h.

3.3.4 Preparation dip coating with of concentration of PPG-4000 NPs on air filter

10%v/v of PPG-4000 was prepared as a stock solution by weighting 10 ml of PPG-4000 dissolve in 490 ml of IPA solution. Preparation concentration of PPG-4000 of 0.1%, 1.0% and 5.0% v/v was pipetted of 2.5, 25 and 125 ml from 10% v/v PPG-4000 stock solution. 10%w/v P25 was prepared from 8 g of P25 NPs dissolved in 80 ml of IPA solution. The air filter was coated with different concentration of PPG-4000 from 0.1-10.0%v/v with dipping speed of 0.500 mm/s and dried at room temperature for 20 min. The air filter was coated with 10%w/v P25 with speed of 0.500 mm/s and dried at room temperature for 30 min. The air filter was remove organic solvent by dried in oven at 110°C for 1 h.

3.3.5 Preparation dip coating with various concentration of P25 NPs on air filter

Preparation solution for dip coating with different concentrations of P25 NPs from 0.1- 10.0% w/v. Preparation concentration of 1% v/v PPG by 1 ml of PPG-4000 dissolved in 99 ml of IPA solution. Concentrations of P25 from 0.1%, 1.0%, 5.0% and 10.0% w/v preparation from 0.1, 1.0, 5.0 and 10.0 g of P25 dissolved in 100 ml of IPA. Air filters (F9) were coated with 1% v/v PPG-4000 for the first and then, followed by 0.1%, 1.0%, 5.0% and 10.0% w/v concentration of P25 respectively. By dip coating velocity of speed 0.500 mm/s. After dip coating the air filters were dried at room temperature for 30 min and dried at 110°C for 1 h in oven.

3.3.6 Preparation dip coating with P25, TiO₂ and 5% Ag-TiO₂ NPs on air filter

1% v/v PPG-4000 was prepared by adding 1 ml of PPG-4000 into 99 ml of IPA solution. P25, TiO₂ and 5% Ag-TiO₂ solution were coated with 10% w/v concentration on air filters. 10% w/v of TiO₂ and 5% Ag-TiO₂, weighing 10 g of TiO₂ and 5% Ag-TiO₂ dissolved in 100 ml of IPA solution. 10% w/v P25, weighting 8 g of P25 NPs dissolved in 80 ml of IPA solution. Firstly, F9 air filter was dip-coated with 1% v/v PPG-4000. Then, air filter was dip-coated with 10% w/v of TiO₂, 5% Ag-TiO₂ solution as a top respectively. The air filter was coated with each solution was dried at room temperature for 30 min and dried at 110°C for 1 h in oven.

3.3.7 Preparation dip coating for self-cleaning test on air filters

Air filter was coated with followed by 3.2.4-3.2.6 section, was coated with 100% wt- oleic acid at dipping speed of 10.0 mm/s. The air filter was dried at room temperature for 30 min and dried in oven at 70°C for 40 min. Then, air filter was irradiated with UV light (351 nm wavelength) for 15, 45, 90, 120, 180, 240, 360 and 1440 min in photocatalytic chamber reactor. Contact angle technique was determined self-cleaning followed by International Organization for Standardization (ISO) 27448 of TiO₂, P25 and Ag-TiO₂ NPs on air filter.

3.3.8 Antibacterial activity test of air filters

The American Association of Textile Chemists and Colorists (AATCC) 100 standard method, the quantitative method, modified with International Organization for Standardization (ISO) 27447 was used to study the antibacterial activity of treated air filter sample. The air filters were treated with autoclave at 121°C for 15 mins before antibacterial test. The stock solution of the bacterial culture was prepared in nutrient agar solution with the concentration number of 1×10^5 colony forming units/mL (CFU/mL). 1 mL of bacterial culture solution was poured on circular air filter specimens then the air filters were incubated at $35 \pm 2^\circ\text{C}$ with 95% relative humidity under dark and UV light irradiation. After incubation, the specimens were diluted with 100 ml of DI water in 250 ml laboratory bottle (DURAN). The bottle was shaken vigorously at least for 1 min. Serial dilution of the culture solution was made with 0.85% NaCl sterile solution. A series of the solutions in saline was prepared ranging from 10^1 to 10^6 CFU/mL and the diluted solutions were spread on agar plates by automated spiral plate (Automated 4000). The number of viable bacterial colonies on the agar plate before and after treatment was counted and the results were reported as percentage of bacterial reduction calculated as follows:

$$\text{Bacteria reduction (R) \%} = \frac{A-B}{A} \times 100$$

Where A and B are the number of bacterial colonies recovered from the untreated and the treated samples respectively, after inoculation. %R is the percentage of bacterial colony reduction⁽⁵⁴⁾.

CHAPTER 4

RESULTS AND DISCUSSION

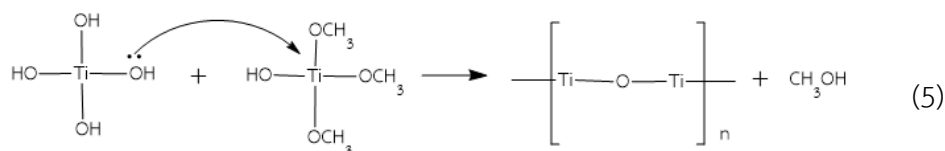
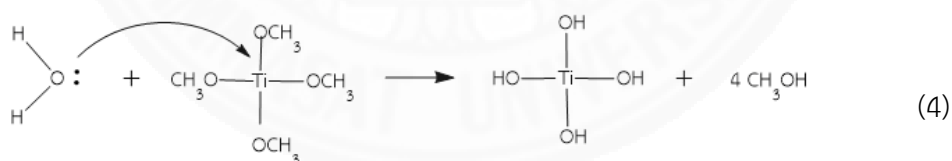
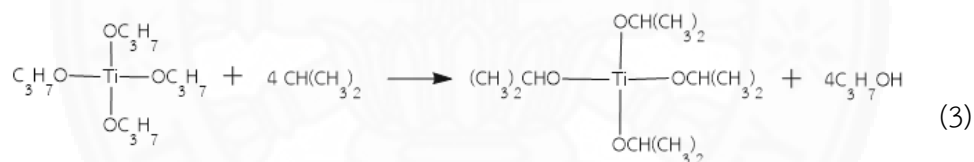
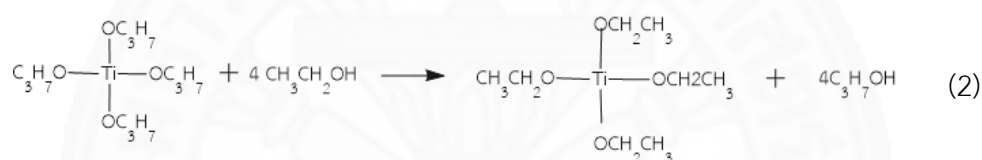
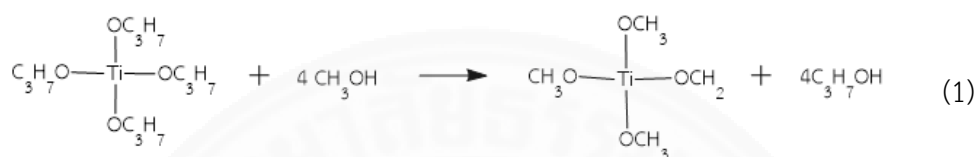
4.1 Synthesis of TiO₂ NPs

In this study need to synthesized TiO₂ NPs with high surface area then, from literature review found the effect of alcohol type is one parameter affect particle size of TiO₂ for high surface area. Therefore, we need to synthesized TiO₂ NPs with various alcohol types namely methanol, ethanol and isopropanol, respectively.

4.1.1 Effect of alcohol type on TiO₂ synthesis.

The morphology and particle size of synthesized TiO₂ with different solvents were investigated by TEM as shown in Figure 4.1. It was observed that there was the aggregation of all spherical TiO₂ particles. The results show that the particle size of TiO₂ synthesized with different solvents including TiO₂-M, TiO₂-E and TiO₂-P were 8.1±2.1, 10.1±2.1 and 10.0±1.9 nm, respectively. Figure 4.2 shows particle size and size distribution from DLS. The results show that the smallest particle size with narrow size distribution was found to be 205.4±18.6 nm for TiO₂-M compared to those of TiO₂-E (254.8±45.3 nm) and TiO₂-P (303.5±13.7 nm) as shown in Table 4.1. Moreover, the degree of aggregation of particles was found to increase with alkyl chain of alcohol. It was observed that the degree of aggregation of particles increased as following TiO₂-P > TiO₂-E > TiO₂-M, respectively which TiO₂-P powder presented the larger particle size than TiO₂-E and TiO₂-M powder⁽⁵⁵⁾. It was observed that particle size from TEM presented the same trend with particle size from DLS. The synthesis of TiO₂ using methanol as a solvent provided the smallest particle size compared to that using ethanol and isopropanol. Because methanol has the smallest molecular size which shows the highest reactivity and lowest steric hindrance compared to those of ethanol and isopropanol. Methanol can quickly react with precursor of TiO₂ (TTIP) leading to

the fastest titanium alkoxide, $\text{Ti}(\text{OCH}_3)_4$ formation in alcoholic permutation reaction mechanism of sol-gel reaction of TiO_2 NPs can be written as shown in equation (1) - (3). This can cause the fastest hydrolysis and condensation reaction leading to the fastest growth of TiO_2 nucleation and provided smallest nanoparticles of TiO_2 ⁽⁵⁶⁾ as shown in equation (4) – (5).



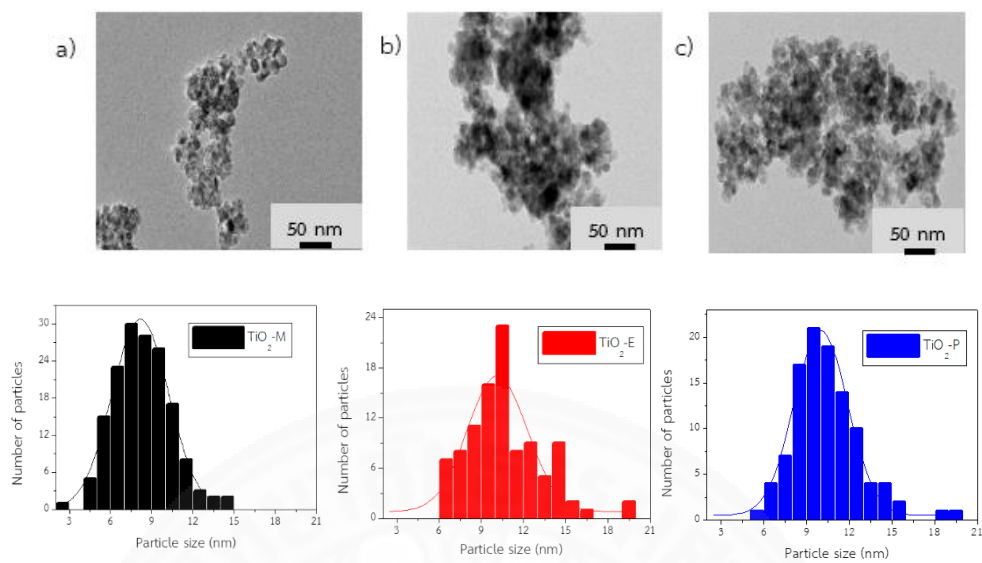


Figure 4.1 TEM images and size distribution of synthesized TiO₂ with different solvents a) TiO₂-M, b) TiO₂-E and c) TiO₂-P.

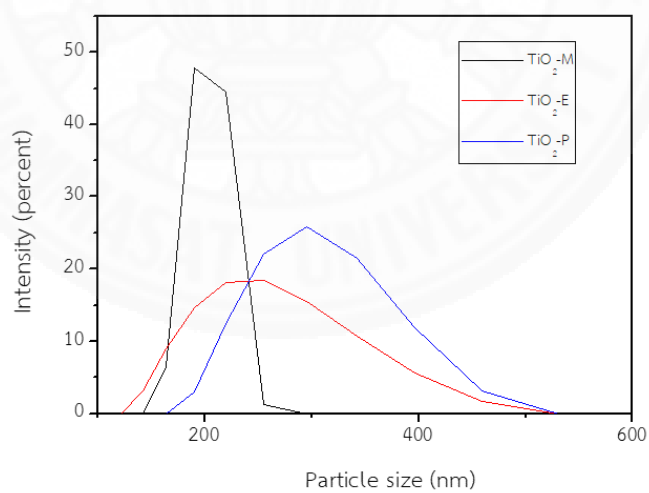


Figure 4.2 Particle size and size distribution of TiO₂ with different solvents from DLS

Table 4.1. Particle size of TiO₂ with different solvents from DLS.

Sample	Particle size (nm)	PDI
TiO ₂ -M	205.4±18.6	0.58±0.05
TiO ₂ -E	254.8±45.3	0.32±0.02
TiO ₂ -P	303.5±13.7	0.50±0.04

The photocatalytic activity of TiO₂ with the degradation of MB under UV light is shown in Figure 4.3. It is assumed as the pseudo-first order reaction of photocatalytic activity where the slope of graph relates to the kinetic constant rate (k) of reaction. The results show that the kinetic constant rate of TiO₂-M, TiO₂-E and TiO₂-P was 13.1×10^{-4} , 9.5×10^{-4} and $8.5 \times 10^{-4} \text{ min}^{-1}$, respectively. TiO₂ synthesized by using methanol as a solvent provided the highest photocatalytic activity with 50% degradation of MB within 10 h. This was in good agreement with the smallest particle size of TiO₂-M obtained from TEM and DLS.

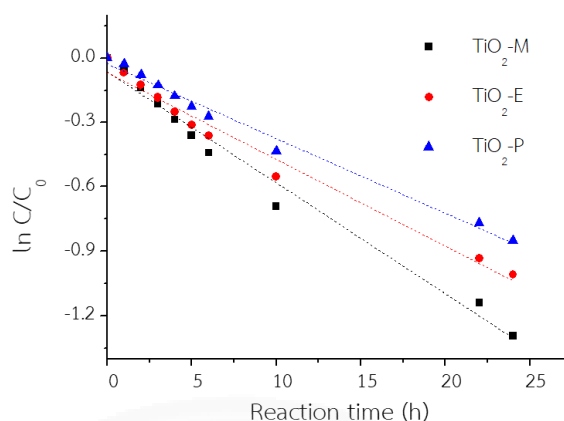


Figure 4.3 Photocatalytic activity with the degradation of MB solution of synthesized TiO₂ particles obtained from different solvents.

4.1.2 Effect of calcination temperature on TiO₂ synthesis

The effect of calcination temperature on phase transition was investigated by XRD. XRD pattern of TiO₂ before and after calcination at different temperatures from 300°C to 800°C is shown in Figure 4.4. Anatase phase is the tetragonal structure and consists of the characteristic peaks at $2\Theta = 25.3, 36.9$ and 37.8° corresponding to (101), (103) and (104) planes, respectively referenced from Joint Committee on Powder Diffraction Standard (JCPDS card no. 21-1272). Rutile phase is also the tetragonal structure and presents diffraction peaks at $2\Theta = 27.4, 36.1, 39.2, 54.3, 56.6, 62.7, 64.0, 69.0$ and 69.8° corresponding to (110), (101), (200), (211), (220), (002), (310), (301) and (112) planes, (JCPDS card no. 21-1276), respectively. Orthorhombic as shown in brookite phase presents diffraction peaks at $2\Theta = 25.3, 36.2$ and 55.2° corresponding to (120), (012) and (241) planes (JCPDS card no. 29-1360). At low calcination temperature from 25°C to 500°C, the broader peaks of XRD patterns were observed which could be attributed to high amorphous structure of TiO₂. With increasing calcination temperature above 600°C, it was found that the crystallinity of

TiO₂ increased due to the sharper and narrower peaks of XRD patterns. The crystallinity increased with increasing calcination temperature since higher ordering of the structure of TiO₂ particles leads to the sharper and narrower X-ray peaks. There was a mixture of anatase and brookite phases when calcination temperature was increased from 25°C to 500°C. The anatase and brookite phases were completely converted to rutile phase at 800°C. The relationship between calcination temperature and percentage of phase content is shown in Figure 4.5. When calcination temperature was increased from 300°C to 600°C, anatase phase increased from 29% to 42% wt. whereas brookite phase decreased from 71% to 28%wt. Rutile phase was obtained at calcination temperature over 500°C. Calcination temperature of TiO₂ powder between 600°C to 700°C, it was observed that anatase phase decreased from 53% to 38%wt. whereas rutile phase increased from 46% to 62%wt. The 100%wt. of rutile phase was found at calcination temperature of 800°C. Therefore, calcination temperature promoted phase transition and crystallinity of TiO₂ powder.

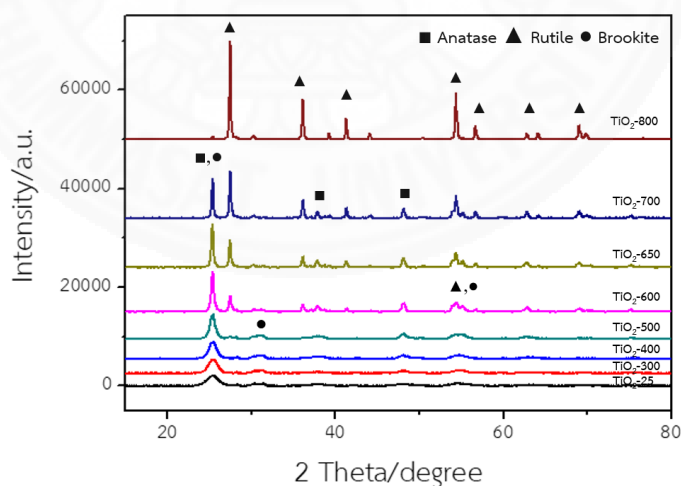


Figure 4.4 XRD patterns of TiO₂ particles before and after calcination at different temperatures.

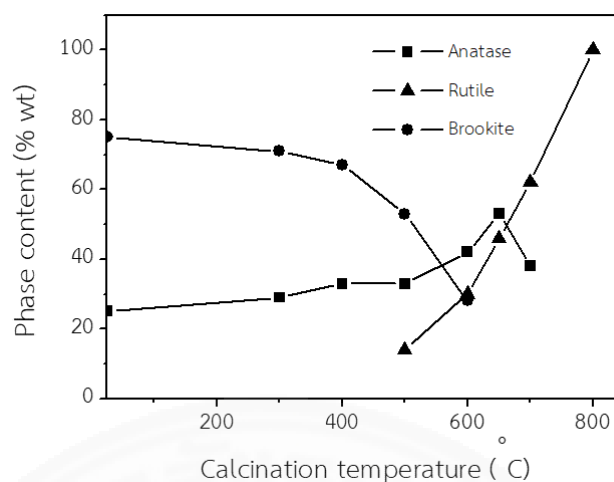


Figure 4.5 Relationship between calcination temperatures from 0°C to 800°C and percentage of phase content (%wt.).

Figure 4.6 shows TEM images of synthesized TiO_2 with different calcination temperatures from 300°C to 800°C. All TiO_2 particles were spherical in shape with the agglomeration and aggregation of crystals. The results show that at low calcination temperature of 300°C showed the mixture of anatase(101) and brookite (111) phase with d-spacing of 3.520 and 3.465 nm was observed for TiO_2 -300. When increasing calcination temperature to 600°C, there were three phases composed of anatase (101), brookite (111) and rutile (110) phases with d-spacing of 3.520, 3.465 and 3.247 nm, respectively. TiO_2 -700 showed mixed anatase (101) and rutile (200) phases with d-spacing of 3.520 and 2.290 nm, respectively. TiO_2 -800 showed dominate rutile phase (110) with d-spacing of 3.247 nm. Moreover, Figure 4.7 shows selected area electron diffraction (SAED) images of TiO_2 particles. The results show that there was a mixture of anatase (211) and brookite (221) phases was observed for TiO_2 -300. When calcination temperature was increased from 300°C to 600°C, there were three phases composed of anatase (316), rutile (111) and brookite (113) phases, respectively.

Selected area electron diffraction patterns showed anatase (220) and rutile (210) phases for TiO₂-700 and showed only rutile (210) phase for TiO₂-800. Therefore, XRD, TEM and SAED images confirmed phase synthesis of TiO₂ powder strongly depend on calcination temperature. Phase transition synthesis of TiO₂ presented from anatase and brookite phases at low calcination temperature to rutile phase at high calcination temperature.



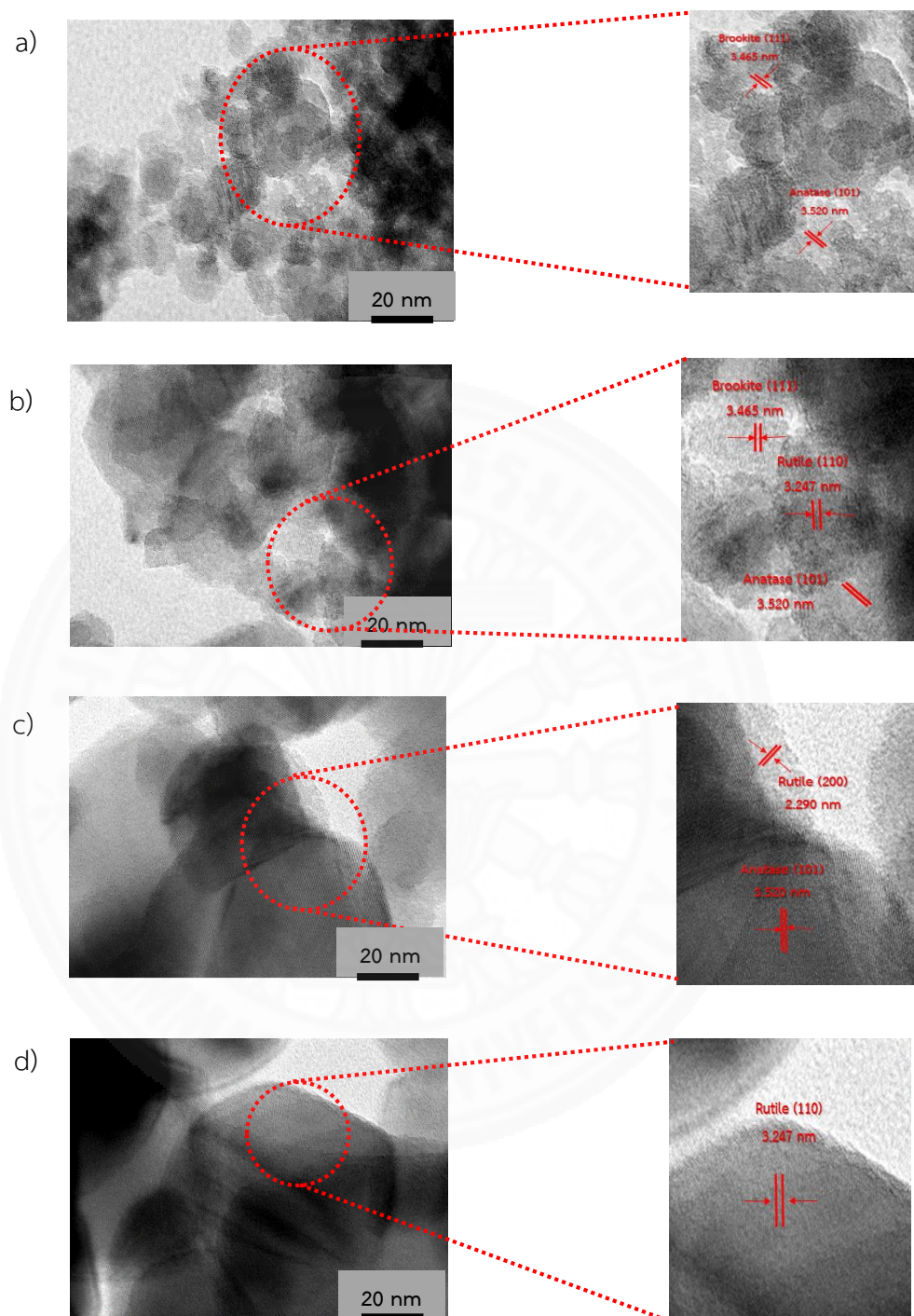


Figure 4.6 TEM images of TiO_2 particles calcined at a) 300°C, b) 600°C, c) 700°C and d) 800°C.

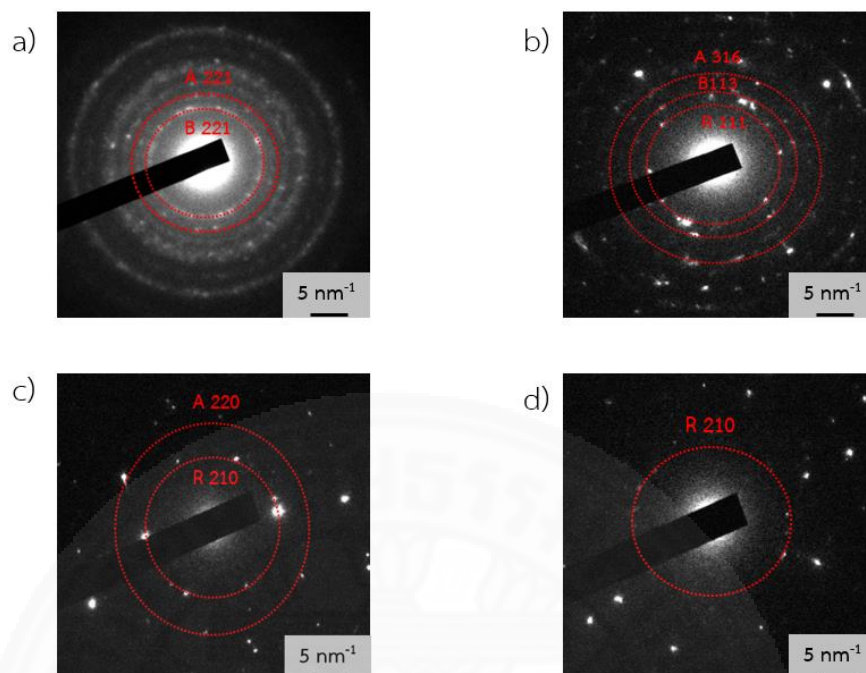


Figure 4.7 Selected area electron diffraction (SAED) images of TiO_2 particle calcined at a) 300°C , b) 600°C , c) 700°C and d) 800°C .

The particle size of TiO_2 with different calcination temperatures was determined from TEM images, the results show that the particle size of TiO_2 -300, TiO_2 -600, TiO_2 -700 and TiO_2 -800 were 8.6 ± 1.7 , 18.7 ± 3.7 , 27.6 ± 8.2 and 81.6 ± 21.6 nm, respectively as shown in Appendix A Figure A1. It was observed that increasing of calcination temperature leads to increasing of particle size and crystallite size of TiO_2 particles. The crystallite size shown in TEM images (Figure 4.7) was in good agreement with that obtained from XRD data as shown in table 4.2. When the calcination temperature increased from 300°C to 800°C , the crystallite size of anatase, rutile and brookite phases was increased. Because calcination temperature presented phase transition from anatase to rutile phase at high temperature. Crystallite size of anatase phase most stable at less than 11 nm, rutile phase showed stable crystallite size more than 35 nm and brookite phase presented stable crystallite size between 11-35 nm,

respectively⁽⁵⁷⁾. When increasing of calcination temperature from 0°C to 600°C, the crystallite size of anatase phase showed stable while crystallite size of brookite phase showed unstable, then anatase phase was increased whereas brookite phase was decreased. When considering calcination temperature from 600 to 800°C crystallite size of rutile phase showed stable while crystallite size of anatase phase showed unstable. Then anatase phase presented transfer to rutile phase and showed completely rutile phase at 800°C. This indicates that crystallite size of TiO₂ powder was increased due to large crystallite size of rutile phase. Therefore, calcination temperature has a strong effect on phase transition, particle size and crystallite size of TiO₂ particles.

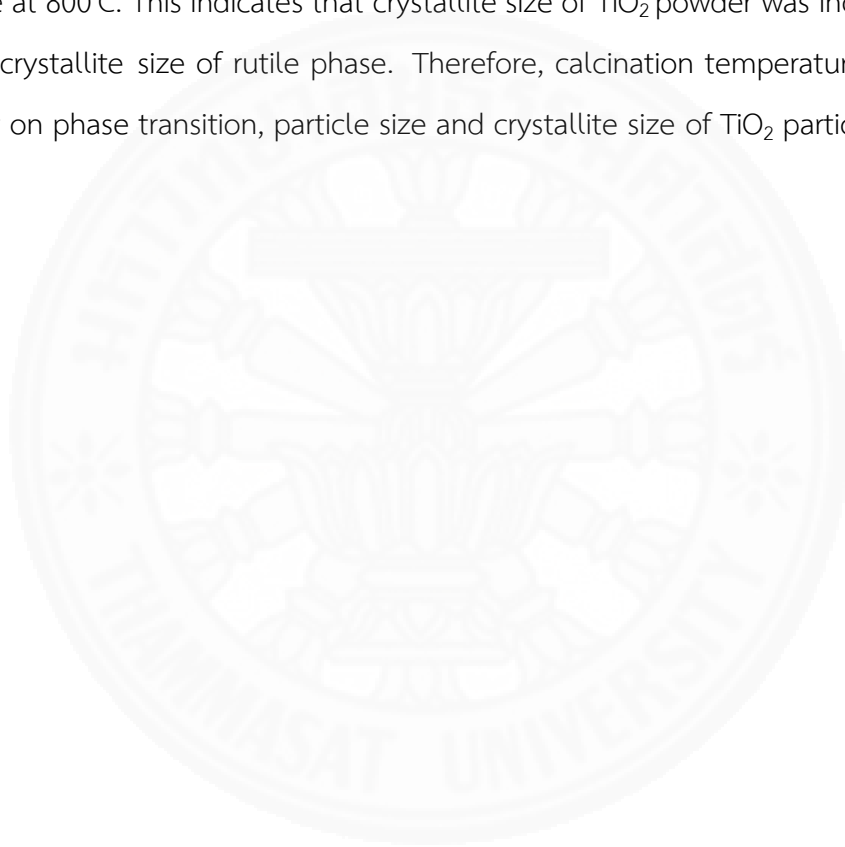


Table 4.2 Crystallite size of synthesized TiO₂ with calcination temperatures from 300°C to 800°C.

Sample	Crystallite size (nm)		
	Anatase	Rutile	Brookite
TiO ₂ before calcination	6	-	3
TiO ₂ -300	7	-	4
TiO ₂ -400	8	-	5
TiO ₂ -500	12	4	5
TiO ₂ -600	20	19	6
TiO ₂ -650	23	25	-
TiO ₂ -700	30	32	-
TiO ₂ -800	-	52	-

Figure 4.8 shows photocatalytic activity of synthesized TiO₂ particles with different calcination temperature from 300°C to 800°C and compared to commercial P25 TiO₂ nanoparticles as a reference. The results show that P25 showed the highest photocatalytic activity with the kinetic constant rate of $3.19 \times 10^{-3} \text{ min}^{-1}$. However, when considering synthesized TiO₂ from TiO₂-300 to TiO₂-800, TiO₂-600 showed the highest photocatalytic activity with the kinetic constant rate of $1.70 \times 10^{-3} \text{ min}^{-1}$ as shown in Figure 4.9. Increasing of calcination temperature from TiO₂-300 to TiO₂-400, we found kinetic constant rate increased from 0.50×10^{-3} to $0.85 \times 10^{-3} \text{ min}^{-1}$.

It was observed that TiO₂-300 and TiO₂-400 showed the mixture of anatase and brookite phases and there was an increase of anatase phase from 29% to 33% wt. The anatase phase provides high photocatalytic activity compared to rutile and brookite phases. Because anatase phase is an indirect band gap structure while rutile and brookite phases appear to be the direct band gap one. Indirect band gap structure shows longer lifetime of electron and hole pair separation than direct band gap due to the lower recombination of e⁻ - h⁺ pairs. Moreover, anatase TiO₂ has longer lifetime of charge carriers than rutile TiO₂ and brookite TiO₂⁽²⁹⁾. With increasing calcination temperature from 500°C to 600°C, the kinetic constant rate was increased from 0.96x10⁻³ to 1.70x10⁻³ min⁻¹. This indicates that it was composed of the mixture of three phases including anatase, rutile and brookite phases which showed higher photocatalytic activity than the mixture two phases of anatase and brookite. TiO₂-600 showed higher photocatalytic activity than TiO₂-500 because TiO₂-600 showed more percentage anatase phase (42% wt.) than TiO₂-500 (33% wt.) and showed ratio of anatase to rutile of 42:30 which suitable for reduce recombination of electron and hole pairs. Then, TiO₂-600 showed the highest photocatalytic activity. With increasing calcination temperature from 600°C to 700°C, kinetic constant was decreased from 1.70x10⁻³ to 1.50x10⁻³ min⁻¹. It is interesting to note that even though the anatase phase was increased from 42%wt. (TiO₂-600) to 53%wt. (TiO₂-650), the kinetic constant was decreased from 1.70x10⁻³ to 1.55x10⁻³ min⁻¹. It was noticed that the crystallite size of anatase and rutile was increased as shown in Table 4.2 and this can lead to the lower surface area of TiO₂-650 compared to that of TiO₂-600. It is therefore the dominance of crystallite size for the decrease of photocatalytic activity between TiO₂-600 and TiO₂-700 over the phase dominance. At calcination temperature of 800°C, it shows the lowest kinetic constant of 0.18x10⁻³ min⁻¹ because TiO₂-800 consisted of only rutile phase and had the largest crystallite size of 52 nm. Due to the direct band gap structure of rutile phase, there is the fast recombination of electron-hole pairs leading to the lowest photocatalytic activity of TiO₂-800.

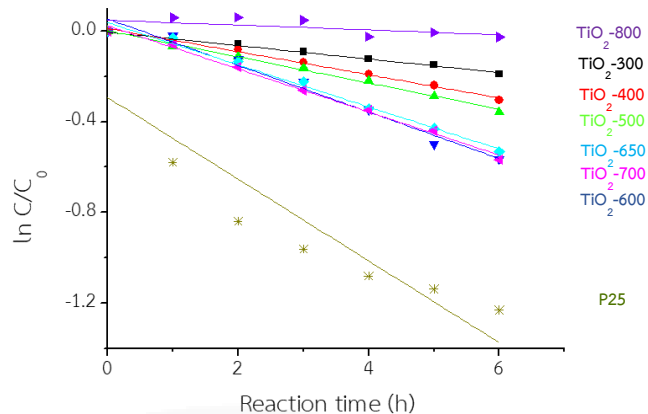


Figure 4. 8 Photocatalytic degradation of MB of synthesized TiO₂ with different calcination temperatures and P25 NPs under UV irradiation.

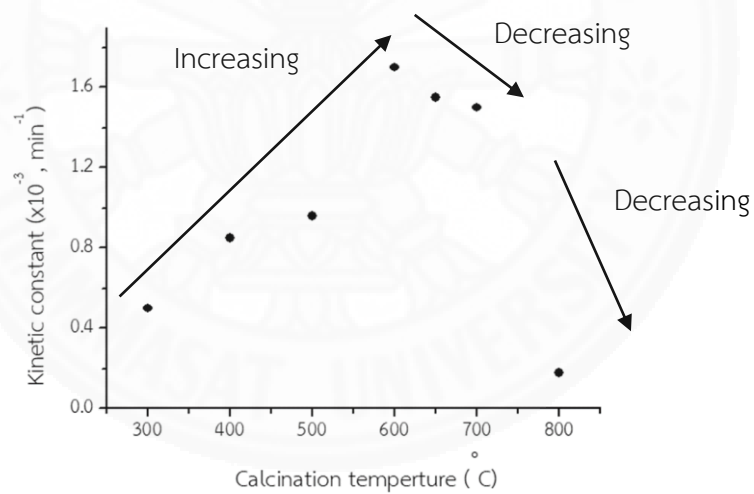


Figure 4.9 Relationship between kinetic constant and calcination temperatures from 300°C to 800°C.

4.2 Synthesis of Ag-TiO₂ powder

4.2.1 Effect of different concentrations of Ag on photocatalytic activity of Ag-TiO₂

Ag-TiO₂ powder presents the mixture of anatase, rutile, brookite phases and silver as shown in XRD patterns in Figure 4.10. Anatase phase is the tetragonal structure and presented the diffraction peaks at $2\Theta = 25.3, 48.0$ and 54.0° corresponding to (101), (200) and (105) planes, respectively (JCPDS card no.21-1272). Tetragonal structure also presented in rutile phase and presented peaks at $2\Theta = 27.4, 36.1, 41.2, 54.3$ and 64.0° belonging to (110), (101), (111), (211) and (310) planes, respectively (JCPDS card no. 21-1276). Orthorhombic structure presented in brookite phase and showed peaks at $2\Theta = 25.3, 30.8, 49.2^\circ$ corresponding to (120), (121) and (132) planes, respectively (JCPDS card no. 29-1360). Ag is cubic structure and consists of the characteristic peaks at $2\Theta = 38.1, 44.3, 64.4$ and 77.4° corresponding to (111), (200), (220) and (311) planes (JCPDS card no. 65-2871). Figure 4.11 presents photocatalytic activity of synthesized TiO₂ and Ag-TiO₂ powder with different concentrations of Ag. P25 TiO₂ commercial (anatase (75% wt.) and rutile (25% wt.) phases) showed the highest photocatalytic activity with kinetic constant rate of $3.19 \times 10^{-3} \text{ min}^{-1}$ (data not shown in graph). However, focus on TiO₂ and Ag-TiO₂ powders with different concentrations of Ag, the results show that Ag-TiO₂ showed higher photocatalytic activity than TiO₂ under UV light. Table 4.3 shows the kinetic constant rate of TiO₂ and Ag-TiO₂ with different concentrations of Ag. It was observed that the highest photocatalytic activity with kinetic constant rate of $2.15 \times 10^{-3} \text{ min}^{-1}$ was achieved at 5% Ag-TiO₂ powder. The kinetic constant rate strongly increased from 1.83×10^{-3} to $2.15 \times 10^{-3} \text{ min}^{-1}$ when concentration of Ag increased from 3% to 5% by mole. This is because the effect concentration of Ag affect crystallite size of Ag-TiO₂ powder. It was observed that when increasing concentration of Ag from 3% to 5% by mole, the crystallite size anatase phase decreased from 26 nm to 16 nm as shown in

Figure 4.12. These crystallite size of anatase phase showed stable and then, anatase phase was increased from 15.9% to 33.0% wt. as shown in Figure 4.13 which anatase phase provided the highest photocatalytic activity compared to rutile and brookite phases. Because anatase phase is an indirect band gap structure leading to the lower recombination of electron and hole pair than rutile and brookite phases which are a direct band gap structure. When considering Ag-TiO₂ powder between 6% and 10% by mole, the kinetic constant rate was decreased from 1.79×10^{-3} to $1.57 \times 10^{-3} \text{ min}^{-1}$ due to reduction of anatase phase from 31.21% to 26.43% wt. Moreover, when increasing concentration of Ag from 3% to 10% by mole, the crystallinity of Ag-TiO₂ particles was decreased from 81.7% to 70.0% as shown in Table 4.4. Because the effect of Ag⁺ ion presented defect in the lattice of TiO₂ and showed weaken oligomer network of TiO₂⁽⁵⁸⁾. Then, crystallinity of Ag-TiO₂ decreased, when increasing concentration of Ag.

Figure 4.14 shows TEM images to further confirm phase of synthesized TiO₂ and Ag-TiO₂ particles. It was found that TiO₂ and Ag-TiO₂ powder were composed of anatase, rutile, and brookite phases and Ag-TiO₂ also showed metallic of silver. For example, TiO₂ powder in Figure 4.15 (a) included anatase (004), rutile (110) and brookite (012) phases with d-spacing of 2.378, 3.247 and 2.476 nm, respectively. 3% Ag-TiO₂ in Figure 4.15 (b) showed anatase (112), rutile (101), brookite (012) and silver (200) and silver (111) with d-spacing of 2.332, 2.487, 2.467, 2.043 and 2.359, respectively. With increasing of Ag concentration, it was observed that an increase of Ag NPs size on the surface of TiO₂. Moreover, from selected area electron diffraction (SAED) images as shown in Figure 4.15, TiO₂ and 3-10% by mole Ag-TiO₂ powders showed polycrystalline structure observed from diffuse diffraction ring images. For instance, TiO₂ consisted of anatase (103), rutile (110) and brookite (113) phases. 3% Ag-TiO₂ was composed of anatase (112), rutile (110), brookite (123) and silver (200). When the concentration of Ag was increased, the diffuse diffraction ring of Ag-TiO₂ particles was decreased. This indicated that the concentration of Ag affects crystallinity of Ag-TiO₂ particles correlating well with XRD data.

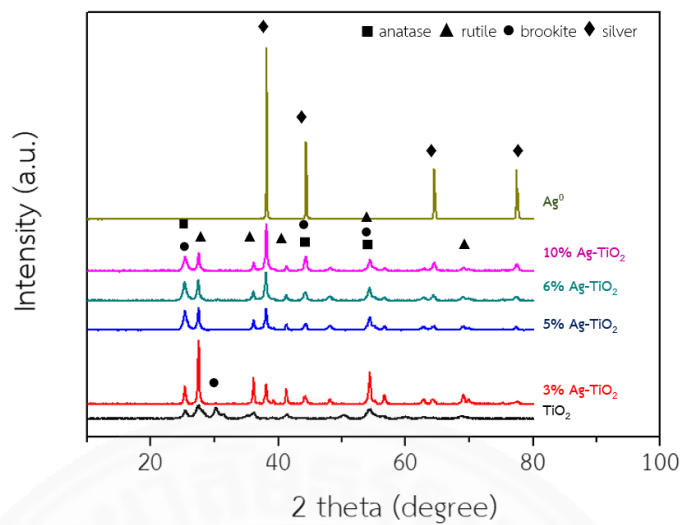


Figure 4.10 XRD patterns of synthesized TiO_2 , Ag and 3-10% by mole Ag-TiO_2 after calcination at 600°C for 4h.

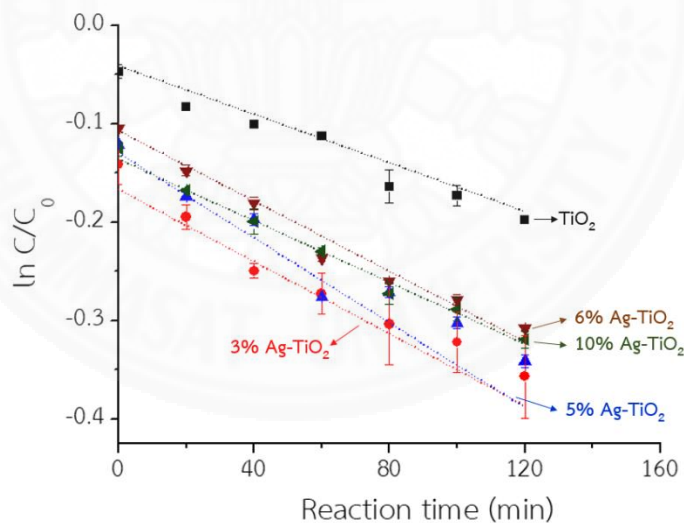
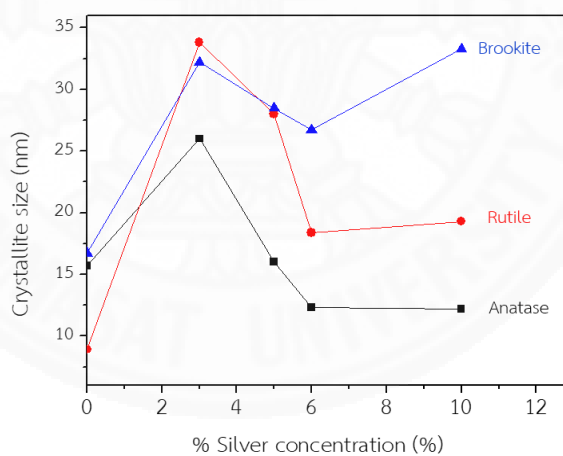


Figure 4.11 Photocatalytic activity of TiO_2 and Ag-TiO_2 with different concentrations of Ag under UV light for 2 h.

Table 4.3 Kinetic constant (k) of TiO₂ and Ag-TiO₂ with different concentrations of Ag.

Sample	Kinetic constant ($\times 10^{-3} \text{ min}^{-1}$)
TiO ₂	1.23
3% Ag-TiO ₂	1.83
5% Ag-TiO ₂	2.15
6% Ag-TiO ₂	1.79
10% Ag-TiO ₂	1.57

Figure 4.12 Crystallite size of anatase, rutile and brookite phases of TiO₂ and Ag-TiO₂ with different concentrations of Ag from 3 to 10% mole.

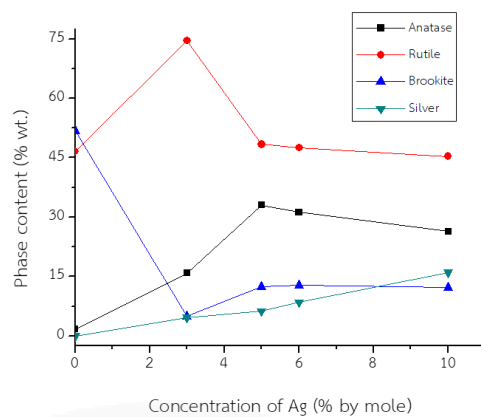


Figure 4.13 Relationship between % phase content of TiO_2 and % Ag concentrations of Ag-TiO_2 .

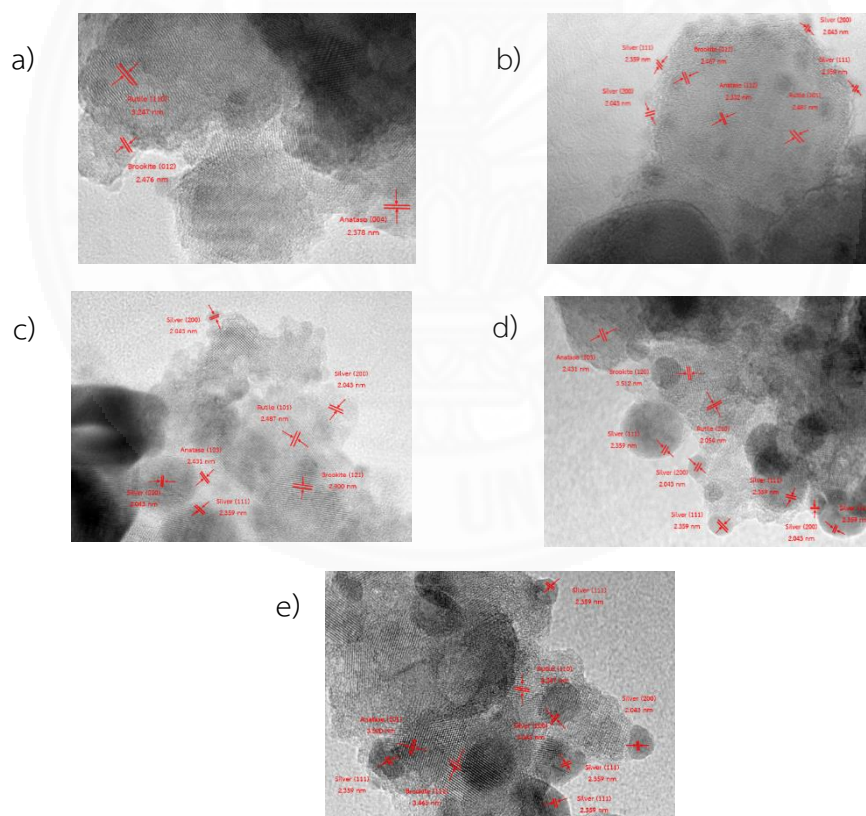


Figure 4.14 TEM images with d-spacing of a) TiO_2 b) 3% Ag-TiO_2 , c) 5% Ag-TiO_2 , d) 6% Ag-TiO_2 and e) 10% Ag-TiO_2 .

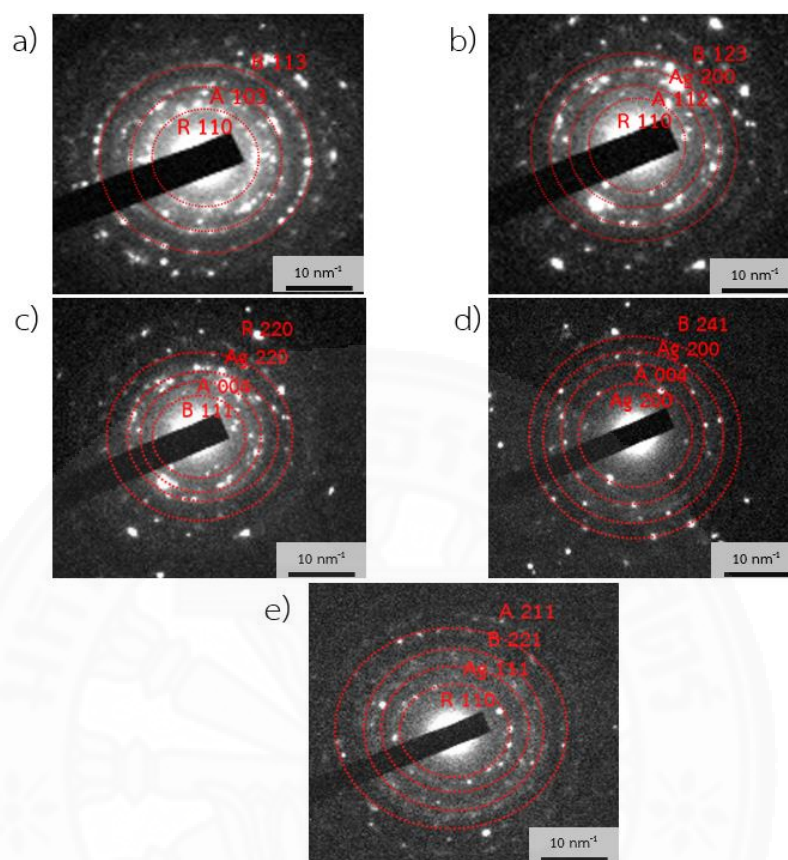


Figure 4.15 Selected area electron diffraction images of a) TiO₂, b) 3% Ag-TiO₂, c) 5% Ag-TiO₂, d) 6% Ag-TiO₂ and e) 10% Ag-TiO₂ particles.

Table 4.4 Percentage of crystallinity and amorphous of synthesized TiO₂, Ag and Ag-TiO₂ with different concentrations of Ag.

Sample	Crystallinity (%)	Amorphous (%)
TiO ₂	61.4	38.6
Ag	87.7	17.3
3% Ag-TiO ₂	81.7	18.3
5% Ag-TiO ₂	75.5	24.5
6% Ag-TiO ₂	72.7	27.3
10% Ag-TiO ₂	70.0	30.0

Besides, the particle size of TiO₂, 3%, 5%, 6% and 10% by mole of Ag-TiO₂ powders was 16.4±5.2, 34.0±9.1, 23.0±7.4, 21.8±7.2 and 28.5±9.6 nm, respectively as shown in Appendix B Figure B.1. It can be seen that the particle size of all Ag-TiO₂ nanoparticles was higher than that of TiO₂ powder. Because the effect concentration of Ag⁺ ion affect phase transition of Ag-TiO₂ powder and then, the particle size of Ag-TiO₂ was increased. With increasing concentration of Ag from 0% to 3% by mole, rutile phase showed the highest phase content of 74.57%wt. and rutile presented the largest crystallite size stable more than 35 nm compared to anatase and brookite phase crystallite size. Then, the particle size of 3% Ag-TiO₂ showed the highest particle size. When considering particle size rang 3% to 10% by mole of Ag-TiO₂ trend to small particle size due to decreasing of rutile phase content from 74.57% to 45.39%wt. which the crystallite size of rutile was decreased. Then, it showed small particle size of Ag-TiO₂ powder. This results were in good agreement with the crystallite

size of TiO_2 and 3-10% by mole Ag- TiO_2 obtained from XRD data as shown in Figure 4.12. The surface area of TiO_2 and Ag- TiO_2 with different concentrations of Ag was investigated by BET. Moreover, pore volume and pore diameter were determined by N_2 adsorption-desorption isotherms with Barrett-Joyner-Halenda (BJH) method as shown in Table 4.5. The results show that Ag- TiO_2 with different concentrations of Ag showed higher specific surface area than TiO_2 except at 3% Ag- TiO_2 . 3% Ag- TiO_2 shows the lowest surface area of $13.97 \text{ m}^2/\text{g}$ which was well correlated to the largest particle size of $34.0 \pm 9.1 \text{ nm}$. 5% Ag- TiO_2 powder provided the highest surface area of $32.12 \text{ m}^2/\text{g}$. This results confirms the highest photocatalytic activity of 5% Ag- TiO_2 as previously mentioned because it presented the highest active site for photocatalytic activity under UV light. When increasing concentration of Ag above 5%, the surface area was decreased to $27.52 \text{ m}^2/\text{g}$ at 6% Ag- TiO_2 and slightly increased to $30.25 \text{ m}^2/\text{g}$ at 10% Ag- TiO_2 . Due to a number of Ag NPs at higher concentrations, the Ag NPs preferred to aggregate and deposited onto the surface of TiO_2 leading to an increase of particle size and low surface area of Ag- TiO_2 powder. This results also support the lowest photocatalytic activity of 6% and 10% by mole Ag- TiO_2 compared to 5% Ag- TiO_2 . The pore volume of all Ag- TiO_2 nanoparticles was lower than that of TiO_2 nanoparticles since some small Ag nanoparticles could be block in the pore volume of TiO_2 powder during the doping step. The pore diameter of TiO_2 and 3-10% by mole Ag- TiO_2 showed in the range of 3-50 nm as shown in Figure D.1 in Appendix D. This indicates that both TiO_2 and Ag- TiO_2 performed mesoporous structure. Figure 4.16 shows the isotherm of TiO_2 and Ag- TiO_2 nanoparticles with different concentrations of Ag from 3% to 10% by mole. The results show that TiO_2 and Ag- TiO_2 powders provided the hysteresis loop as the type V in isotherm corresponding to a capillary condensation phenomena associated with the mesoporous porous structure. The type of hysteresis loop was H3 with a slit shape pore according to IUPAC⁽⁵⁹⁾.

Table 4.5 Surface area, pore volume and pore diameter of TiO₂ and Ag-TiO₂ with different concentrations of Ag measured by BET and N₂ adsorption-desorption isotherm.

Sample	S _{BET} (m ² /g)	PV (cm ³ /g)	PD (nm)
TiO ₂	18.62	0.38	3.42, 20.30
3% Ag-TiO ₂	13.97	0.22	3.22, 50.09
5% Ag-TiO ₂	32.12	0.25	3.70, 27.44
6% Ag-TiO ₂	27.52	0.24	3.67, 27.26
10% Ag-TiO ₂	30.25	0.26	3.69, 27.72

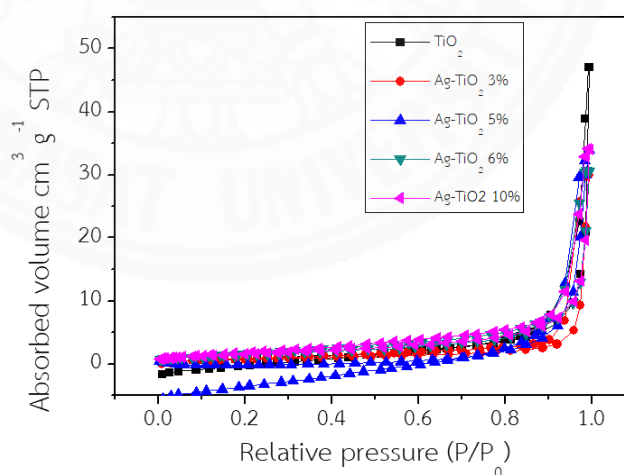


Figure 4.16 Isotherm from N₂ adsorption-desorption of TiO₂ and Ag-TiO₂ nanoparticles with different concentrations of Ag from 3-10% by mole.

To deeper understanding the mechanism why Ag-TiO₂ showed higher photocatalytic activity than TiO₂, it can be attributed to Schottky barrier between Ag and TiO₂. As already discussed above in TEM and SEM-EDS images as shown in Figure 4.14, Figure 4.17-4.18 and Appendix Figure C1-C3, respectively, Ag NPs were deposited onto the surface of TiO₂ as heterojunction. This can lead to the mechanism of Schottky barrier⁽⁶⁰⁾ and the photocatalytic reaction as shown in Figure 4.19. Ag NPs can act as electron sink for electron from conduction band of TiO₂. This can enhance the charge transfer and reduce the recombination of electron-hole pairs leading to an increase of photocatalytic reaction.

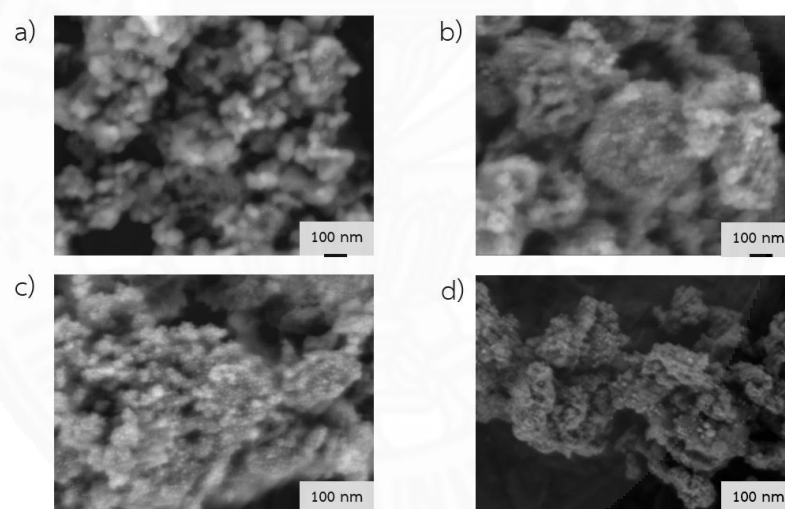


Figure 4.17 Back scattered electron (BSE) images of a) 3% Ag-TiO₂, b) 5% Ag-TiO₂, c) 6% Ag-TiO₂ and d) 10% Ag-TiO₂.

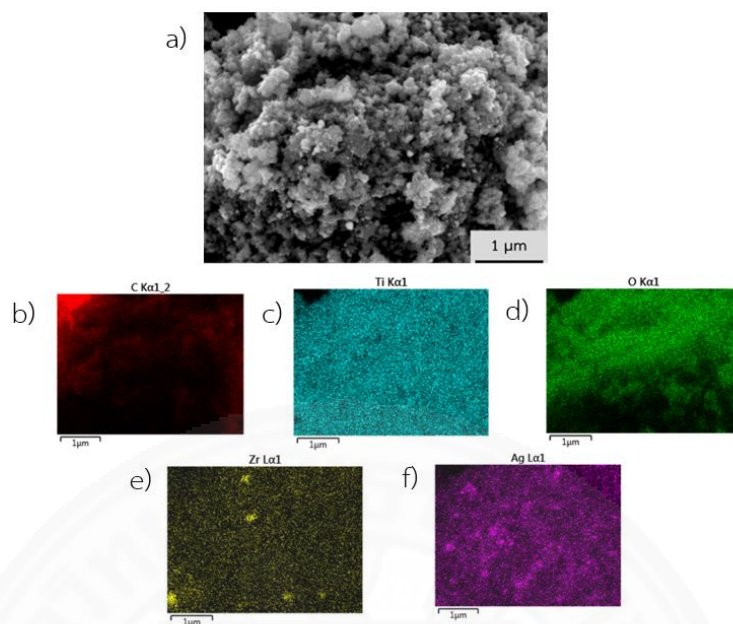


Figure 4.18 Energy Dispersive X-ray Spectroscopy (EDS) mapping of a) SEM image 3% Ag-TiO₂ particles, b) EDS mapping of C, c) EDS mapping of Ti, d) EDS mapping of O, e) EDS mapping of Zr and f) EDS mapping of Ag.

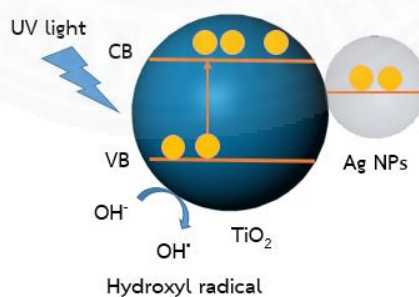


Figure 4.19 Mechanism of photocatalytic activity of Ag-TiO₂ powder under UV light

4.2.2 Effect of different concentrations of Ag on antibacterial activity

The MIC of TiO₂, P25 and Ag-TiO₂ with different concentrations of Ag was estimated by using *Staphylococcus aureus* (*S. aureus*) 8739 as a gram positive and *Escherichia coli* (*E. coli*) 6538P as a gram negative bacteria. Table 4.6 shows MIC and MBC of TiO₂, P25 and Ag-TiO₂ with different concentrations of Ag under dark and UV light conditions. The results showed that MIC of microorganism growth was unable to observe in TiO₂ and P25 under dark condition because TiO₂ and P25 did not present photocatalytic activity. When considering under UV light, TiO₂ showed MIC value of *E. coli* and *S. aureus* of 1.250 mg/ml higher than that of P25 of 0.625 mg/ml. This indicates that P25 shows higher antibacterial activity than TiO₂ powder. When considering Ag-TiO₂ with different concentrations of Ag from 3% to 10% by mole, the results show that under dark condition MIC of *E. coli* and *S. aureus* of 3% to 10% by mole Ag-TiO₂ particles were 0.312 to 0.625 mg/ml and 0.625 to 1.250 mg/ml, respectively. MIC of *E. coli* and *S. aureus* under UV light of 3% to 10% Ag-TiO₂ particles were 0.625-1.250 mg/ml and 1.250 mg/ml, respectively. It should be noted that under dark and UV light conditions the antibacterial activity was influenced by Ag NPs. MBC of 3-10% by mole Ag-TiO₂ was in the range of 0.625-2.500 mg/ml *E. coli* under dark and UV light conditions. MBC of Ag-TiO₂ was found to be 1.250-5.00 mg/ml and 2.500 mg/ml of *S. aureus* under dark and UV light conditions. MIC and MBC of *E. coli* were lower than those of *S. aureus* due to the thicker cell wall structure of gram positive compared to gram negative bacteria. Besides, Ag⁺ preferred to attach on gram negative due to the different ion⁵⁰. Because gram negative bacteria has more lipopolysaccharides which composed of phosphate (PO₄³⁻) in their structure than gram positive. The attraction of positive charge of Ag⁺ ion to gram negative bacteria showed higher than gram positive bacteria. Therefore, antibacterial activity of *E. coli* can killer than *S. aureus* bacteria. It was observed that 3-5% Ag-TiO₂ showed higher antibacterial activity due to low MIC and MBC value under dark and UV light. The MBC value of

1.250 mg/ml of 3% Ag-TiO₂ under UV light showed higher antibacterial activity than that under dark condition (2.500 mg/ml). This can be attributed to the free radical namely superoxide anion (O₂⁻) and hydroxyl radical (OH[•]) generated from the photocatalytic reaction of TiO₂ when 3% Ag-TiO₂ NPs were irradiated with UV light combined with the effect of Ag⁺ ion release to kill bacteria. While considering Ag-TiO₂ under dark condition, the antibacterial activity came only from the effect of Ag⁺ ion release. To conclude that mechanism for antibacterial activity under dark and UV light irradiation as shown in Figure 4.20. Back scattered electron (BSE) images from FE-SEM of Ag-TiO₂ with different concentrations of Ag were shown in Figure 4.18. It was observed that the brighter small particles deposited on the surface of TiO₂ were Ag NPs due to the heavier atoms or molecules of Ag compared to TiO₂. When increasing concentrations of Ag from 3% to 10% by mole, the results showed an increase of number of particles and particle size of Ag deposited on surface of TiO₂ (as shown in Appendix C1-C3). EDS mapping as shown in Figure 4.19 of 3% Ag-TiO₂ powder confirmed that Ag NPs were uniformly deposited onto the surface of TiO₂ powder. With increasing concentration of Ag from 3% to 10% by mole of Ag-TiO₂, the results show that an increase of number and more aggregation of Ag NPs on surface of TiO₂ as shown in Appendix C1-C3.

Diffuse reflectance spectra (DRS) of TiO₂ and Ag-TiO₂ powders with different concentrations of Ag from 3% to 10% by mole were shown in Figure 4.21 to investigate the absorption. The results show that Ag-TiO₂ showed absorption in both UV and visible region whereas TiO₂ only absorbed in UV region (in wavelength 200-400 nm). Ag-TiO₂ with different concentrations of Ag presented absorption extend into the visible region due to Surface Plasmon Resonance (SPR) of Ag NPs⁽⁶¹⁾. Free electrons of Ag nanoparticles occurred collective oscillation electrons of metal by photon and then, the oscillating electrons showed resonance in the visible regions. Both EDS and DRS results confirmed that Ag NPs deposited on surface of TiO₂ powder. Moreover, the

energy band gap of TiO₂ and Ag-TiO₂ can calculate from DRS method using Kubella-Munk function shows equation as follow:

$$\alpha(h\nu) = B(h\nu - E_g)^2 \quad (6)$$

Where α is the extinction coefficient, h is the Planck's constant (J·S), ν is the light frequency (s⁻¹), B is the absorption constant, E_g is the energy band gap (eV) and n is the value of the specific transition, n = 2 for indirect band gap and n = 1/2 for direct band gap, respectively⁽⁶²⁾. Energy band gap of TiO₂ and 3-10% by mole Ag-TiO₂ can be obtained by using Tauc plot as shown in Figure E.1 in Appendix E and can be calculated by extrapolation of the slope of graph for direct band gap structure. It was observed that all Ag-TiO₂ NPs presented lower energy band gap lower than TiO₂ powder as shown in Table 4.7. This indicates that some Ag⁰ can dope in to TiO₂ network in hydrolysis and condensation reaction in sol-gel method and Ag doping leading to create localized energy levels near valance or conduction band of TiO₂. Then, the energy band gap of TiO₂ was decreased from 3.13 to 2.83 eV when adding concentration of 3% Ag-TiO₂. With increasing concentration of Ag from 3% to 10% by mole of Ag-TiO₂, energy band gap decreased from 2.83 to 2.72 eV except 5% Ag-TiO₂ showed increasing energy band gap of 2.95 eV.

Table 4. 6 Minimum inhibitory concentration (MIC) and minimum bactericidal concentration (MBC) of TiO_2 , P25 and Ag-TiO_2 at different concentrations of Ag under dark and UV light conditions.

Sample	MIC (mg/ml)				MBC (mg/ml)			
	<i>E. coli</i>		<i>S. aureus</i>		<i>E. coli</i>		<i>S. aureus</i>	
	Dark	UV light	Dark	UV light	Dark	UV light	Dark	UV light
P25	-	0.625	-	0.625	-	10.000	-	5.000
TiO_2	-	1.250	-	1.250	-	10.000	-	10.000
3% Ag-TiO_2	0.625	0.625	1.250	1.250	2.500	1.250	2.500	2.500
5% Ag-TiO_2	0.625	0.625	1.250	1.250	1.250	1.250	1.250	2.500
6% Ag-TiO_2	0.625	1.250	1.250	1.250	1.250	2.500	2.500	2.500
10% Ag-TiO_2	0.312	0.625	0.625	1.250	0.625	0.625	5.000	2.500

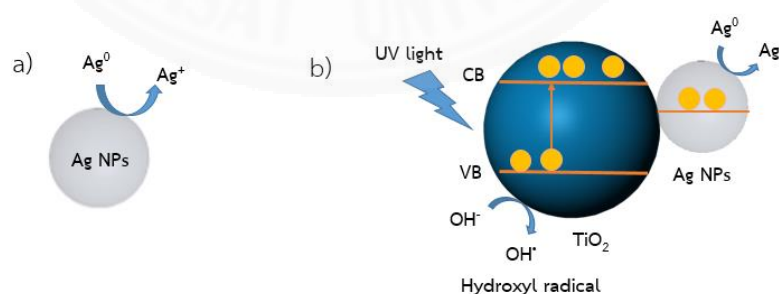


Figure 4.20 Mechanism antibacterial activity of Ag-TiO_2 powder under a) dark and b) UV light conditions.

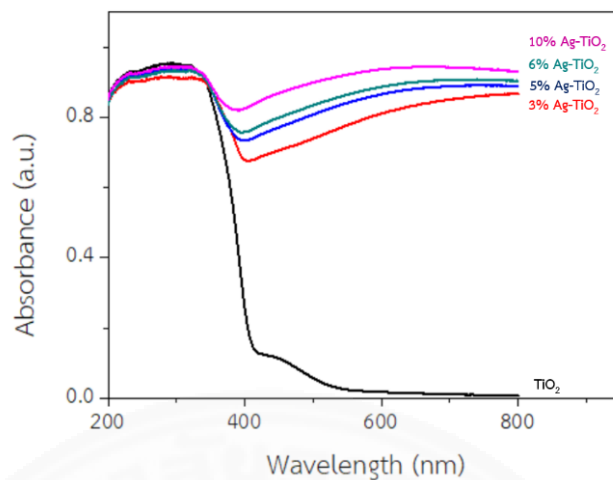


Figure 4.21 Diffuse reflectance spectra (DRS) of TiO_2 and 3-10% by mole Ag-TiO_2 nanoparticles.

Table 4.7 Energy band gap of TiO_2 and 3-10% Ag-TiO_2 nanoparticles.

Sample	TiO_2	3% Ag-TiO_2	5% Ag-TiO_2	6% Ag-TiO_2	10% Ag-TiO_2
Energy band gap (eV)	3.13	2.83	2.95	2.77	2.72

4.3 Dip coating of TiO₂, P25 and Ag-TiO₂ NPs on air filter

In this part, the study parameters for dip coating of nanomaterials including TiO₂, P25 and Ag-TiO₂ on air filter were investigated for uniformly distribution of material, good self-cleaning and high antibacterial activity. The study parameters included dipping speed, concentration of PPG-4000 as a binder, and concentration of materials including P25 and 5% Ag-TiO₂ which can have much influence on the coating of materials on air filters.

4.3.1 Effect of dipping speed on air filters for self-cleaning and antibacterial activity application

The dipping speed of dip-coating method was the first parameter that was studied to see the effect of P25 coating on F9 air filters. The relationship between the reduction rate of *E. coli* and dipping speed was presented in Figure 4.22. It is interesting to note that the high antibacterial activity above 99% was observed at all dipping speed from 0.167 to 1.000 mm/s of 10%w/v P25 solution under both dark and UV light conditions. This phenomena can be speculated to be the effect of PPG-4000 which acts as a binder⁽⁶³⁾. PPG-4000 has the structure of polymer chain can produce hydroxyl group which can kill bacteria. Furthermore, the self-cleaning performance was also studied and shown in Table 4.8. The coated air filters with 9%v/v PPG-4000 and 10%w/v P25 with different dipping speeds were dipped into 100% oleic acid acted as the contaminate molecules. It was found that the dipping speed of 0.167 mm/s showed the highest self-cleaning rate of $3.21 \times 10^{-3} \text{ min}^{-1}$. An example of how to calculate the self-cleaning rate was illustrated in Appendix F. The self-cleaning results indicated that air filter coated with the dipping speed of 0.167 mm/s presented the highest photocatalytic activity. The higher self-cleaning rate obtained, the more photocatalytic activity occurred. To explain in more detail, when the P25 NPs were excited by UV light, the highly active molecular including hydroxyl radical and

superoxide anion were generated from the photocatalytic reaction, and could be reacted with oleic acid molecular coated on air filter. This reaction can cause the self-cleaning by elimination of oleic acid contaminants leading to the smaller contact angle obtained. It was obviously observed that the coated air filters with P25 NPs was charged from hydrophobic to super-hydrophilic property after self-cleaning reaction. In addition, FE-SEM was employed to study the morphology and adhesion of P25 NPs on air filters. FE-SEM images of coated air filters with different dipping speeds were shown in Figure 4.23. There were agglomeration and aggregation of P25 NPs observed in all coated air filters. However, the air filter coated with 0.500 mm/s (see in Figure 4.23 d)) presented the least agglomeration and clogging between fibers compared to others dipping speeds. Moreover, 0.500 mm/s coated air filter was shown the good adhesion of P25 NPs on air filters after considering the obtained results from above mentioned, the dipping speed of 0.500 mm/s was chosen for next steps of study due to the optimal condition for good adhesion of material and antibacterial with high self-cleaning rate and suitable time for coating.

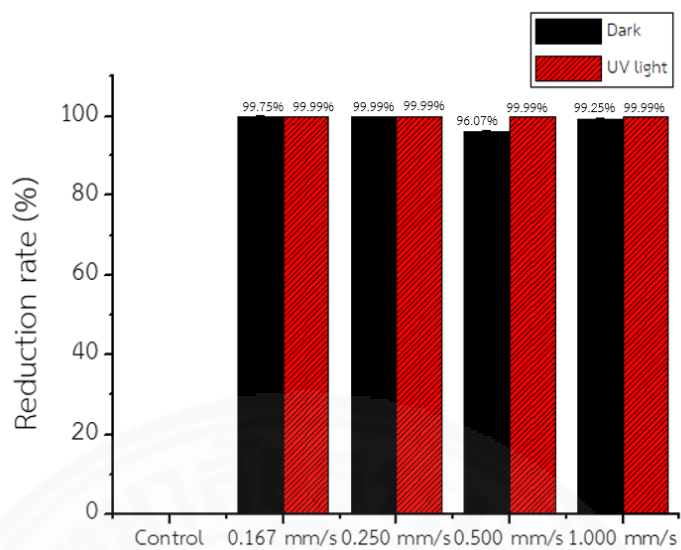


Figure 4.22 Reduction rate of *E. coli* with air filters coated with different dipping speeds under dark and UV light condition.

Table 4.8 Self-cleaning rate of air filters coated with various dipping speeds from 0.167 to 1.000 mm/s of 10%w/v P25 and 9%v/v PPG-4000 as a binder.

Dipping speed (mm/s)	Rate constant of self-cleaning (k) ($\times 10^{-3}$, min^{-1})
0.167	3.21
0.250	1.72
0.500	2.15
1.000	1.12

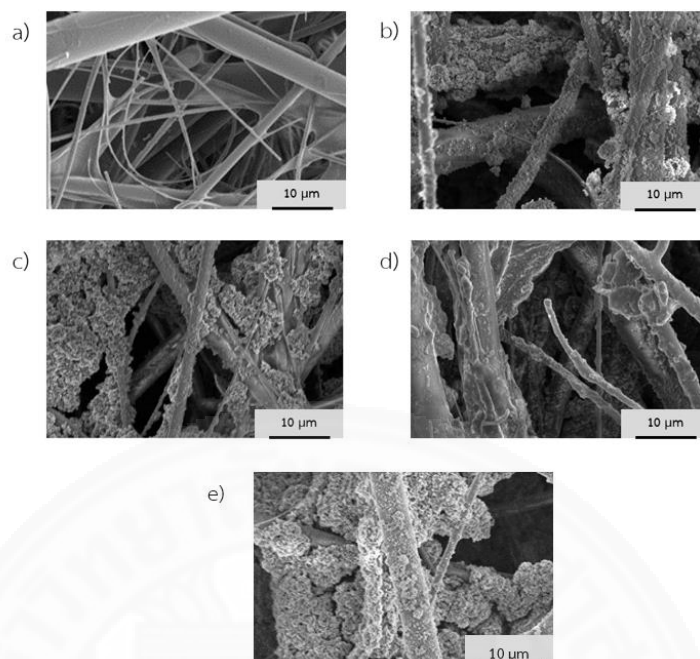


Figure 4.23 FE-SEM images a) uncoated F9 air filter and coated air filters with 9%v/v of PPG-4000 and 10%w/v of P25 NPs with different dipping speeds of b) 0.167 mm/s, c) 0.250 mm/s, d) 0.500 mm/s, and e) 1.000 mm/s.

4.3.2 Effect of PPG-4000, IPA and P25 NPs self-cleaning and antibacterial on air filter

Air filters coated by PPG-4000, IPA, P25 and, PPG-4000-IPA-P25 showed inhibiting the growth of bacteria compared to control as shown in Figure 4.24. However, air filter was coated by IPA showed 0% reduction rate under UV light condition. This indicates that IPA did not have the antibacterial activity under UV light. It was observed that the air filter coated by PPG-4000 showed quite high bacterial reduction of 92.42% and 97.79% under dark and UV light conditions, respectively. This indicates that PPG-4000 acts as antibacterial reagent. While IPA showed rather low antibacterial activity of 11.13% under dark condition. The air filter was coated by only

commercial P25 showed antibacterial activity of *E. coli* of 63.62% and 99.98% under dark and UV light conditions, respectively. The air filters coated with PPG-4000, IPA and P25 demonstrated the highest antibacterial activity of 95.34% and 99.99% under dark and UV light conditions, respectively. This can be attributed to the effect of reactive oxygen species (ROS) of P25 generated under UV light via the photocatalytic reaction and effect of PPG-4000 as antibacterial agent for antibacterial activity. These ROS and antibacterial agent can further react with the membrane of bacteria and cause the bacterial death^(54,64). Due to the performance of PPG-4000 which showed high antibacterial activity, the optimal concentration of PPG-4000 was then investigated to reduce the antibacterial activity of PPG-4000. However, the good adhesion of P25 on air filter and good self-cleaning should not be reduced and would be considered with further study in next step.

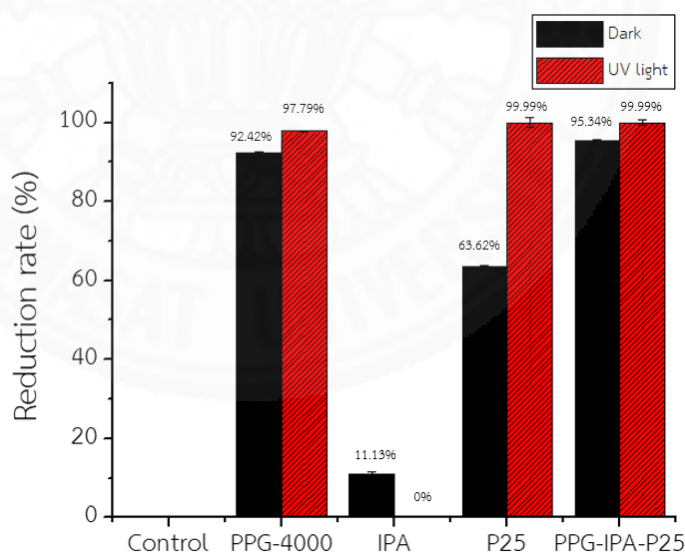


Figure 4.24 Reduction of *E. coli* on different F9 air filters with different coating agents including PPG, IPA, P25, and PPG+P25+IPA employing AATCC 100-1999 and ISO 27447 under dark and UV light conditions for 6h.

4.3.3 Effect of concentration of PPG-4000 on self-cleaning and antibacterial air filter

The effect of different concentration of PPG-4000 coated on air filter on the number concentration of *E. coli* after incubation under dark and UV light condition was studied. Figure 4.25 shows the percentage of bacterial reduction of air filters coated on different concentrations of PPG-4000. It was observed that the reduction rate of *E. coli* was found to be at 0% antibacterial activity at the concentration of PPG-4000 below 1.0%v/v under dark and UV light conditions. On the other hands, when the concentration of PPG-4000 increased to 5.0%v/v, the reduction rate of *E. coli* was increased to 16.59% and 53.59% under dark and UV light conditions, respectively. 10% v/v of PPG-4000 showed the highest percentage reduction rate of *E. coli* of 99.99% under dark and UV light conditions. This indicates that PPG-4000 can act as antibacterial agent due to the hydrophilic property of PPG-4000. PPG-4000 molecules are able to freely pass across the outer membrane of bacteria and then react with the cytoplasmic membrane. This can cause the damage of bacterial cell and affect the leakage of phosphate and finally cell bacterial death⁽⁶³⁾.

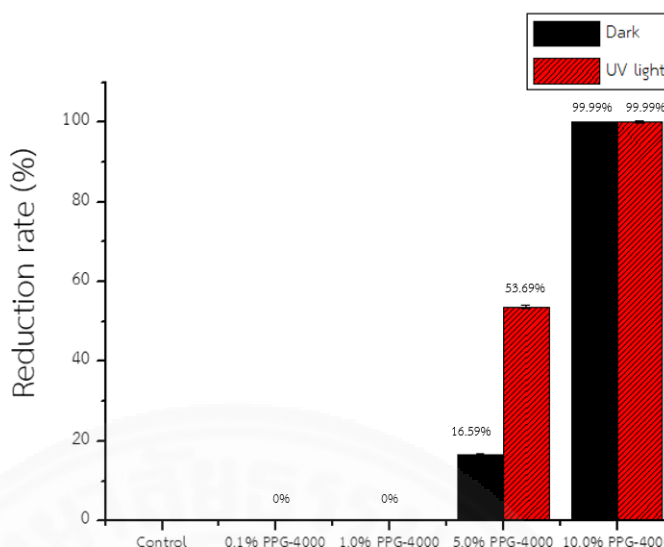


Figure 4.25 Reduction rate of *E. coli* on air filter coated with different concentrations of PPG-4000 employing modified AATCC 100 and ISO 27447 under dark and UV light conditions.

When air filters were coated with both PPG-4000 and 10% w/v P25 TiO₂, the number concentration of *E. coli* left after incubation with dark and UV light conditions for 6 h was observed. Figure 4.26 shows the rate of reduction of *E. coli* on air filters coated with different concentrations of PPG-4000 and 10% w/v P25 after incubation under dark and UV light for 6 h. It was observed that under dark condition the air filter coated with 0.1% v/v PPG-4000 and 10% w/v P25 NPs did not present the antibacterial activity with 0% reduction rate while under UV light it showed very high antibacterial activity of 99.99%. Considering under dark condition, when the concentration of PPG-4000 increased from 1.0% to 10.0% v/v, the reduction rate was increased from 68.26% to 99.99%. Under UV light condition, it is interesting to note that all air filters consisting of both PPG-4000 and 10% w/v P25 show the highest percentage of bacterial reduction of 99.99%. This is because the synergistic effect of PPG-4000 and photocatalytic P25 generating reactive oxygen species (ROS). These ROS can react with cell membrane which cause the bacteria death⁽⁶⁴⁾ and PPG-4000 acts as

antibacterial agent for antibacterial activity. In addition, the self-cleaning of air filters coated with different concentrations of PPG-4000 and top-coating with combine P25 NPs is shown in Table 4.9. The results show that the highest self-cleaning rate of $10.8 \times 10^{-4} \text{ min}^{-1}$ was obtained with the air filter coated with 10.0% v/v PPG-4000 and 10% w/v of P25. The higher the concentration of PPG-4000, the higher self-cleaning rate obtained. It was observed that when the concentration of PPG-4000 was increased 100 times from 0.1% to 10.0% v/v, the self-cleaning rate was increased twice from $5.77 \times 10^{-4} \text{ min}^{-1}$ to $10.80 \times 10^{-4} \text{ min}^{-1}$. Figure 4.27 shows FE-SEM images of air filters coated with different concentrations of PPG-4000 and 10% w/v P25 NPs. It was observed that there were much higher aggregation and agglomeration of P25 powder deposited on air fiber and covered the pores or clogged the pores between fibers for 0.1%, 5.0% and 10.0% v/v PPG-4000 (see Figure 4.27 b), d) and e)) compared to that of 1.0% v/v PPG-4000 (Figure 4.27 c)). Therefore, 1.0% v/v of PPG-4000 coated on air filter was considered to be the most suitable concentration to coat on air filter before coating with P25 NPs due to the results from bacterial reduction and material adhesion efficiency as already mentioned above.

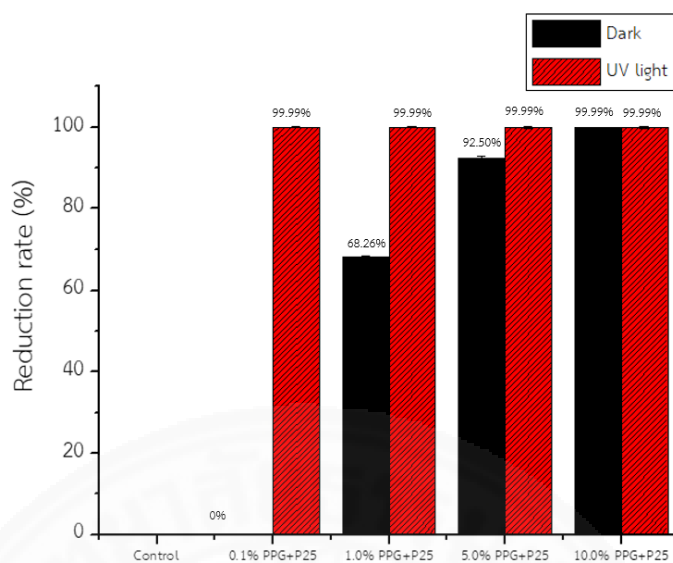


Figure 4.26 Reduction rate of *E. coli* on air filter coated with different concentrations of PPG-4000 and then coated with 10% w/v P25 NPs tested by of AATCC 100 under dark and UV light conditions.

Table 4.9 Self-cleaning rate of air filters coated with various concentrations of PPG-4000 from 0.1 to 10.0%v/v and then top-coated with 10% w/v P25 NPs.

Sample	Self-cleaning rate k ($\times 10^{-4}$, min^{-1})
0.1% PPG+P25	5.77
1.0% PPG+P25	7.27
5.0% PPG+P25	7.53
10.0% PPG+P25	10.80

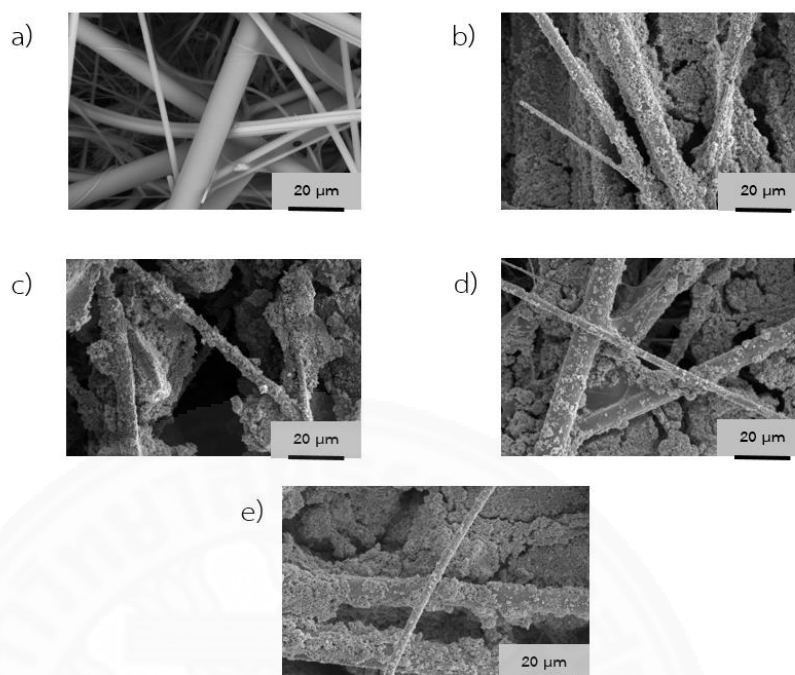


Figure 4.27 FE-SEM images of a) uncoated F9 air filter and air filters was coated with different concentrations of PPG-4000 of b) 0.1%, c) 1.0%, d) 5.0%, and e) 10.0% v/v and top-coated with 10%w/v P25 NPs.

4.3.4 Effect of concentration of P25 NPs on self-cleaning and antibacterial air filters

Figure 4.28 shows FE-SEM images of air filters with different concentrations of P25 NPs from 0.1% to 10.0% w/v. It was observed that when concentration of P25 NPs was increased from 0.1% to 10%w/v, the aggregation and agglomeration of P25 powders deposited on air fiber and covered the pores between fibers seemed to be increased, performance of air filter with different concentrations of P25 as shown in Table 4.11, the results show that increasing of concentration of P25 NPs on air filter from 0.1% to 10.0%w/v, self-cleaning rate was increased from

6.08×10^{-4} to $26.50 \times 10^{-4} \text{ min}^{-1}$. The higher amount of P25 deposited on air filters, the higher photocatalytic activity occurred and leading to the higher self-cleaning rate. The percentage of bacterial reduction of *E. coli* on coated air filters with different concentrations of P25 NPs after incubation under dark and UV light for 6 is shown in Figure 4.30. The results demonstrate that under dark condition air filters coated with P25 from 0.1% to 5.0%w/v cannot inhibit the growth of *E. coli* with 0% reduction due to the requirement of UV light for photocatalytic P25. However, it is interesting to note that air filter coated with 10%w/v P25 NPs showed antibacterial activity with the reduction rate of 56.01%. Because 10%w/v is high concentration of P25 NPs can kill bacteria under dark condition. On the other hands, under UV light condition the percentage reduction rate of *E. coli* reduction was triply increased from 31.63% to 99.99% when the concentration of P25 was increased from 0.1%, 10%w/v. The highest antibacterial activity was achieved with the concentration of P25 NPs at 10% w/v under dark and UV light. This indicates that the more P25 used, the higher antibacterial activity obtained due to the photocatalytic activity of P25 which generates ROS. These ROS can react with cell membrane which causes the bacterial death⁽⁶⁴⁾.

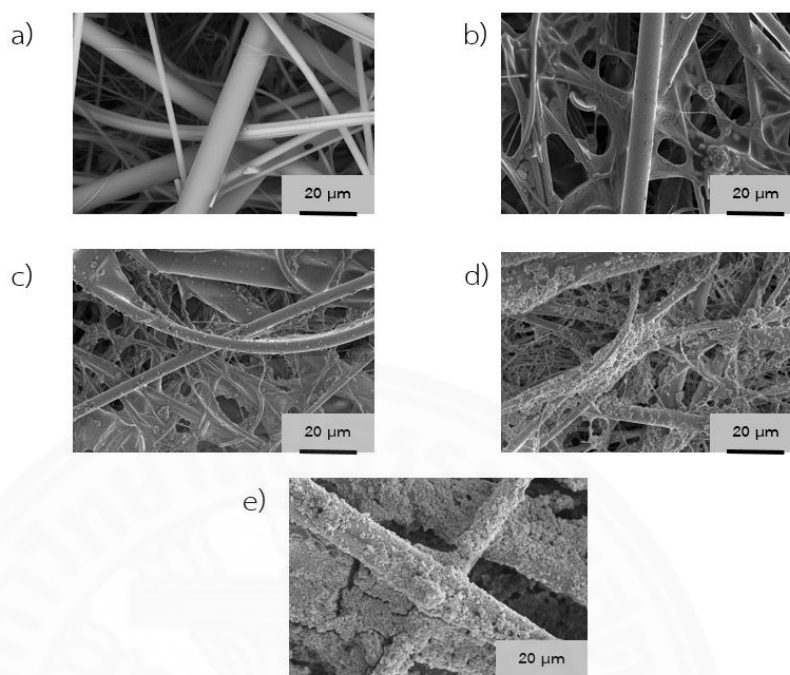


Figure 4.28 FE-SEM images of a) uncoated F9 air filter and air filters coated with various concentrations of P25 b) 0.1%, c) 1.0%, d) 5.0% and e) 10.0%w/v.

Table 4.10 Self-cleaning rate of air filters coated with various concentrations of P25 from 0.1 to 10.0%w/v.

Sample	Self-cleaning rate k ($\times 10^{-4} \text{ min}^{-1}$)
0.1% w/v P25	6.08
1.0% w/v P25	7.47
5.0% w/v P25	24.70
10.0% w/v P25	26.50

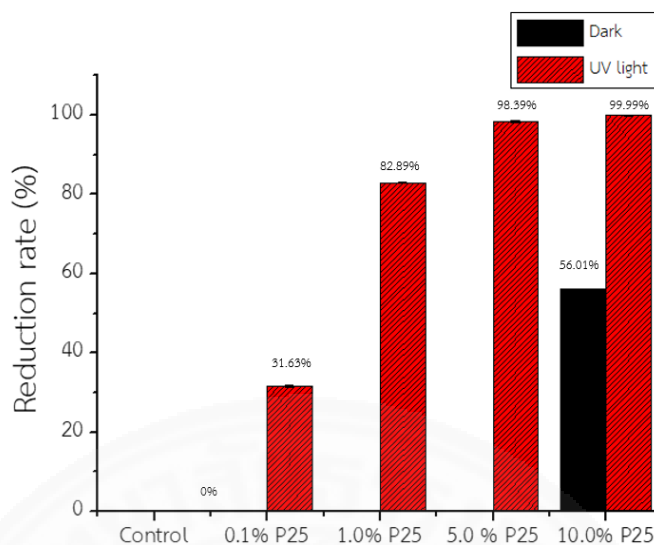


Figure 4.29 Reduction rate of *E. coli* on air filters coated with different concentrations of P25 NPs from 0.1% to 10.0%w/v and 1.0% v/v PPG-4000 employing the modified AATCC 100 under dark and UV light conditions.

4.3.5 Effect of different materials including of 10% w/v P25 NPs, TiO₂ and 5% Ag-TiO₂ on self-cleaning and antibacterial air filters

FE-SEM images of air filter coated with 10% w/v of TiO₂, P25 and 5% Ag-TiO₂ are shown in Figure 4.30. The results show that air filter coated with P25 NPs showed better uniformly distribution on air filter than that of air filter coated with synthesized TiO₂ and 5% Ag-TiO₂ presented higher aggregation of powders on air filter and cover the gap between fiber with less adhesion. When considering self-cleaning rate of air filters coated with 10% w/v of P25, TiO₂ and 5% Ag-TiO₂ particles is shown in Table 4.11. The results show that air filter coated with P25 NPs showed the highest self-cleaning rate of $26.5 \times 10^{-4} \text{ min}^{-1}$. This indicates that P25 NPs presented the highest photocatalytic activity compared to synthesized TiO₂ and 5% Ag-TiO₂. However, it should be noted that from FE-SEM results it was noticed that there were a less amount of TiO₂ and Ag-TiO₂ NPs deposited on air filters. This can cause the less amount of

active NPs on air filter leading to the less photoactive and lower self-cleaning rate of synthesized TiO_2 and Ag- TiO_2 coated air filters. The percentage of bacterial reduction on air filters coated with 10% w/v of P25 NPs, TiO_2 and 5% Ag- TiO_2 after incubating under dark and UV light for 6 h is shown in Figure 4.31. It was observed that air filter coated with synthesized TiO_2 NPs cannot inhibit the growth of *E. coli* with 0% reduction rate under both dark and UV light. This result was speculated to be the result of fast precipitation of synthesized TiO_2 solution between dip-coating leading to the less amount of NPs deposited on air filter. Consequently, the coated air filter cannot show the bacterial reduction. Concerning the air filter coated with P25, it showed on antibacterial activity (only 2.37%) under dark condition, while it showed the strong antibacterial activity under UV light condition. 5% Ag- TiO_2 showed the highest antibacterial activity with reduction rate of *E. coli* of 99.99% under both dark and UV light conditions. From the antibacterial activity results, this can be explained that Ag in Ag- TiO_2 has a strong effect on inhibiting the bacterial growth due to the releasing of Ag^+ ion. These Ag^+ ion can penetrate into the cell membrane of bacteria causing the DNA damage and cell bacterial death. From EDS mapping of 5% Ag- TiO_2 as shown in Figure 4.32, it was observed that distribution of Ti, O and Ag atoms on the air filter which corresponds to the distribution of Ag- TiO_2 NPs on air filter from FE-SEM image (see Figure 4.32 a)).

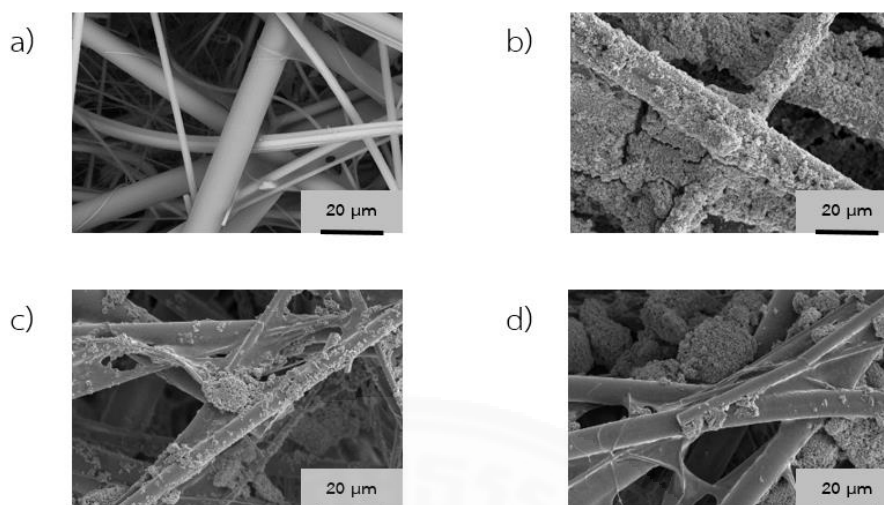


Figure 4.30 FE-SEM images of a) uncoated F9 air filter and air filter coated with b) 10%w/v P25, c) 10%w/v synthesized TiO_2 , and d) 5% Ag-TiO_2 .

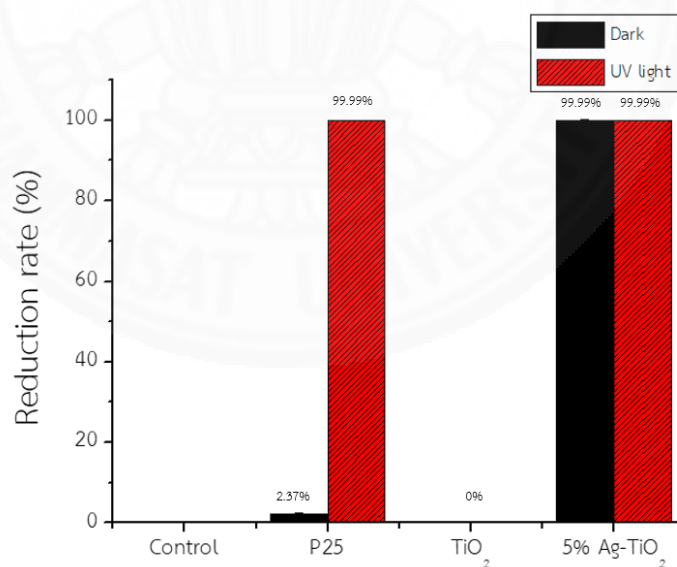


Figure 4.31 Reduction rate of *E. coli* on air filter with 10% w/v P25, TiO_2 , and 5% Ag-TiO_2 employing the modified AATCC 100 under dark and UV light conditions.

Table 4.11 Self-cleaning rate of air filters coated with 10%w/v of P25, TiO₂, and 5% Ag-TiO₂.

Sample	Self-cleaning rate ($\times 10^{-4}$, min ⁻¹)
P25	26.50
TiO ₂	5.62
5% Ag-TiO ₂	10.70

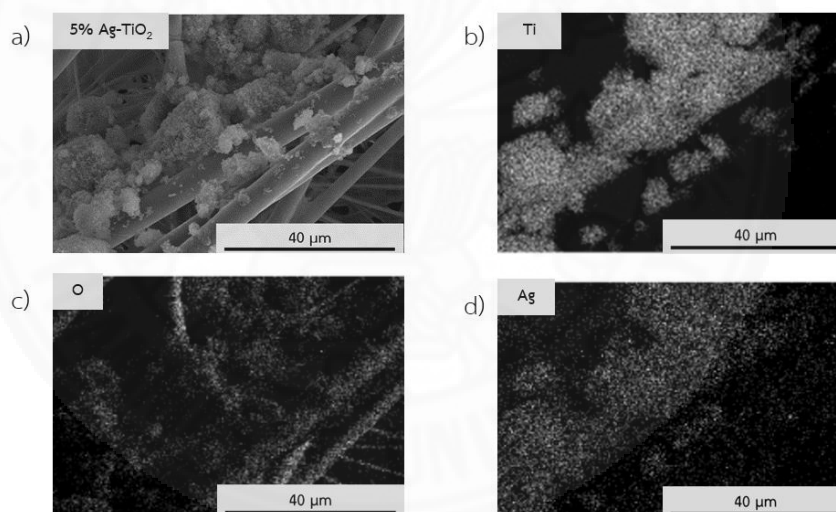


Figure 4.32 (a) FE-SEM image of air filter coated with 10%w/v of 5% Ag-TiO₂, b) Ti, c) O, and d) Ag.

CHAPTER 5

CONCLUSIONS AND RECOMMENDATIONS

5.1 CONCLUSION

TiO₂ nanoparticles were successfully synthesized by DWBMS synthesized method using methanol as a solvent providing the smallest particle size of 8.1±2.1 nm and showing the highest photocatalytic activity of 8.5×10⁻⁴ min⁻¹. Calcination temperature has strong effect on phase transition, crystallinity, crystallite size and particle size of TiO₂ NPs. The highest photocatalytic activity of synthesized TiO₂ NPs was achieved at 600°C with the kinetic constant rate of 1.70×10⁻³ min⁻¹. Ag-TiO₂ NPs was successfully synthesized by DWBMS method using methanol as a solvent and calcined at 600°C for 4 h. The optimal amount of Ag in Ag-TiO₂ was found to be at 5% by mole Ag-TiO₂ which showed the strongest photocatalytic activity with the kinetic constant rate of 2.02×10⁻³ min⁻¹ due to its smallest particle size and highest surface area. The optimal doping of 3-5% by mole Ag-TiO₂ showed the antibacterial activity with the suitable MIC and MBC about 0.625-2.500 mg/ml. The highest self-cleaning rate of 2.15×10⁻³ min⁻¹ and high antibacterial activity of 99.99% under UV light was achieved at 0.500 mm/s. The optimal condition of PPG-4000 for dip coating is 1%v/v PPG-4000. The optimal concentration of 1%v/v PPG-4000 and 10%w/v P25 showed the highest antibacterial activity of 99.99% under UV light and showed the uniform distribution on air filter. The optimal conditions for coating of 5% Ag-TiO₂ on air filter is 1%v/v PPG-4000 and 10%w/v of 5% Ag-TiO₂ powder with dipping speed of 0.500 mm/s.

5.2 Recommendations and outlook

Since 5% Ag-TiO₂ still has an issue of particle precipitation during dip-coating process causing the less amount of 5% Ag-TiO₂ depositing on air filters and leading to the low self-cleaning rate, the suitable of dip-coating process and surfactant

material is needed to enhance the dipping solution during the dip coating process. Furthermore, the challenge of reducing the dominant effect of Ag^+ ion on antibacterial activity under both dark and UV light conditions consequently, the optimal concentration of 5% Ag-TiO_2 should be investigated to reduce the antibacterial activity under dark condition and enhance the antibacterial activity under UV light condition. Last but not least, the photocatalytic activity and antibacterial activity of all Ag-TiO_2 NPs should be studied under visible light condition.



REFERENCES

1. World Health Organization. (2017). *Tuberculosis (TB)*. accessed June 8, 2018. World Health Organization Country Office from Thailand. Website: http://www.who.int/tb/publications/global_report/en/
2. Le Ouay B, Stellacci F. Antibacterial activity of silver nanoparticles: a surface science insight. *Nano Today*. 2015;10(3):339-54.
3. Yoon KY, Byeon JH, Park CW, Hwang J. Antimicrobial effect of silver particles on bacterial contamination of activated carbon fibers. *Environmental science & technology*. 2008;42(4):1251-5.
4. Joe YH, Ju W, Park JH, Yoon YH, Hwang J. Correlation between the antibacterial ability of silver nanoparticle coated air filters and the dust loading. *Aerosol Air Qual Res*. 2013;13:1009-18.
5. Gupta S, Tripathi M. A review of TiO₂ nanoparticles. 2011. 1639-57 p.
6. Chuaybamroong P, Chotigawin R, Supothina S, Sribenjalux P, Larpkittaworn S, Wu CY. Efficacy of photocatalytic HEPA filter on microorganism removal. *Indoor Air*. 2010;20(3):246-54.
7. Limmongkon Y, Johns J, Charentanyarak L. Preparation of a TiO₂-coated photocatalytic air filter for use with an electrostatic air filter pack for xylene removal. *Science Asia*. 2013;39:284-93.
8. Cai Y, Strømme M, Welch K. Disinfection Kinetics and Contribution of Reactive Oxygen Species When Eliminating Bacteria with TiO₂ Induced Photocatalysis. *Journal of Biomaterials and Nanobiotechnology*. 2014;5(3):200-9.
9. Pelaez M, Nolan NT, Pillai SC, Seery MK, Falaras P, Kontos AG, et al. A review on the visible light active titanium dioxide photocatalysts for environmental applications. *Applied Catalysis B: Environmental*. 2012;125:331-49.

10. Tobaldi D, Piccirillo C, Pullar R, Gualtieri A, Seabra M, Castro P, et al. Silver-modified nano-titania as an antibacterial agent and photocatalyst. *The Journal of Physical Chemistry C*. 2014;118(9):4751-66.
11. Pham T-D, Lee B-K. Feasibility of silver doped TiO₂/glass fiber photocatalyst under visible irradiation as an indoor air germicide. *International journal of environmental research and public health*. 2014;11(3):3271-88.
12. Avciata O, Benli Y, Gorduk S, Koyun O. Ag doped TiO₂ nanoparticles prepared by hydrothermal method and coating of the nanoparticles on the ceramic pellets for photocatalytic study: Surface properties and photoactivity. *Journal of Engineering Technology and Applied Sciences*. 2016;1(1).
13. Zhang H, Chen G. Potent antibacterial activities of Ag/TiO₂ nanocomposite powders synthesized by a one-pot sol-gel method. *Environmental science & technology*. 2009;43(8):2905-10.
14. Jung HJ, Sohn Y, Sung HG, Hyun HS, Shin WG. Physicochemical properties of ball milled boron particles: dry vs. wet ball milling process. *Powder Technology*. 2015;269:548-53.
15. Kment Š, Gregora I, Kmentová H, Novotná P, Hubička Z, Krýsa J, et al. Raman spectroscopy of dip-coated and spin-coated sol-gel TiO₂ thin films on different types of glass substrate. *Journal of sol-gel science and technology*. 2012;63(3):294-306.
16. Faustini M, Louis B, Albouy PA, Kuemmel M, Grosso D. Preparation of sol-gel films by dip-coating in extreme conditions. *The Journal of Physical Chemistry C*. 2010;114(17):7637-45.
17. Touam T, Atoui M, Hadjoub I, Chelouche A, Boudine B, Fischer A, et al. Effects of dip-coating speed and annealing temperature on structural, morphological and optical properties of sol-gel nano-structured TiO₂ thin films. *The European Physical Journal-Applied Physics*. 2014;67(3).

18. Morones JR, Elechiguerra JL, Camacho A, Holt K, Kouri JB, Ramírez JT, et al. The bactericidal effect of silver nanoparticles. *Nanotechnology*. 2005;16(10):2346.
19. Ruparelia JP, Chatterjee AK, Duttagupta SP, Mukherji S. Strain specificity in antimicrobial activity of silver and copper nanoparticles. *Acta biomaterialia*. 2008;4(3):707-16.
20. Sinha R, Karan R, Sinha A, Khare S. Interaction and nanotoxic effect of ZnO and Ag nanoparticles on mesophilic and halophilic bacterial cells. *Bioresource technology*. 2011;102(2):1516-20.
21. Jiang W, Mashayekhi H, Xing B. Bacterial toxicity comparison between nano-and micro-scaled oxide particles. *Environmental pollution*. 2009;157(5):1619-25.
22. Hu X, Li G, Yu JC. Design, fabrication, and modification of nanostructured semiconductor materials for environmental and energy applications. *Langmuir*. 2009;26(5):3031-9.
23. Seven O, Dindar B, Aydemir S, Metin D, Ozinel M, Icli S. Solar photocatalytic disinfection of a group of bacteria and fungi aqueous suspensions with TiO₂, ZnO and Sahara desert dust. *Journal of Photochemistry and Photobiology A: Chemistry*. 2004;165(1-3):103-7.
24. Shimura K, Yoshida H. Heterogeneous photocatalytic hydrogen production from water and biomass derivatives. *Energy & Environmental Science*. 2011;4(7):2467-81.
25. Khaki MRD, Shafeeyan MS, Raman AAA, Daud WMAW. Application of doped photocatalysts for organic pollutant degradation-A review. *Journal of environmental management*. 2017;198:78-94.
26. Hirakawa T, Yawata K, Nosaka Y. Photocatalytic reactivity for O₂ and OH radical formation in anatase and rutile TiO₂ suspension as the effect of H₂O₂ addition. *Applied Catalysis A: General*. 2007;325(1):105-11.

27. Krishna MG, Vinjanampati M, Purkayastha DD. Metal oxide thin films and nanostructures for self-cleaning applications: current status and future prospects. *The European Physical Journal-Applied Physics*. 2013;62(3).
28. Elgh B, Yuan N, Cho HS, Magerl D, Philipp M, Roth SV, et al. Controlling morphology, mesoporosity, crystallinity, and photocatalytic activity of ordered mesoporous TiO₂ films prepared at low temperature. *APL Materials*. 2014;2(11):113313.
29. Zhang J, Zhou P, Liu J, Yu J. New understanding of the difference of photocatalytic activity among anatase, rutile and brookite TiO₂. *Physical Chemistry Chemical Physics*. 2014;16(38):20382-6.
30. Hurum DC, Agrios AG, Gray KA, Rajh T, Thurnauer MC. Explaining the enhanced photocatalytic activity of Degussa P25 mixed-phase TiO₂ using EPR. *The Journal of Physical Chemistry B*. 2003;107(19):4545-9.
31. Pan X, Yang M-Q, Fu X, Zhang N, Xu Y-J. Defective TiO₂ with oxygen vacancies: synthesis, properties and photocatalytic applications. *Nanoscale*. 2013;5(9):3601-14.
32. Zaleska A. Doped-TiO₂: a review. *Recent patents on engineering*. 2008;2(3):157-64.
33. Hajipour MJ, Fromm KM, Ashkarran AA, de Aberasturi DJ, de Larramendi IR, Rojo T, et al. Antibacterial properties of nanoparticles. *Trends in biotechnology*. 2012;30(10):499-511.
34. Liu R, Wang P, Wang X, Yu H, Yu J. UV- and visible-light photocatalytic activity of simultaneously deposited and doped Ag/Ag (I)-TiO₂ photocatalyst. *The Journal of Physical Chemistry C*. 2012;116(33):17721-8.
35. Dunnill CW, Page K, Aiken ZA, Noimark S, Hyett G, Kafizas A, et al. Nanoparticulate silver coated-titania thin films—Photo-oxidative destruction of stearic acid under different light sources and antimicrobial effects under hospital lighting conditions. *Journal of Photochemistry and Photobiology A: Chemistry*. 2011;220(2-3):113-23.

36. Tobaldi D, Piccirillo C, Pullar R, Gualtieri A, Seabra M, Castro P, et al. Silver-modified nano-titania as an antibacterial agent and photocatalyst. *The Journal of Physical Chemistry C*. 2014;118(9):4751-66.
37. Pham T-D, Lee B-K. Effects of Ag doping on the photocatalytic disinfection of *E. coli* in bioaerosol by Ag-TiO₂/GF under visible light. *Journal of colloid and interface science*. 2014;428:24-
38. Zhang Y, Wang T, Zhou M, Wang Y, Zhang Z. Hydrothermal preparation of Ag-TiO₂ nanostructures with exposed {001}/{101} facets for enhancing visible light photocatalytic activity. *Ceramics International*. 2017;43(3):3118-26.
39. Behnajady M, Modirshahla N, Shokri M, Rad B. Enhancement of photocatalytic activity of TiO₂ nanoparticles by silver doping: photodeposition versus liquid impregnation methods. *Global NEST Journal*. 2008;10(1):1-7.
40. Mogal SI, Gandhi VG, Mishra M, Tripathi S, Shripathi T, Joshi PA, et al. Single-step synthesis of silver-doped titanium dioxide: influence of silver on structural, textural, and photocatalytic properties. *Industrial & Engineering Chemistry Research*. 2014;53(14):5749-58.
41. Yoldas BE. Hydrolysis of titanium alkoxide and effects of hydrolytic polycondensation parameters. *Journal of Materials Science*. 1986;21(3):1087-92.
42. Behnajady M, Eskandarloo H, Modirshahla N, Shokri M. Investigation of the effect of sol-gel synthesis variables on structural and photocatalytic properties of TiO₂ nanoparticles. *Desalination*. 2011;278(1):10-7.
43. Park HK, Kim DK, Kim CH. Effect of solvent on titania particle formation and morphology in thermal hydrolysis of TiCl₄. *Journal of the American Ceramic Society*. 1997;80(3):743-9.
44. García-Serrano J, Gómez-Hernández E, Ocampo-Fernández M, Pal U. Effect of Ag doping on the crystallization and phase transition of TiO₂ nanoparticles. *Current Applied Physics*. 2009;9(5):1097-105.
45. Mosquera AA, Albella JM, Navarro V, Bhattacharyya D, Endrino JL. Effect of silver on the phase transition and wettability of titanium oxide films. *Scientific reports*. 2016;6:32171.

46. Kment Š, Gregora I, Kmentová H, Novotná P, Hubička Z, Krýsa J, et al. Raman spectroscopy of dip-coated and spin-coated sol-gel TiO₂ thin films on different types of glass substrate. *Journal of sol-gel science and technology*. 2012;63(3):294-306.
47. Scriven L. Physics and applications of dip coating and spin coating. *MRS Online Proceedings Library Archive*. 1988;121.
48. Yimsiri P, Mackley M. Spin and dip coating of light-emitting polymer solutions: Matching experiment with modelling. *Chemical Engineering Science*. 2006;61(11):3496-505.
49. Rodriguez CL, Weathers J, Corujo B, Peterson P. Formulating water-based systems with propylene-oxide-based glycol ethers. *Journal of Coatings Technology*. 2000;72(6):67-72.
50. Sarah M, Hasmi B, Shariffudin S, Hashim H, Herman S, editors. Crack-Free TiO₂ Thin Film via Sol-Gel Dip Coating Method: Investigation on Molarity Effect. *IOP Conference Series: Materials Science and Engineering*; 2018: IOP Publishing.
51. Bahadur J, Agrawal S, Panwar V, Parveen A, Pal K. Antibacterial properties of silver doped TiO₂. *Macromolecular Research*. 2016;24(6):488-93.
52. Monshi A, Foroughi MR, Monshi MR. Modified Scherrer equation to estimate more accurately nano-crystallite size using XRD. *World Journal of Nano Science and Engineering*. 2012;2(3):154-60.
53. Foster HA, Ditta IB, Varghese S, Steele A. Photocatalytic disinfection using titanium dioxide: spectrum and mechanism of antimicrobial activity. *Applied Microbiology and Biotechnology*. 2011;90(6):1847-68.
54. Montazer M, Behzadnia A, Pakdel E, Rahimi MK, Moghadam MB. Photo induced silver on nano titanium dioxide as an enhanced antimicrobial agent for wool. *Journal of Photochemistry and Photobiology B: Biology*. 2011;103(3):207-14.
55. Chen H-S, Kumar RV. Sol-gel TiO₂ in self-organization process: growth, ripening and sintering. *RSC Advances*. 2012;2(6):2294-301.
56. Soltani N, Saion E, Erfani M, Rezaee K, Bahmanrokh G, Drummen GP, et al. Influence of the polyvinyl pyrrolidone concentration on particle size and dispersion of

57. Li J-G, Ishigaki T. Brookite rutile phase transformation of TiO₂ studied with monodispersed particles. *Acta materialia*. 2004;52(17):5143-50.
58. Nolan NT, Seery MK, Hinder SJ, Healy LF, Pillai SC. A systematic study of the effect of silver on the chelation of formic acid to a titanium precursor and the resulting effect on the anatase to rutile transformation of TiO₂. *The Journal of Physical Chemistry C*. 2010;114(30):13026-34.
59. AlOthman ZA. A review: fundamental aspects of silicate mesoporous materials. *Materials*. 2012;5(12):2874-902.
60. Avciata O, Benli Y, Gorduk S, Koyun O. Ag doped TiO₂ nanoparticles prepared by hydrothermal method and coating of the nanoparticles on the ceramic pellets for photocatalytic study: Surface properties and photoactivity. *Journal of Engineering Technology and Applied Sciences*. 2016;1(1):34-50.
61. Das R, Nath SS, Chakdar D, Gope G, Bhattacharjee R. Synthesis of silver nanoparticles and their optical properties. *Journal of Experimental Nanoscience*. 2010;5(4):357-62.
62. López R, Gómez R. Band-gap energy estimation from diffuse reflectance measurements on sol-gel and commercial TiO₂: a comparative study. *Journal of sol-gel science and technology*. 2012;61(1):1-7.
63. Darwish RM, Bloomfield SF. Effect of ethanol, propylene glycol and glycerol on the interaction of methyl and propyl p-hydroxybenzoate with *Staphylococcus aureus* and *Pseudomonas aeruginosa*. *International Journal of Pharmaceutics*. 1997;147(1):51-60.
64. Li Y, Zhang W, Niu J, Chen Y. Mechanism of photogenerated reactive oxygen species and correlation with the antibacterial properties of engineered metal-oxide nanoparticles. *ACS nano*. 2012;6(6):5164-73.

APPENDICES



APPENDIX A

Particle size and size distribution of TiO_2 was synthesized DWBMS method with different calcination temperatures

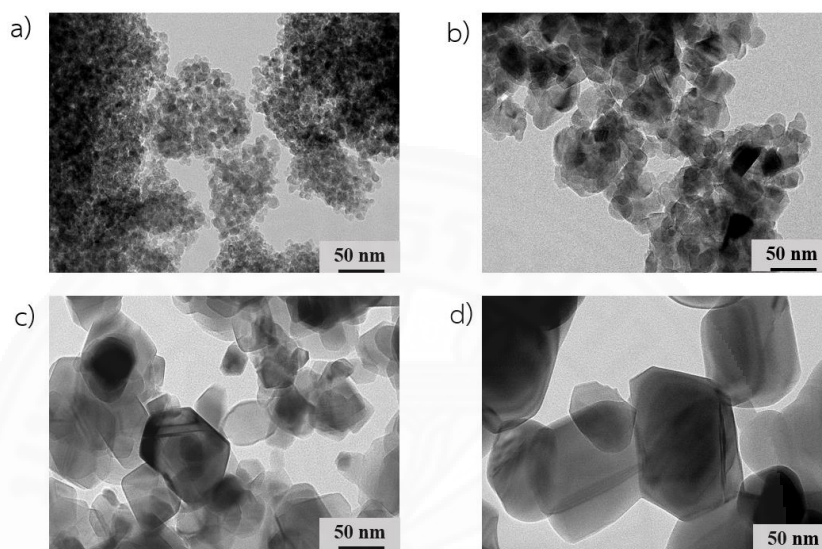


Figure A.1 TEM images of a) TiO_2 -300, b) TiO_2 -600, c) TiO_2 -700, and d) TiO_2 -800.

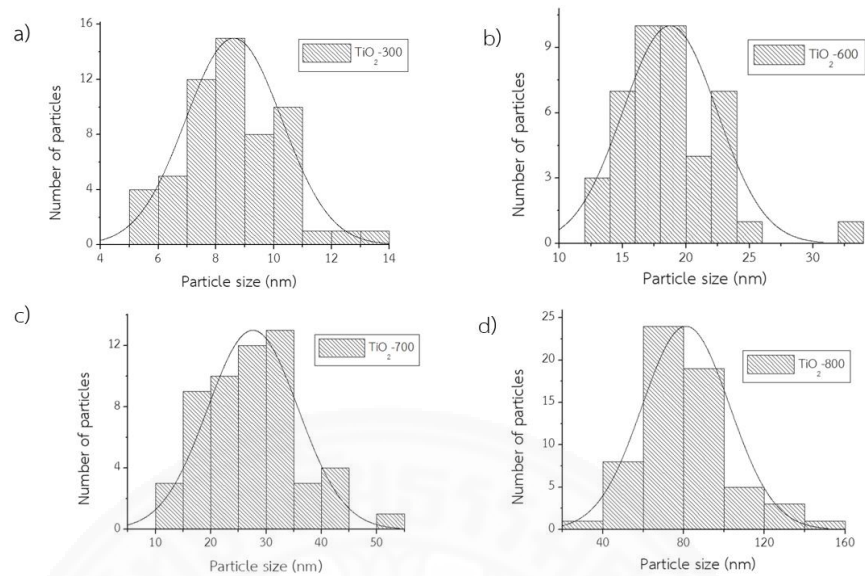


Figure A.2 Size distribution of a) TiO_2 -300, b) TiO_2 -600, c) TiO_2 -700, and d) TiO_2 -800.

APPENDIX B

Particle size and size distribution of Ag-TiO₂ synthesized via DWBMS method with different concentrations of Ag

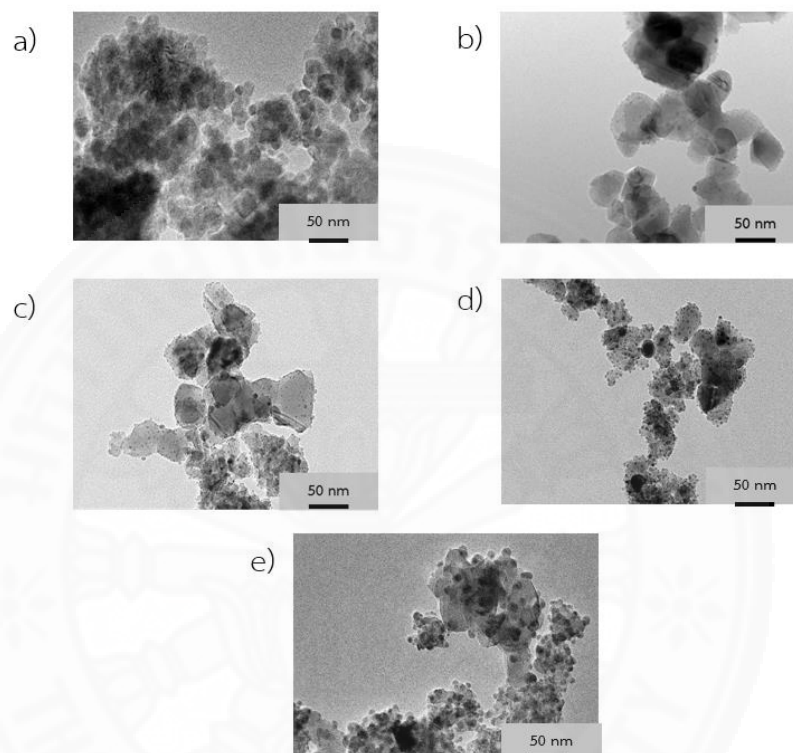


Figure B.1 TEM images of a) TiO₂ and b) 3% Ag-TiO₂, c) 5% Ag-TiO₂, d) 6% Ag-TiO₂, and e) 10% Ag-TiO₂.

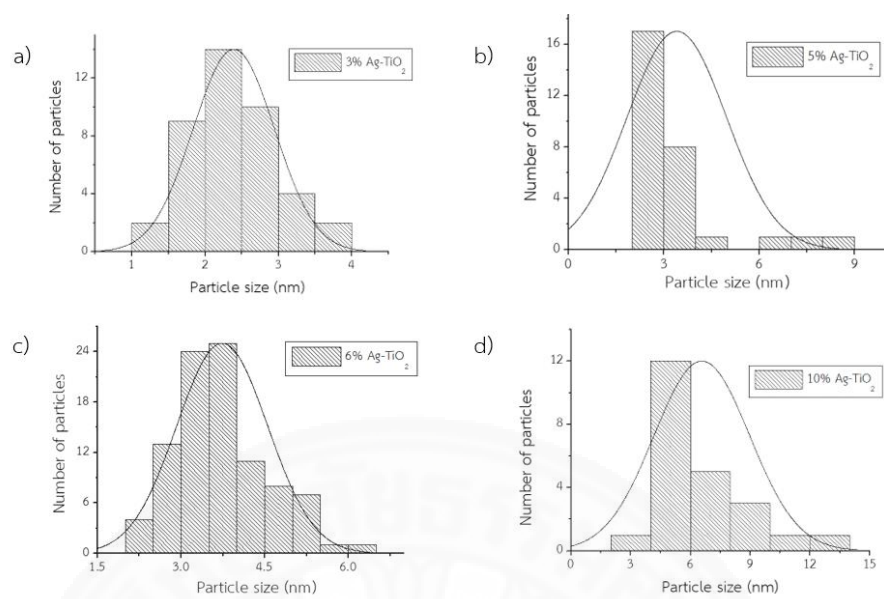
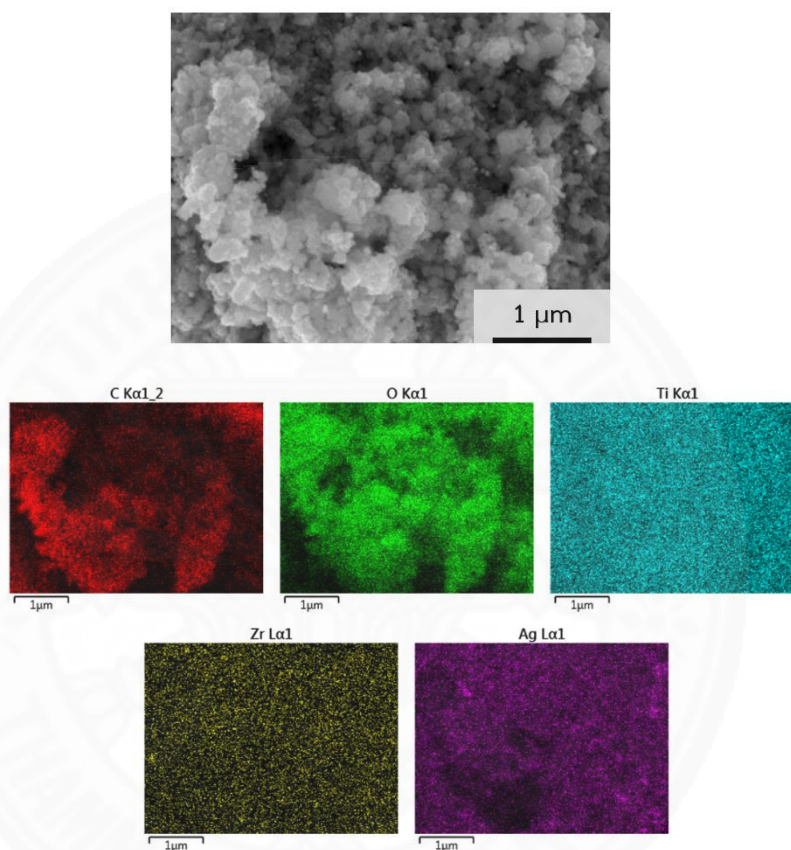


Figure B.2 Size distribution of a) 3% Ag-TiO₂, b) 5% Ag-TiO₂, c) 6% Ag-TiO₂, and d) 10% Ag-TiO₂.

APPENDIX C

Energy Dispersive Spectroscopy of Ag-TiO₂ synthesized via DWBMS
method with different concentrations of AgFigure C.1 EDS mapping of 5% Ag-TiO₂ particles.

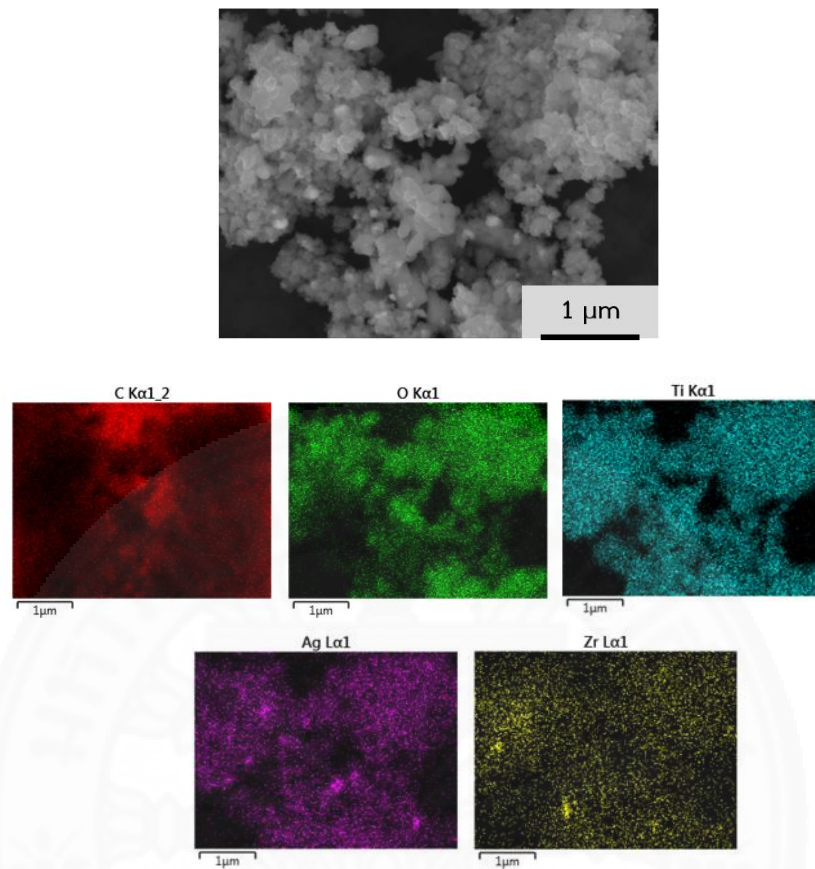


Figure C.2 EDS mapping of 6% Ag-TiO₂ particles.

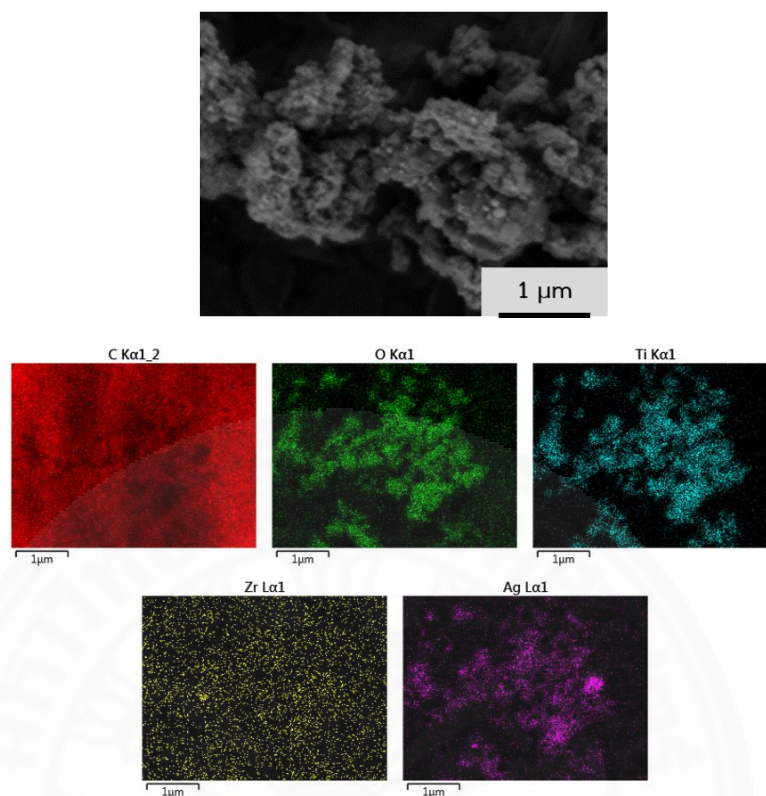


Figure C.3 EDS mapping of 10% Ag-TiO₂ particles.

APPENDIX D

Pore size distribution of TiO_2 and Ag-TiO_2 with different concentrations of Ag from 3 to 10% by mole

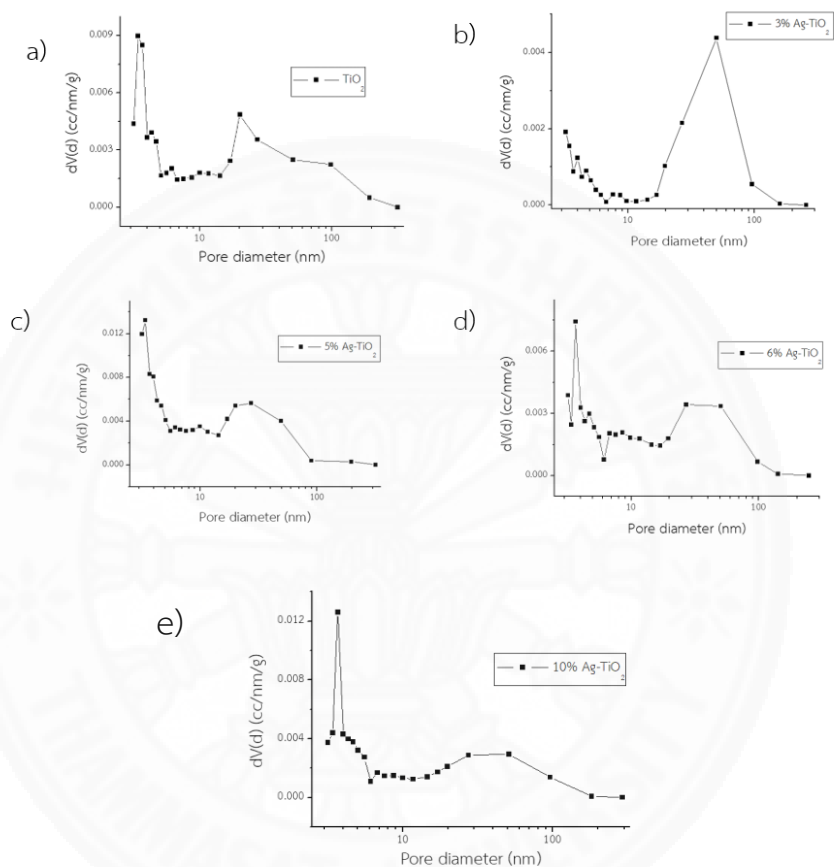


Figure D.1 Pore size distribution of a) TiO_2 , b) 3% Ag-TiO_2 , c) 5% Ag-TiO_2 , d) 6% Ag-TiO_2 , and e) 10% Ag-TiO_2 .

APPENDIX E

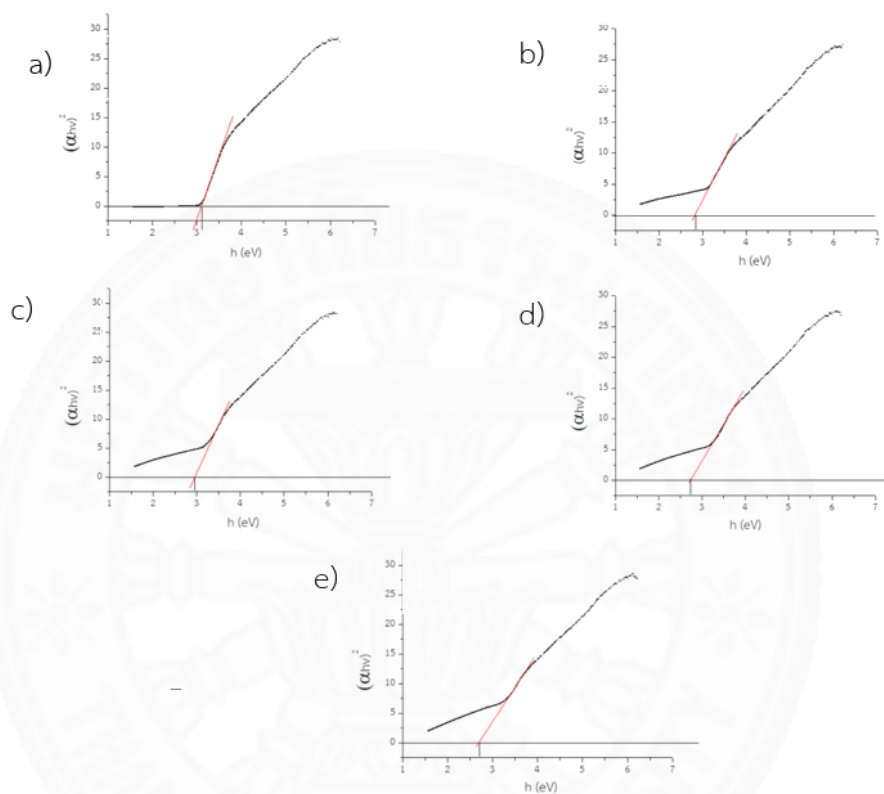
Energy band gap of TiO_2 and Ag-TiO_2 powder with different concentrations of Ag

Figure E.1 Energy band gap of a) TiO_2 , b) 3% Ag-TiO_2 , c) 5% Ag-TiO_2 , d) 6% Ag-TiO_2 , and e) 10% Ag-TiO_2 .

APPENDIX F

**Concentration of *E. coli* on air filter for antibacterial activity on AATCC
100-1999 under dark and UV light conditions**

Table F.1 Concentration of *E. coli* on F9 air filters coated with different dipping speeds of 0.167, 0.250, 0.500 and 1.000 mm/s under dark and light conditions.

Sample	Concentration of <i>E. coli</i> (CFU/ml)	
	Dark	UV light
Control-1	$(5.05 \pm 1.45) \times 10^9$	$(1.02 \pm 0.13) \times 10^9$
0.167 mm/s	$(1.27 \pm 0.13) \times 10^7$	$(1.00 \pm 0.00) \times 10^5$
0.250 mm/s	$(1.00 \pm 0.00) \times 10^5$	$(1.00 \pm 0.00) \times 10^5$
Control-2	$(6.03 \pm 0.21) \times 10^9$	$(9.30 \pm 1.70) \times 10^9$
0.500 mm/s	$(2.37 \pm 0.72) \times 10^8$	$(1.00 \pm 0.00) \times 10^5$
1.000 mm/s	$(4.49 \pm 1.40) \times 10^7$	$(1.00 \pm 0.00) \times 10^5$

Percentage of bacterial reduction calculated as follows:

$$\text{Bacteria reduction (\%R)} = \frac{A-B}{A} \times 100 \quad (1)$$

Where A and B are the number of bacterial colonies recovered from the untreated and the treated samples, respectively after inoculation. %R is the percentage of bacterial colony reduction⁽⁵⁴⁾.

An example of calculation of at air filter coated with 0.167 mm/s is illustrated as follows:

$$\text{Bacteria reduction (\%R)} = \frac{(5.0 \times 10^9) - (1.2 \times 10^7)}{5.05 \times 10^9} \times 100$$

$$\text{Then, bacterial reduction (\% R)} = 99.75 \%$$

Standard deviation can be calculated from this equation

$$SD = \sqrt{\left(\frac{SD}{X_{average}}\right)^2 + \left(\frac{SD}{Y_{average}}\right)^2} \quad (2)$$

Then, SD = 0.30

Table F.2 Concentration of *E. coli* on F9 air filters coated with different concentrations of PPG-4000 under dark and UV light conditions.

Sample	Concentration of <i>E. coli</i> (CFU/ml)	
	Dark	UV light
Control-1	$(5.56 \pm 1.14) \times 10^9$	$(1.02 \pm 0.13) \times 10^9$
0.1%v/v PPG-4000	$(7.58 \pm 1.33) \times 10^9$	$(3.30 \pm 0.23) \times 10^9$
1.0%v/v PPG-4000	$(9.34 \pm 1.94) \times 10^9$	$(3.22 \pm 0.29) \times 10^9$
Control-2	$(7.48 \pm 0.48) \times 10^9$	$(4.25 \pm 1.33) \times 10^9$
5.0%v/v PPG-4000	$(6.24 \pm 1.57) \times 10^9$	$(1.97 \pm 0.43) \times 10^9$
10.0%v/v PPG-4000	$(1.00 \pm 0.00) \times 10^5$	$(1.00 \pm 0.00) \times 10^5$

Table F.3 Concentration of *E. coli* on F9 air filters coated with different concentrations of PPG-4000 and top-coated with 10%w/v P25 NPs under dark and light conditions.

Sample	Concentration of <i>E. coli</i> (CFU/ml)	
	Dark	UV light
Control-1	$(5.56 \pm 1.14) \times 10^9$	$(1.02 \pm 0.13) \times 10^9$
0.1%v/v PPG-4000+P25	$(1.26 \pm 0.67) \times 10^9$	$(1.00 \pm 0.00) \times 10^5$
1.0%v/v PPG-4000+P25	$(1.76 \pm 0.21) \times 10^9$	$(1.00 \pm 0.00) \times 10^5$
Control-2	$(7.48 \pm 0.48) \times 10^9$	$(4.25 \pm 1.33) \times 10^9$
5.0%v/v PPG-4000+P25	$(5.60 \pm 2.35) \times 10^8$	$(1.00 \pm 0.00) \times 10^5$
10.0%v/v PPG-4000+P25	$(1.00 \pm 0.00) \times 10^5$	$(1.00 \pm 0.00) \times 10^5$

Table F.4 Concentration of *E. coli* on F9 air filters coated with different concentrations of P25 NPs and 1%v/v of PPG-4000 under dark and UV light conditions.

Sample	Concentration of <i>E. coli</i> (CFU/ml)	
	Dark	UV light
Control-1	$(6.72 \pm 0.80) \times 10^9$	$(6.19 \pm 0.77) \times 10^9$
0.1%w/v P25	$(8.51 \pm 1.42) \times 10^9$	$(4.23 \pm 0.99) \times 10^5$
1.0%w/v P25	$(7.60 \pm 2.13) \times 10^9$	$(1.06 \pm 0.10) \times 10^5$
Control-2	$(7.72 \pm 0.61) \times 10^9$	$(4.47 \pm 0.77) \times 10^9$
5.0%w/v P25	$(8.74 \pm 1.93) \times 10^8$	$(7.20 \pm 0.42) \times 10^5$
10.0%w/v P25	$(3.40 \pm 0.40) \times 10^5$	$(1.00 \pm 0.00) \times 10^5$

Table F.5 Concentration of *E. coli* on F9 air filters coated with 10%w/v of P25, TiO₂ and 5% Ag-TiO₂ and pre-coated with 1%v/vPPG-4000 under dark and UV light conditions.

Sample	Concentration of <i>E. coli</i> (CFU/ml)	
	Dark	UV light
Control-1	$(7.58 \pm 0.57) \times 10^9$	$(2.78 \pm 0.15) \times 10^9$
10%w/v P25	$(7.40 \pm 1.29) \times 10^9$	$(1.00 \pm 0.00) \times 10^5$
10%w/v TiO ₂	$(8.00 \pm 1.40) \times 10^9$	$(4.19 \pm 0.79) \times 10^9$
10%w/v 5% Ag-TiO ₂	$(1.00 \pm 0.00) \times 10^5$	$(1.00 \pm 0.00) \times 10^5$

APPENDIX G

Self-cleaning rate of air filters coated with different speeds and concentrations of PPG-4000, P25 NPs, TiO₂ and 5% Ag-TiO₂

Table G.1 Contact angle of F9 air filters coated with 10%w/v P25 NPs with 0.167 mm/s irradiated by UV light from 0 to 24 h.

UV irradiation (h)	Contact angle of air filter (degree)				
	Point 1	Point 2	Point 3	Point 4	Point 5
0.00	55.52	43.62	35.60	56.23	40.71
0.25	59.64	37.67	58.40	51.55	53.09
0.75	38.18	46.31	59.10	53.30	47.49
1.50	52.01	48.83	46.67	41.46	58.44
2.00	50.47	40.64	58.32	40.98	31.97
3.00	48.61	59.42	58.93	41.70	31.65
4.00	45.87	31.35	40.41	34.11	28.25
6.00	27.25	25.13	21.30	37.09	32.27
24.00	43.82	38.38	38.13	51.04	47.10

Table G.2 Contact angle of F9 air filter coated with 10%w/v P25 NPs with 0.250 mm/s irradiated by UV light from 0 to 24 h.

UV irradiation (h)	Contact angle of air filter (degree)				
	Point 1	Point 2	Point 3	Point 4	Point 5
0.00	61.85	44.18	54.94	30.61	31.01
0.25	59.50	54.82	40.22	53.87	49.05
0.75	54.13	51.86	58.30	41.13	57.56
1.50	56.27	56.42	58.79	57.16	56.94
2.00	29.29	53.08	49.22	56.10	54.58
3.00	47.80	52.48	42.92	54.52	49.49
4.00	44.58	49.35	38.58	36.47	24.39
6.00	43.80	40.90	36.27	41.79	43.88
24.00	22.49	41.68	34.01	43.96	39.11

Table G.3 Contact angle of air filter coated with 10%w/v P25 NPs with 0.500 mm/s irradiated by UV light from 0 to 24 h.

UV irradiation (h)	Contact angle of air filter (drgree)				
	Point 1	Point 2	Point 3	Point 4	Point 5
0.00	42.54	47.19	40.78	48.81	34.75
0.25	50.84	50.43	54.65	31.02	53.54
0.75	49.80	42.93	28.89	53.68	43.74
1.50	51.13	54.84	31.59	31.50	41.22
2.00	37.71	53.70	43.10	40.73	43.31
3.00	22.40	38.16	26.15	28.43	34.88
4.00	46.59	40.39	35.88	43.82	42.98
6.00	21.81	38.24	35.39	29.94	31.50
24.00	28.80	37.41	33.04	34.89	28.52

Table G.4 Contact angle of air filter coated with 10%w/v P25 NPs with 1.000 mm/s irradiated by UV light from 0 to 24 h.

UV irradiation (h)	Contact angle of air filter (degree)				
	Point 1	Point 2	Point 3	Point 4	Point 5
0.00	43.53	45.48	52.60	43.52	44.89
0.25	48.14	50.23	49.36	41.21	40.04
0.75	44.76	44.43	47.46	38.13	45.03
1.50	36.98	42.86	45.02	31.04	40.35
2.00	38.66	39.33	40.50	41.93	31.73
3.00	33.01	36.19	39.91	36.51	33.09
4.00	30.05	33.17	34.33	35.83	40.25
6.00	32.91	39.27	38.55	42.18	38.79
24.00	36.02	29.69	34.04	36.32	33.72

An equation for calculation of self-cleaning can be written as follows:

$$\ln \frac{C}{C_0} = -kt + \text{constant} \quad (1)$$

Where k is the constant of contact angle of water (min)

$$f(t) = \frac{[\cos\phi(t) - \cos\phi_2]}{[\cos\phi_1 - \cos\phi_2]} \quad (2)$$

Where $\phi(t)$ = contact angle at time, ϕ_1 = contact time at start and ϕ_2 = contact time at final. From Table G.1 the air filter coated with 0.167 mm/s can find average $\cos\phi_1 = 0.68$ and then, can substitute in equation 2

$$f(t) = \frac{\cos\phi(t) - 1}{0.32} \quad (3)$$

so, it can substitute $\cos\phi(t)$ at different time from 0.25 to 24 h in equation 3 as shown in table G.5.

Table G.5 Natural logarithm of $f(t)$ of contact angle of air filters coated with P25 NPs with different dipping speeds irradiated by UV light from 0 to 24 h.

UV irradiation (h)	$\ln f(t)$			
	Velocity of dipping speed (mm/s)			
	0.167	0.250	0.500	1.000
0.25	0.20	0.24	0.23	0.02
0.75	0.08	0.28	0.06	-0.1
1.50	0.10	0.42	-0.01	-0.31
2.00	-0.01	0.15	0.04	-0.35
3.00	0.07	0.16	-0.67	-0.49
4.00	-0.49	-0.27	-0.05	-0.55
6.00	-0.93	-0.18	-0.59	-0.36
24.00	-0.13	-0.40	-0.53	-0.59

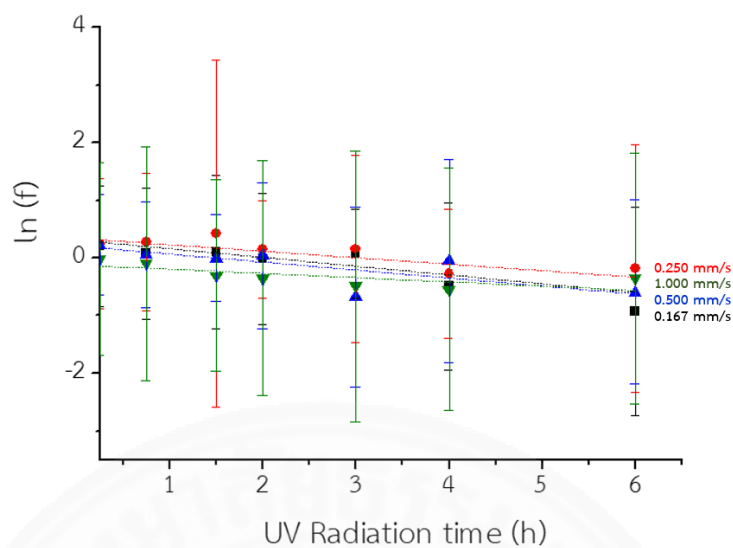


Figure G.1 Relationship between UV irradiation time and $\ln f(t)$ of F9 air filters coated with different dipping speeds of 10%w/v P25 solution.

Table G.6 Contact angle of F9 air filter coated with 0.1%v/v PPG-4000 and 10%w/v P25 NPs irradiated by UV light from 0 to 24 h.

UV irradiation (h)	Contact angle of air filter (°)				
	Point 1	Point 2	Point 3	Point 4	Point 5
0.00	36.74	30.04	41.32	39.18	38.75
0.25	30.20	33.45	36.91	32.86	36.76
0.75	35.49	33.78	40.01	38.21	36.21
1.50	39.23	37.89	41.38	43.36	44.32
2.00	24.55	33.91	30.25	34.86	41.12
3.00	27.32	38.01	37.70	31.59	43.54
4.00	36.27	38.86	31.27	34.67	36.17
6.00	40.02	39.39	34.10	36.80	41.93
24.00	38.44	35.10	29.54	32.74	36.95

Table G.7 Contact angle of F9 air filter coated with 1.0%v/v PPG-4000 and 10%w/v P25 NPs irradiated by UV light from 0 to 24 h.

UV irradiation (h)	Contact angle of air filter (°)				
	Point 1	Point 2	Point 3	Point 4	Point 5
0.00	43.58	39.57	33.01	34.56	28.56
0.25	42.48	51.31	51.99	46.89	33.37
0.75	37.37	34.14	32.96	36.94	32.09
1.50	32.28	39.21	33.39	42.47	42.87
2.00	35.36	37.79	38.69	44.93	42.64
3.00	45.24	44.98	45.29	41.39	43.43
4.00	42.19	31.31	42.05	39.12	36.85
6.00	35.72	36.43	44.73	31.53	35.16
24.00	33.92	37.74	38.60	42.85	35.59

Table G.8 Contact angle of F9 air filter coated with 5.0%v/v PPG-4000 and 10%w/v P25 NPs irradiated by UV light from 0 to 24 h.

UV irradiation (h)	Contact angle of air filter (°)				
	Point 1	Point 2	Point 3	Point 4	Point 5
0.00	29.24	32.77	28.67	33.42	31.91
0.25	33.39	22.19	35.00	37.61	28.80
0.75	26.46	27.25	36.86	28.05	24.06
1.50	35.05	26.02	28.17	25.18	36.40
2.00	25.30	27.34	35.10	32.39	29.98
3.00	37.08	29.45	29.90	27.41	27.73
4.00	29.60	36.33	44.25	42.00	44.34
6.00	34.76	36.56	32.38	38.39	34.14
24.00	29.39	29.89	35.79	38.46	34.47

Table G.9 Contact angle of F9 air filter coated with 10.0%v/v PPG-4000 and 10%w/v P25 NPs irradiated from 0 to 24 h.

UV irradiation (h)	Contact angle of air filter (°)				
	Point 1	Point 2	Point 3	Point 4	Point 5
0.00	43.73	38.00	38.45	42.39	39.67
0.25	35.22	36.74	37.35	33.30	41.05
0.75	39.14	41.08	40.25	36.51	32.82
1.50	27.08	30.36	36.87	40.12	42.19
2.00	38.88	39.24	43.45	43.94	40.02
3.00	31.25	35.46	32.39	32.17	31.31
4.00	31.07	36.14	24.42	39.82	39.41
6.00	30.26	34.14	31.64	31.34	29.83
24.00	28.84	33.02	34.53	32.81	33.66

Table G.10 Natural logarithm of $f(t)$ contact angle of air filters coated with different concentrations of PPG-4000 from 0.1 to 10.0 %v/v and top-coated with 10%w/v P25 irradiated by UV light from 0 to 24 h.

UV irradiation (h)	$\ln f(t)$			
	Concentration of PPG-4000 (% v/v)			
	0.1	1.0	5.0	10.0
0.25	-0.2	0.46	0	-0.14
0.75	-0.05	-0.06	-0.19	-0.08
1.50	0.17	0.12	-0.01	-0.2
2.00	-0.24	0.21	0.05	0.07
3.00	-0.09	0.39	-0.31	-0.38
4.00	-0.12	0.13	-0.2	-0.26
6.00	0.04	0.05	0.06	-0.45
24.00	-0.17	0.10	0.04	-0.38

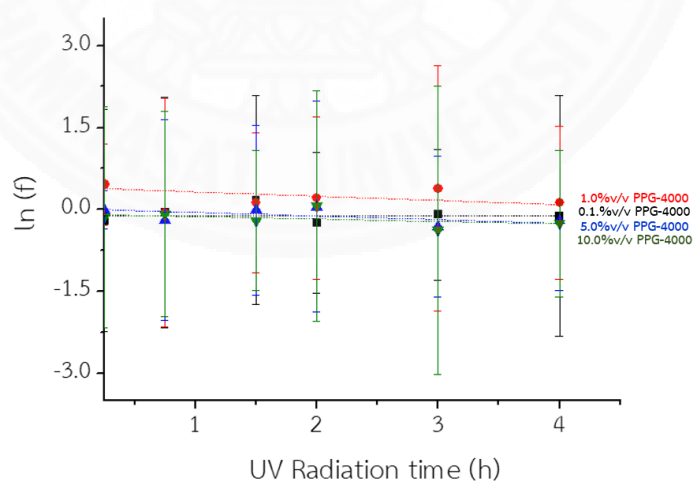


Figure G.2 Relationship between UV irradiation time and $\ln f(t)$ of F9 air filter coated with different concentrations of PPG-4000 from 0.1% to 10.0%v/v.

Table G.11 Contact angle of F9 air filter coated with 1.0%v/v PPG-4000 and 0.1%w/v P25 NPs irradiated by UV light from 0 to 24 h.

UV irradiation (h)	Contact angle of air filter (°)				
	Point 1	Point 2	Point 3	Point 4	Point 5
0.00	43.68	43.39	45.40	45.87	40.50
0.25	39.46	39.91	45.25	39.52	31.95
0.75	34.16	36.81	33.87	36.92	35.18
1.50	39.40	35.91	39.50	37.07	37.35
2.00	28.76	33.71	31.85	34.50	31.75
3.00	33.83	34.66	35.88	32.79	40.35
4.00	28.21	36.36	41.48	34.59	39.40
6.00	36.23	34.92	28.43	35.09	31.11
24.00	37.68	35.76	36.10	34.06	32.88

Table G.12 Contact angle of F9 air filter coated with 1.0%v/v PPG-4000 and 1.0%w/v P25 NPs from 0 to 24 h.

UV irradiation (h)	Contact angle of air filter (°)				
	Point 1	Point 2	Point 3	Point 4	Point 5
0.00	39.65	44.06	40.19	44.18	35.28
0.25	33.56	33.82	43.00	39.62	42.30
0.75	41.00	35.76	39.76	35.93	38.90
1.50	37.43	37.03	32.05	40.75	31.91
2.00	43.59	34.93	32.12	40.16	33.68
3.00	38.42	41.14	38.43	31.06	38.65
4.00	35.11	34.75	34.81	27.04	37.97
6.00	34.75	32.73	35.01	33.18	33.11
24.00	33.98	28.41	29.99	21.95	34.39

Table G.13 Contact angle of F9 air filter coated with 1.0%v/v PPG-4000 and 5.0% w/v P25 NPs irradiated by UV light from 0 to 24 h.

UV irradiation (h)	Contact angle of air filter (°)				
	Point 1	Point 2	Point 3	Point 4	Point 5
0.00	31.75	41.72	46.26	47.55	43.96
0.25	32.03	33.19	47.44	42.60	38.80
0.75	33.01	34.06	33.57	28.27	34.76
1.50	35.88	37.06	37.86	34.37	44.12
2.00	41.83	38.66	34.56	38.37	42.77
3.00	35.32	36.61	34.98	32.97	30.95
4.00	23.57	31.83	28.88	30.94	29.08
6.00	23.25	20.43	26.14	25.91	25.92
24.00	23.55	30.36	22.93	29.57	24.70

Table G.14 Contact angle of F9 air filter coated with 1.0%v/v PPG-4000 and 10.0% w/v P25 NPs irradiated by UV light from 0 to 24 h.

UV irradiation (h)	Contact angle of air filter (°)				
	Point 1	Point 2	Point 3	Point 4	Point 5
0.00	45.85	47.25	42.73	48.93	46.38
0.25	34.91	47.24	41.15	37.93	40.92
0.75	40.41	41.49	42.20	41.71	39.51
1.50	38.83	42.53	42.75	45.19	38.08
2.00	31.58	28.00	29.42	39.84	34.09
3.00	28.27	25.14	31.51	32.41	31.33
4.00	30.78	27.19	34.83	34.38	29.68
6.00	26.45	26.52	29.49	25.85	23.73
24.00	25.45	27.11	27.14	27.95	31.79

Table G.15 Natural logarithm of $f(t)$ of contact angle of air filters coated with different concentrations of PPG-4000 from 0.1 to 10.0%v/v and top-coated with 10%w/v P25 irradiated by UV light from 0 to 24 h.

UV irradiation (h)	$\ln F(t)$			
	Concentration of PPG 4.000 (%v/v)			
	0.1	1.0	5.0	10.0
0.25	-0.21	-0.09	-0.15	-0.08
0.75	-0.41	-0.11	-0.49	-0.05
1.50	-0.28	-0.23	-0.21	-0.03
2.00	-0.6	-0.17	-0.14	-0.49
3.00	-0.41	-0.14	-0.41	-0.67
4.00	-0.37	-0.33	-0.73	-0.57
6.00	-0.54	-0.35	-1.07	-0.91
24.00	-0.42	-0.58	-0.91	-0.8

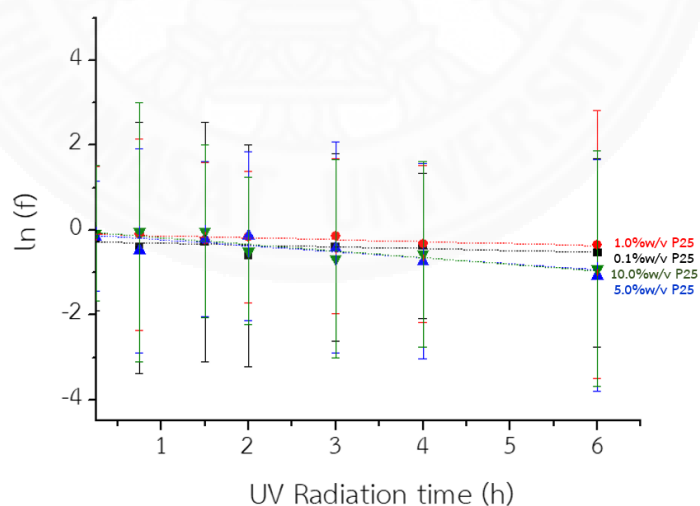


Figure G.3 Relationship between UV irradiation time and $\ln f(t)$ of F9 air filter coated with different concentration of P25 NPs from 0.1% to 10.0%w/v.

Table G.16 Contact angle of F9 air filter coated with 1.0%v/v PPG-4000 and 10.0% w/v 5% Ag-TiO₂ irradiation by UV light from 0 to 24 h.

UV irradiation (h)	Contact angle of air filter (°)				
	Point 1	Point 2	Point 3	Point 4	Point 5
0.00	33.94	38.21	34.69	33.78	31.03
0.25	34.85	34.99	35.73	30.45	34.22
0.75	25.15	32.78	29.47	29.17	22.05
1.50	23.14	26.18	30.06	30.85	21.54
2.00	23.15	27.50	27.62	27.63	23.14
3.00	29.85	24.94	27.00	24.54	26.55
4.00	26.71	28.63	27.48	28.46	25.54
6.00	21.28	25.59	25.57	26.25	26.33
24.00	17.86	17.35	13.75	25.41	26.07

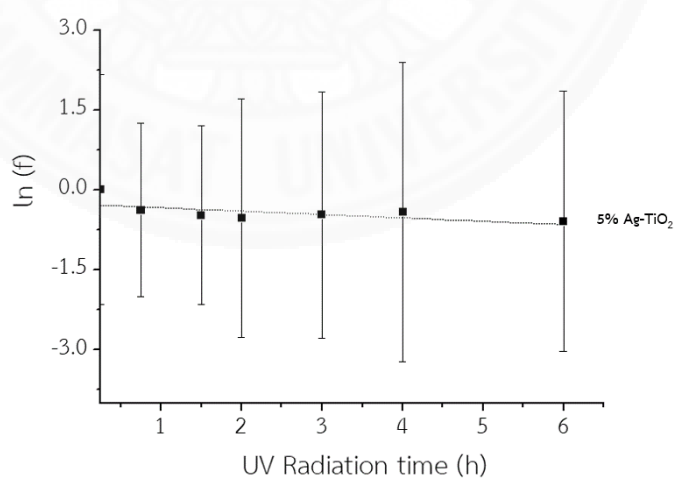


Figure G.4 Relationship between UV irradiation time and $\ln f(t)$ of F9 air filter coated with 10%w/v of 5% Ag-TiO₂.

BIOGRAPHY

Name	Miss Siripond Phomma
Date of Birth	September 3, 1992.
Educational Attainment	Academic Year 2015: Bachelor of Science in Industrial Chemistry, Kasetsart university, Thailand.
Scholarship	Year 2017: Graduate Research Funding for Master Student from Faculty of Chemical Engineering, Thammasart university (001/2/2559) and Thailand Graduate Institute of Science and Technology (TGIST) (SCA-CO-2560-4582-TH).
Publications	<p>Siripond S, Sapcharoenkun C, Wutikhun T, Kasamechonchung P, Eksangsri T. Synthesis of TiO₂ Nanoparticles with High Photocatalytic Activity by Wet Ball Milling Sol-Gel Method. The 7th International Thai Institute of Chemical Engineering and Applied Chemistry Conference (ITICHE2017), October 19-20, 2017, Shangri-La Hotel, Bangkok.</p>
Work Experiences	Year 2015 Position: Researcher and Development Work place: Supreme production co., ltd.